Institute of Paper Science and Technology

STATUS REPORTS

To The

CHEMICAL RECOVERY

PROJECT ADVISORY COMMITTEE

March 24, 1994

IPST

Atlanta, Georgia

INSTITUTE OF PAPER SCIENCE AND TECHNOLOGY
PURPOSE AND MISSION STATEMENT

The Institute of Paper Science and Technology is a unique organization whose charitable, educational, and scientific purpose evolves from the singular relationship between the Institute and the pulp and paper industry which has existed since 1929. The purpose of the Institute is fulfilled through three missions, which are:

- to provide high quality students with a multidisciplinary graduate educational experience which is of the highest standard of excellence recognized by the national academic community and which enables them to perform to their maximum potential in a society with a technological base; and
- to sustain an international position of leadership in dynamic scientific research which is participated in by both students and faculty and which is focused on areas of significance to the pulp and paper industry; and
- to contribute to the economic and technical well-being of the nation through innovative educational, informational, and technical services.

ACCREDITATION

The Institute of Paper Science and Technology is accredited by the Commission on Colleges of the Southern Association of Colleges and Schools to award the Master of Science and Doctor of Philosophy degrees.

NOTICE AND DISCLAIMER

The Institute of Paper Science and Technology (IPST) has provided a high standard of professional service and has put forth its best efforts within the time and funds available for this project. The information and conclusions are advisory and are intended only for internal use by any company who may receive this report. Each company must decide for itself the best approach to solving any problems it may have and how, or whether, this reported information should be considered in its approach.

IPST does not recommend particular products, procedures, materials, or service. These are included only in the interest of completeness within a laboratory context and budgetary constraint. Actual products, procedures, materials, and services used may differ and are peculiar to the operations of each company.

In no event shall IPST or its employees and agents have any obligation or liability for damages including, but not limited to, consequential damages arising out of or in connection with any company's use of or inability to use the reported information. IPST provides no warranty or guaranty of results.

CHEMICAL RECOVERY

1994 ANNUAL SPRING RESEARCH REVIEW

TABLE OF CONTENTS

TABLE OF CONTENTS (continued)

KRAFT RECOVERY FURNACE MODELING CAPABILITY

PROJECT 3605

Robert Horton
Steve Lien
Wenrui Yang

March 24, 1994

Institute of Paper Science and Technology
500 10th Street, N.W.
Atlanta, Georgia

TECHNICAL PROGRAM REVIEW

FY 1993-94

Project Title:	KRAFT RECOVERY FURNACE MODELING CAPABILITY
Project Code:	MODEL
Project Number:	3605
Division:	Chemical and Biological Sciences
Project Staff:	R. Horton, S. Lien, W. Yang
FY 93-94 Budget:	$258,000
FY 94-95 Budget:	$190,000

PROGRAM OBJECTIVE:

Support development of a comprehensive model for the fireside processes in a kraft recovery furnace. Provide useful intermediate information to industry as progress is made toward the final model. Work to be done in conjunction with co-workers at UBC, OSU/Abo Akademi, Univ. of Toronto, and other key players.

SUMMARY OF RESULTS:

Collaboration:

IPST's funding for the recovery boiler modeling research has come from two major sources over the past three years: IPST member company dues, and U.S. DOE. A year ago at this time, DOE was considering separate funding of the UBC and IPST efforts. The decision was made to continue DOE funding under the original contract. We continue to collaborate with UBC, OSU, and T.M. Grace, Co., and communication among the research institutions has improved. Joint meetings are held more frequently with participation from all. Joint case studies which involve representatives from each institution are in progress. A time schedule for code transfer from UBC to IPST was agreed upon.

Technical Results:

The majority of IPST research during the last year has been focused in two areas: char bed modeling, and coupled combustion and flow calculation. General applications of the model include simulation of an operational boiler with different liquor nozzles (joint with Ahlstrom, Corp.) and a study of the effects of boiler load on

physical carryover. Student research in support of this project has been directed at developing an improved sulfur reduction model and a NOx model for the recovery boiler.

A new version of the FLUENT CFD code was obtained this year which allows us to describe the char bed shape using curves rather than rectangular steps. This code also permits us to use user-defined subroutines for combustion and multigridding solver techniques. We have developed a technique to predict mass transfer coefficients across a three-dimensional char bed surface. Black liquor combustion chemistry is being coded for use with a bed model that will allow moving boundary conditions which may allow prediction of bed shape.

Dr. Pekka Siiskonen, a Visiting Scientist from Tampella Corp. with experience in char bed modeling, began working with us at IPST in February, 1994.

A preliminary black liquor combustion model has been coded for direct use with CFD codes such as FLUENT and the UBC code. The preliminary combustion model has a crude description of pyrolysis which does not result in a closed energy balance. The coupled combustion and flow simulations allow the prediction of temperature and concentration fields. We will continue to improve the black liquor combustion model as experimental results provide more information about rates and combustion by-products. We are able to use the fully-coupled combustion and flow simulations to test the accuracy of fixed-field methods that were developed earlier.

To date, our FLUENT-based model has been used to study boiler operation in several ways. First, we have conducted sensitivity studies to help validate the simulation technique and the experimentally based model. Second, we have conducted simulations with generalized boiler descriptions to try to learn more about the importance of black liquor firing practice and general boiler behavior. And lastly, we have examined three specific mill boiler operations to help troubleshoot and understand real observations.

GOALS FOR 1994-95

1. Complete a char bed model which includes combustion chemistry and mass transfer coefficient prediction for a three dimensional surface.

2. Develop and incorporate improved energy balance and rate models for the pyrolysis stage of black liquor combustion.

3. Use the model to obtain insight into effects of air distribution and firing practices.

4. Transfer black liquor combustion model developments to UBC.

Student Activities:

The NOx model will continue to be developed using student and external support. Experimental studies will be conducted in support of the black liquor combustion model.

Char Bed Modeling

CFD SIMULATIONS OF THE INTERACTION BETWEEN AIR JETS AND DIFFERENT CHAR BED SHAPES IN RECOVERY FURNACES

Wenrui Yang, Robert R. Horton, and Terry N. Adams

Institute of Paper Science and Technology
500 10th Street, N.W.
Atlanta, GA 30318

December 1993

ABSTRACT

This paper presents the results of investigations of the interaction between air jets and the char bed in a black liquor recovery furnace. A section of the lower furnace region is examined using Computational Fluid Dynamics (CFD). Three char bed shapes and two model geometries are examined. Air flow patterns, shear stress, and mass transfer coefficient on the bed surface are calculated. The results show that the primary air jets have strong impact on the perimeter of the char bed. The profiles for the primary jets depend on the char bed slopes. A steep slope results in fast dissipation and short air jets. Interaction between secondary air jets and the char bed occurs only if the char bed reaches the secondary air level, and the interaction is mainly determined by the air port-to-surface spacing. The shear stress and mass transfer coefficient distributions suggest that a stable char bed for the given air flow patterns may have a slope of about 1:2 and a height just below the secondary air level. This agrees with field observations.

INTRODUCTION

Char bed combustion in black liquor recovery furnaces is an important part of furnace operations. The char bed should have an adequate char burning rate, a high sulfate reduction efficiency, and a stable shape that minimizes particle entrainment and carryover. Interaction of air jets on bed surface is a major factor that affects the combustion processes in the char bed because under normal operation conditions, char bed burning is essentially limited by the rate of oxygen supply (1). Since the oxygen supply depends on air flow patterns, the air jets have significant influence on char combustion and char bed shape. In turn, the shape of the char bed affects air flow patterns by deflecting air jets that impinge on the bed surface (2, 3). A good understanding of the interaction between the air jets and the char bed can help design efficient furnaces and optimize operation conditions.

Computational Fluid Dynamics (CFD) is an efficient method for studying gas flow and combustion processes in recovery furnaces. Applications of the CFD technique to recovery furnace simulations have produced useful results for air flow patterns (4 - 13), temperature and concentration distributions (6 - 8, 14), trajectories of black liquor particles (6, 16), and particle entrainment (16). Simulations of black liquor combustion in a char bed involves chemical reactions, mass transfer, and heat transfer on the bed surface (7, 15). Since the shape of the boundary is not known beforehand, assumed char bed shapes have been used in simulations (2, 3, 7). This may introduce errors in the results; however, such studies can provide information for feasible char bed shapes and may eventually lead to the prediction of char bed shapes from operation conditions.

A limiting factor for CFD simulations of recovery furnaces is that the requirement for computer memory and CPU time can easily exceed practical limits. The overall size of a typical furnace is large relative to its small features, such as air ports. Thus, a CFD furnace model requires large numbers of computational cells to resolve details in a full model. The complexity of the processes in a furnace makes the simulations even more memory and time intensive. An efficient way to reduce the size of a CFD model without losing details is to

simulate a small zone of interest by isolating the zone from the rest of the furnace with suitable boundary conditions. A symmetry plane is the most frequently used boundary type for simplifying recovery furnace simulations (5, 8, 14). This technique is especially helpful for char bed simulations. With reduced simulation zones, smaller computational cells can be used to describe the furnace structure and char bed shape more accurately.

Application of CFD technique to char bed simulations is a complicated problem which involves chemical reactions, transport processes, fluid dynamics, and numerical methods. This paper represents a part of an ongoing study on char bed simulations. In previous articles (2, 3), the effects of grid type and selection of boundary geometry on simulation results were examined. In this work, the interaction between air jets and char beds is studied using CFD simulations in the lower region of a furnace. Gas flow patterns, shear stress and mass transfer coefficient on the bed surface are calculated for different char bed shapes. Feasible char bed shapes are qualitatively described from the distribution patterns of the shear stress and the mass transfer coefficient. In this and the previous studies, CFD simulations are restricted to a slice of the lower furnace region in order to resolve details of the flow patterns with limited computational ability. In a future study, simulations will be carried out in a larger region with a coarser grid to examine the interaction between the char bed and air jets from adjacent furnace walls.

In the following sections, the char bed models will be described, then simulation results for air flow patterns and air jet-char bed interaction will be presented, followed by conclusions from this study.

DESCRIPTION OF CHAR BED MODELS

Attention is focused on the lower furnace region where air jet-char bed interaction takes place. The horizontal cross-section of the full furnace is a 10 m square. The air ports are symmetrically arranged on furnace walls. The primary air ports are 0.05 m wide and 0.3 m high, with an elevation of 0.05 m and a spacing of 0.3 m. The secondary air ports are

0.15 m wide and 0.5 m high, with an elevation of 1.5 m and a spacing of 1.5 m. The inlet air velocities are assumed to be uniform across individual air ports. The primary air velocity is 50 m/s in a 10° downward angle, the secondary air velocity is 80 m/s in the horizontal direction. Heat transfer and chemical reactions are not included in the present study, so an isothermal condition is assumed and the physical properties of air at 1000 °C are used.

To examine effects of char bed shape on the air jet-char bed interaction, three simplified char bed shapes are used in the simulations. All the char beds have straight slopes and flat tops. The char bed surfaces start to rise at 0.15 m from the wall with 1:1, 1:2, or 1:4 slope, and then level off either at 1.775 m above the baseline or at 3.7 m from the wall. The 1:4 slope results in a bed that is only half the height of the beds of 1:1 and 1:2 slopes.

To resolve details of the gas flow patterns, a large number of small computational cells must be used. Therefore, only a small section of the lower furnace region is included in the models. Two arrangements of symmetry planes are considered in this work: a slab geometry and a wedge geometry. The slab models include a uniform width slice of the char bed isolated from the furnace by two parallel and one central symmetry planes and an upper isobaric boundary. The thickness of the slab is 0.75 m, including 2½ primary air ports and ½ secondary air port, as shown in Figure 1. Part of the upper boundary of the computational region is sloped to achieve efficient node distributions. The effect of a sloped boundary on gas flow field is negligible since gas velocity is very low near the sloped boundary. The slab models are equivalent to furnaces with air ports on two infinitely long opposing walls. In this case, the air jets from the other two walls of a four-wall furnace have negligible effect.

In the wedge geometry, one of the side symmetry planes is slightly angled so that the symmetry planes on both sides meet at the furnace center, as shown in Figure 2. This is a rough approximation of a symmetrical furnace with air ports on four walls. As the air jets travel from the wall to the furnace center, the cross-sectional area reduces gradually as if the jets were pushed by air jets from the adjacent walls. With the same inlet air flow rate, the average vertical velocity of the wedge models is twice that of the slab models. Technically, a

wedge model corresponds more closely to a nearly circular furnace with uniformly distributed air ports around the wall. Air jets in the middle of a symmetrical square furnace correspond approximately to a situation between the slab and the wedge models.

The simulations were carried out with FLUENT Version 4.11 (Fluent Inc.), a CFD software based on the finite difference method (17). Body-fitted-coordinate (BFC) grids were used so that the char bed slopes could be represented by smooth boundary conditions (18). In comparison with Cartesian coordinate grids, which must use stairsteps to represent sloped boundaries, BFC grids offer improved accuracy, especially for shear stress and mass transfer coefficient on the sloped surface, and faster convergence speed (3).

All the models in this study have the same number of computational cells ($57\times52\times27\times$ = 80,028). Simulations with nearly 150,000 cells show that the solutions are nearly grid-independent. Slight grid dependence does not affect the utility of the results, as the main interest is in the differences between the models that are more significant than the effects of the grid. The κ-ε turbulence model was used for all computations and the software was run on an IBM RISC/6000 computer, model 550.

RESULTS AND DISCUSSION

Effect of Bed Shape on Gas Flows

In the 1:1 and 1:2 slope models, the char beds reached the secondary air level. Strong interaction between the air jets and the char beds is expected for these models. Figure 3 shows velocity distribution patterns near the boundaries for all cases. An apparent difference between the slab and the wedge models is that the secondary air jets turn upward earlier in the wedge models than in the slab models. However, the primary air jets are only slightly affected by the wedge shape. More discussion about the effects of the wedge shape can be found in a previous paper (2).

In all the models, the primary air jets impinge on the char bed surfaces within a short distance. The slopes of the char beds determine impinging angles of the air jets, and strongly affect the flow patterns. In the case of a 1:1 steep slope, which corresponds to a large impinging angle, the primary jets are deflected abruptly upon impinging on the bed surface. Strong interaction between neighboring jets causes the primaries to dissipate in a short distance. As the slope decreases, the primary jets extend greater distances into the furnace.

A char bed influences the secondary air jets when the height of the bed reaches the secondary air level. For the beds with the same height (1:1 and 1:2 slopes), the 1:1 slope bed is closer to the secondary air port so it has a stronger influence. In the case of a 1:1 slope, (Figures 3(a) and (b)), the secondary jets undergo sudden compression in the y direction and expansion in the z direction. This process enhances dissipation and reduces jet velocity. A high pressure region that is formed at the point of impingement forces the primary air to deviate from its original flow direction. In the case of a 1:2 slope, the slab and the wedge models show remarkably different air jet-char bed interaction. In the slab model, the secondary jet extends horizontally and impinges on the top of the char bed. In the wedge model the secondary air jet turns upward before it contacts the bed surface, resulting in little air jet-char bed interaction. If a char bed is below the secondary air level, it has little apparent effect on the secondary air flows in either the slab or the wedge model (Figure 3(e) and (f)).

Figures 4 and 5 compare average vertical velocities at the upper boundaries. All the models predict a high velocity central core, which is typical for symmetrical air distributions. The wedge models predict higher velocities at the furnace center than the slab models because they have smaller cross-sectional areas and the air jets are forced to turn upward sooner by the converging side boundaries. Impingement of the air jet on the char bed enhances dissipation, as is shown by the decrease of the velocities with increasing char bed slopes in the slab models. The situation is similar for the wedge models, except that the case with a 1:2 slope has a lower velocity at the furnace center than the other cases because a high pressure region above the top of the bed forces the secondary jet to turn upward sooner.

Impacts of Air Jets on Char Bed Surfaces

Impingement of an air jet on a char bed affects the mass and heat transfer processes and redistribution of char particles on the bed surface. All of these processes are related to the shear stress on the bed surface. Figure 6 shows plan views of the shear stress distributions. The bright areas highlight strong interactions between the air jets and the char beds. Generally, the impact of an impinging jet on a surface depends on the air port-to-surface distance and angle of impingement. For the primary air jets, the air port-to-surface distance does not vary significantly with the slope of the char bed, however, the angle of impingement varies with the slope. As the slope of the char bed decreases, the angle of impingement decreases and the primary air jets extend further along the bed surface. As a result, the areas of large shear stress increase in the x direction.

The secondary air ports are a greater distance to the char bed, thus, the effect of air port-to-surface distance is more significant than that of the angle of impingement. Comparing Figures 6(a) and (c), the maximum shear stress due to the secondary air jets decreases from 3.92 Pa to 1.44 Pa when the air port-to-surface distance increases from 1.92 m to 3.7 m. With the same change in distance, the wedge models show an even more remarkable decrease in the shear stress because the secondary air jet no longer impinges on the char bed with the 3.7 m distance. In the case of a 1:4 slope, since the char beds are well below the secondary air level the secondary air jets have no contribution to the shear stress distributions, as can be seen in Figures 6(e) and (f).

The average shear stress distributions are plotted in Figures 7 and 8. The shear stresses due to the primary jets have comparable maximum values that are not very sensitive to the slopes of the char bed. However, the distribution profiles are strongly affected by the slopes. The steeper the slope, the faster the shear stress decreases. In the case of a 1:1 slope, the secondary air jets produce spots of very large shear stress at the top of the char beds. This may be partly due to the angled edges of the flat bed tops. If the char bed surfaces had rounded edges, the shear stress distributions would not change so abruptly.

In the present simulations, the char bed surface is assumed to be smooth. This causes the shear stress to be underestimated because practical char bed surfaces are rough. Roughness parameters would have to be specified for more realistic simulations. The roughness parameter affects the magnitude of the shear stress significantly. However, the distribution patterns would probably not be affected.

Mass transfer on the bed surface plays a major role in determining the rate of char combustion. Mass transfer coefficient can be estimated from the shear stress and velocity using the Chilton-Colburn analogy (19):

$$St_m Sc^{\frac{2}{3}} = \frac{C_f}{2} \tag{1}$$

where $St_m = k/u_p$ is the Stanton number for mass transfer; k is the mass transfer coefficient; u_p is velocity near the surface; Sc is the Schmidt number of the gas (≈ 0.7); C_f is the friction factor, which can be calculated from the shear stress, τ_w, and the velocity by:

$$C_f = \frac{\tau_w}{\frac{1}{2}\rho u_p^2} \tag{2}$$

Combining Equations (1) and (2) to give

$$k = \frac{\tau_w}{\rho u_p} Sc^{-\frac{2}{3}} \tag{3}$$

The above equations have been confirmed to agree with experimental results of black liquor combustion (15). Average mass transfer coefficient for the present models are shown in Figures 9 and 10. As expected, the profiles of the mass transfer coefficient have similar patterns as the shear stress profiles. The distributions of the shear stress and the mass transfer coefficient may provide clues to realistic char bed shapes.

Char Bed Shapes

The shapes of char beds are the results of many physical and chemical processes. The arrival of char particles is mainly determined by black liquor spray patterns and is affected by gas flow patterns. The combustion and redistribution of char particles on the char bed surface depend on air flow patterns, as well as the shape of the bed. Mechanical processes, such as collapse of an undercut bed, will also contribute to the formation of a bed shape.

The air jet-char bed interaction is an important part of char bed formation processes. At typical furnace operation temperatures (> 1000 °C), char combustion by O_2 is essentially controlled by mass transfer. In the areas of air jet impingement, combustion takes place faster than in other areas due to higher O_2 concentration and larger mass transfer coefficient. In the areas where the air jets cannot reach directly, O_2 supply may be deficient, and char gasification by CO_2 and H_2O may become important. The gasification reactions are slower than the combustion by O_2, and these endothermic reactions may reduce the local surface temperature and slow down the reaction rates.

In the cases of 1:1 and 1:4 slopes, the mass transfer coefficient distributions are similar for the slab and the wedge geometries. The char beds with a 1:1 slope represent one extreme where the primary and secondary air jets impinge hard on the bed surfaces. This can result in very nonuniform combustion rate distributions. Very fast combustion can be expected near the bottom and the top surfaces of the char beds. If the char arrival pattern does not cause excessive accumulations in these areas, then the top surface will be burnt off and the bottom surface will be undercut. Consequently, the char bed would collapse, becoming less steep. In contrast, the char combustion rate varies less abruptly on the bed with a 1:4 slope. Faster combustion occurs near the base of the bed where the primary jets impinge on it. As the air flows toward the center of the furnace, O_2 concentration and mass transfer coefficient decrease gradually. Combustion rate at the furnace center can be expected to be lower than that near the walls. This implies that the char bed would have the tendency to grow higher at the center.

The slab and the wedge models with a 1:2 slope show different combustion patterns. The effects of the primary air jets are similar: increasing combustion rate near the base of the bed. The slope of the bed is already small, thus collapse is not likely to occur. The straight slope, however, may change into a complex curved shape. In the slab model, impingement of the secondary jet on the top of the bed creates a fast burning area. This may prevent the char bed from growing higher or steeper since the combustion rate increases quickly with the growth of the bed. Significant decrease of the bed size is not likely either since that would lead to a situation similar to the case of a 1:4 slope. A stable bed shape may have approximately a 1:2 slope with the top at the secondary air jet level. In the wedge model with a 1:2 slope, the secondary air jet does not extend horizontally far enough to reach the char bed. Char combustion rate at the top of the bed is expected to be smaller than that in the corresponding slab model. Therefore, the wedge model would predict a higher char bed than the slab model.

Combustion is only one aspect of the char bed formation process. Accurate prediction of the char bed shape is not possible unless char arrival and mechanical char redistribution processes are also considered. An actual char bed shape is determined by the balance of overall char arrival and removal.

CONCLUSIONS

Interaction between air jets and black liquor char beds has been studied using CFD simulations. Three char bed shapes and two model geometries have been examined. The following conclusions may be drawn from the results.

1. There is strong interaction between primary air jets and char beds. The flow patterns of the jets depend on the slopes of the char beds. The smaller the slope, the further the jets extend, but the weaker the initial impact on the bed.

2. The interaction between secondary air jets and char beds depends on the air port-

to-surface distance. The smaller the distance the stronger the interaction. There is minimal interaction between secondary air jets and a char bed if the char bed is below the secondary air level.

3. Air jet impingements produce areas of high mass transfer coefficients. The distribution of the mass transfer coefficients is very sensitive to the char bed shape. With the assumed air system, a stable char bed may have a slope between 1:4 and 1:1, and a height reaching the secondary air level.

ACKNOWLEDGMENT

This work was supported by the U.S. DOE under contract No. DE-FG02-90CE40936, and IPST member company funding.

REFERENCES

1. Grace, T. M., Lien, S. J., and Brown, C. A., "Char Bed Burning - Laboratory Studies," *Proc. Int'l Chem. Recovery Conf.*, p. 539, 1992.

2. Yang, W., Horton, R. R., and Adams, T. N., "A Comparison of CFD Simulations of Recovery Boiler Char Beds with 2-D and 3-D Geometries," IPST Technical Paper series #483, 1993.

3. Yang, W., Horton, R. R., and Adams, T. N., "CFD Simulations of Recovery Boiler Char Beds with Step and Smooth Surfaces," IPST Technical Paper Series, #478, 1993.

4. Chapman, P. J. and Jones, A. K., "Recovery Boiler Secondary Air System Development Using Experimental and Computational Fluid Dynamics," *Proc. TAPPI Eng. Conf.*, p. 193, 1990.

5. Jones, A. K. and Grace T. M., "A Comparison of Computational and Experimental Methods for Determining the Gas Flow Patterns in the Kraft Recovery Boiler," *Proc. TAPPI Eng. Conf.*, p. 3, 1988.

6. Chapman, P. J. and Jones, A. K., "Recovery Furnace Combustion Modeling Using Computational Fluid Dynamics," *Proc. Int'l Chem. Recovery Conf.*, p. 71, 1992.

7. Sumnicht, D. W., "A Computer Model of a Kraft Char Bed," Ph.D. Thesis, IPC, April, 1989.

8. Vakkilainen, E. K., Adams, T. N., and Horton, R. R., "The Effect of Recovery Furnace Bullnose Designs on Upper Furnace Flow and Temperature Profiles," *Proc. Int'l Chem. Recovery Conf.*, p. 101, 1992.

9. Siiskonen, P., Karvinen, R., Hyoty, P., Migaj, V. K., and Morgoun, A. V., "Combined Physical and Numerical Study of a Multilevel Air System," *Proc. Int'l Chem. Recovery Conf.*, p. 57, 1992.

10. Salcudean, M., Nowak, P., and Abdullah, Z., "Mathematical Modeling of Recovery Furnaces," *Proc. Int'l Chem. Recovery Conf.*, p. 197, 1992.

11. Abdullah, Z., Nowak, P., Salcudean, M., and Gartshore, I. S., "Investigation of Interlaced and Opposed Jet Arrangements for Recovery Furnaces," *Proc. TAPPI Eng. Conf.*, p. 103, 1992.

12. Quick, J. W., Gartshore, I. S., and Salcudean, M., "Interaction of Opposing Jets with Special Relevance to Recovery Furnaces," *Proc. TAPPI Eng. Conf.*, p. 123, 1992.

13. Adams, T. N. and Horton, R. R., "The Effects of Black Liquor Spray on Gas Phase

Flows in a Recovery Boiler," *Proc. TAPPI Eng. Conf.*, p. 81, 1992.

14. Karvinen, R., Hyoty, P., and Siiskonen, P., "The Effect of Dry Solids Contents on Recovery Boiler Furnace Behavior," *Tappi J.* **74**(12), 171(1991).

15. Sutinen, J. E. and Karvinen, R., "Numerical Modeling of Char Bed Phenomena," *Proc. Int'l Chem. Recovery Conf.*, p. 79, 1992.

16. Horton, R. R., Grace, T. M., and Adams, T. N., "The Effects of Black Liquor Spray Parameters on Combustion Behavior in Recovery Furnace Simulations," *Proc. Int'l Chem. Recovery Conf.*, p. 85, 1992.

17. FLUENT User's Guide, Ver. 4.0, Fluent Inc., December 1991.

18. PreBFC User's Guide, Ver. 4.0, Fluent Inc., December 1991.

19. Incropera, F. P. and De Witt, D. P., *Fundamentals of Heat and Mass Transfer*, 2nd ed., John Willey & Sons, New York, 1985.

20. Launder, B. E. and Spalding, D. B., *The Numerical Computation of Turbulent Flows*, Imperial College of Science and Technology, London, 1973.

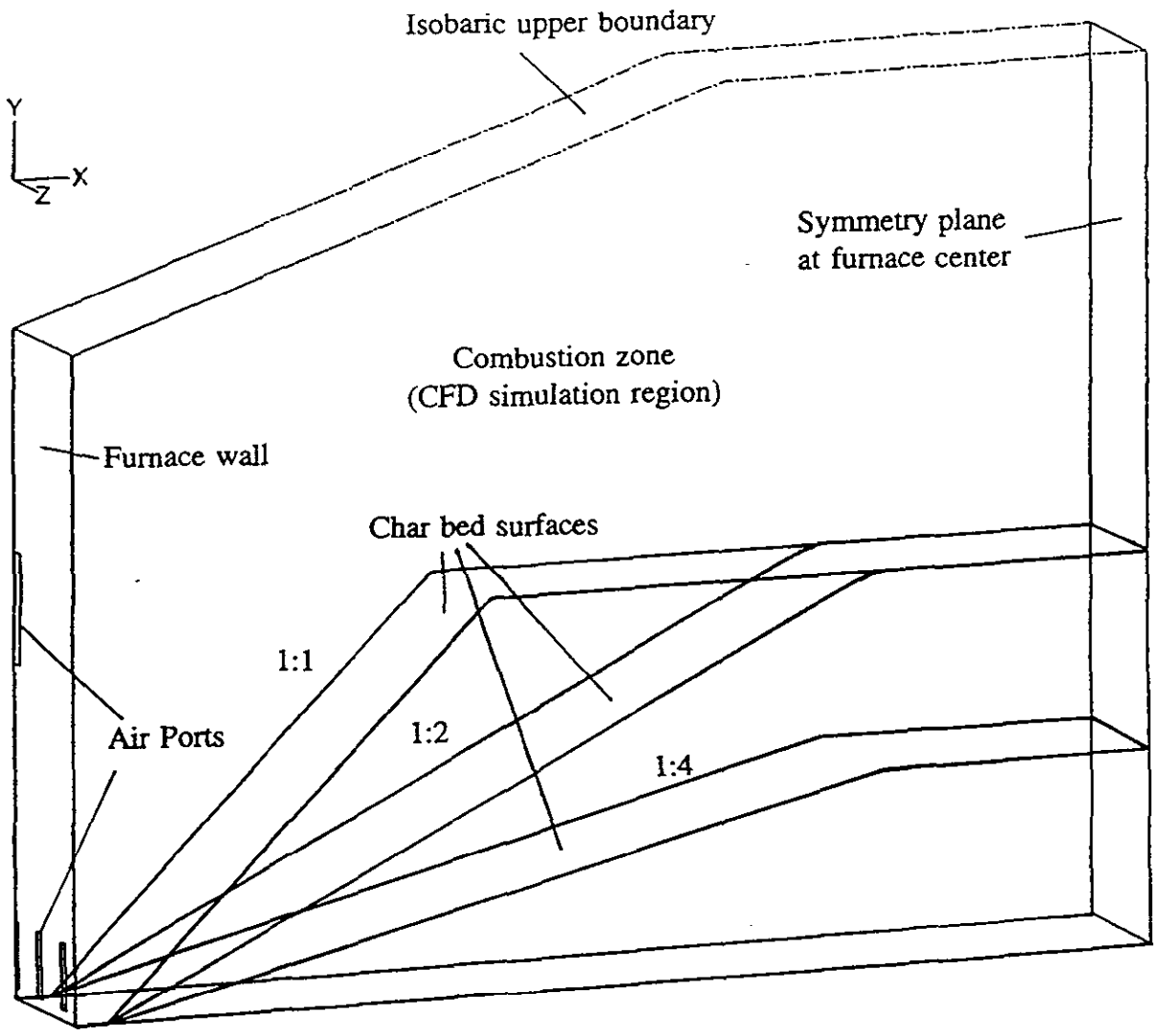

Figure 1. Geometries of slab char bed models with 1:1, 1:2, and 1:4 slopes.

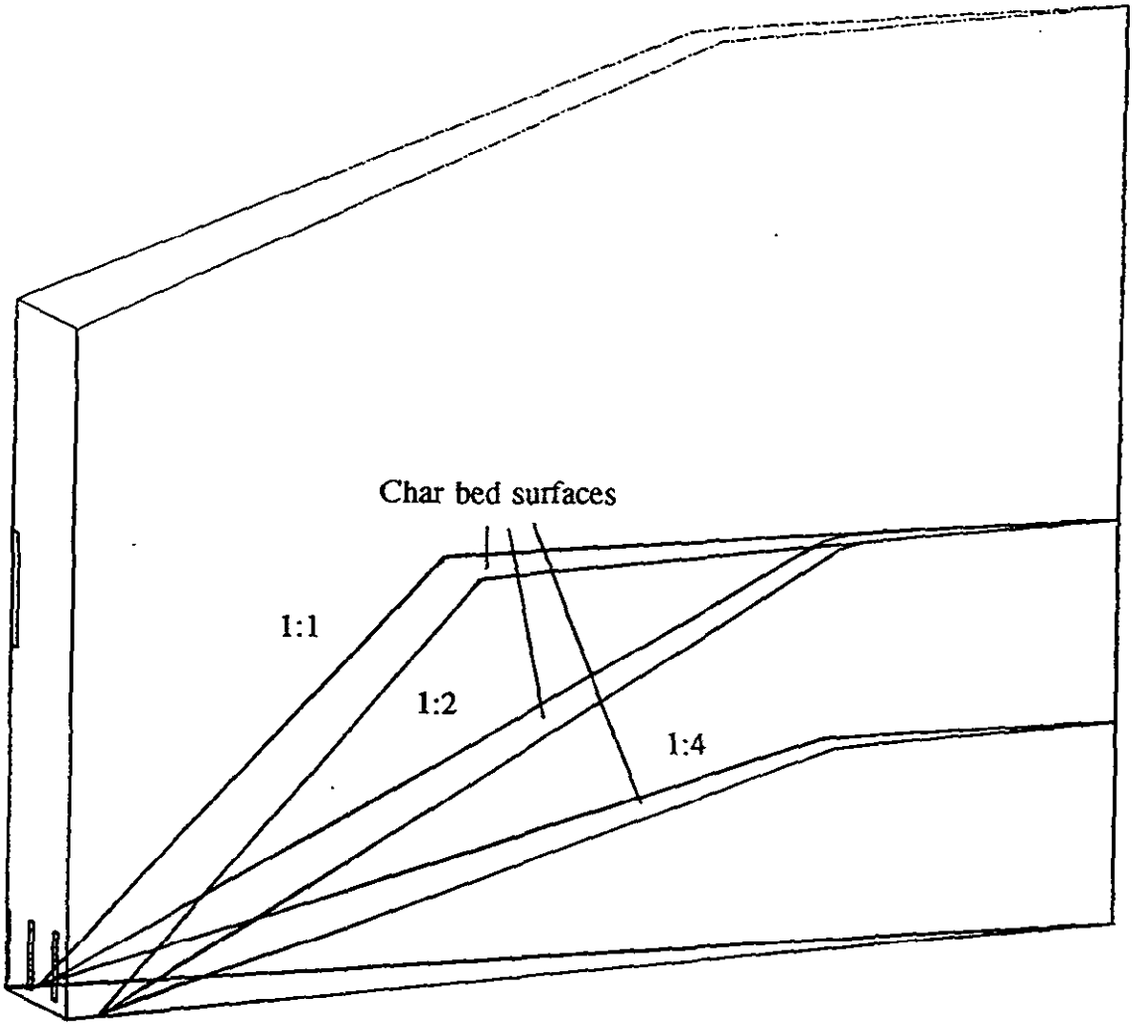

Figure 2. Geometries of wedge char bed models with 1:1, 1:2, and 1:4 slopes.

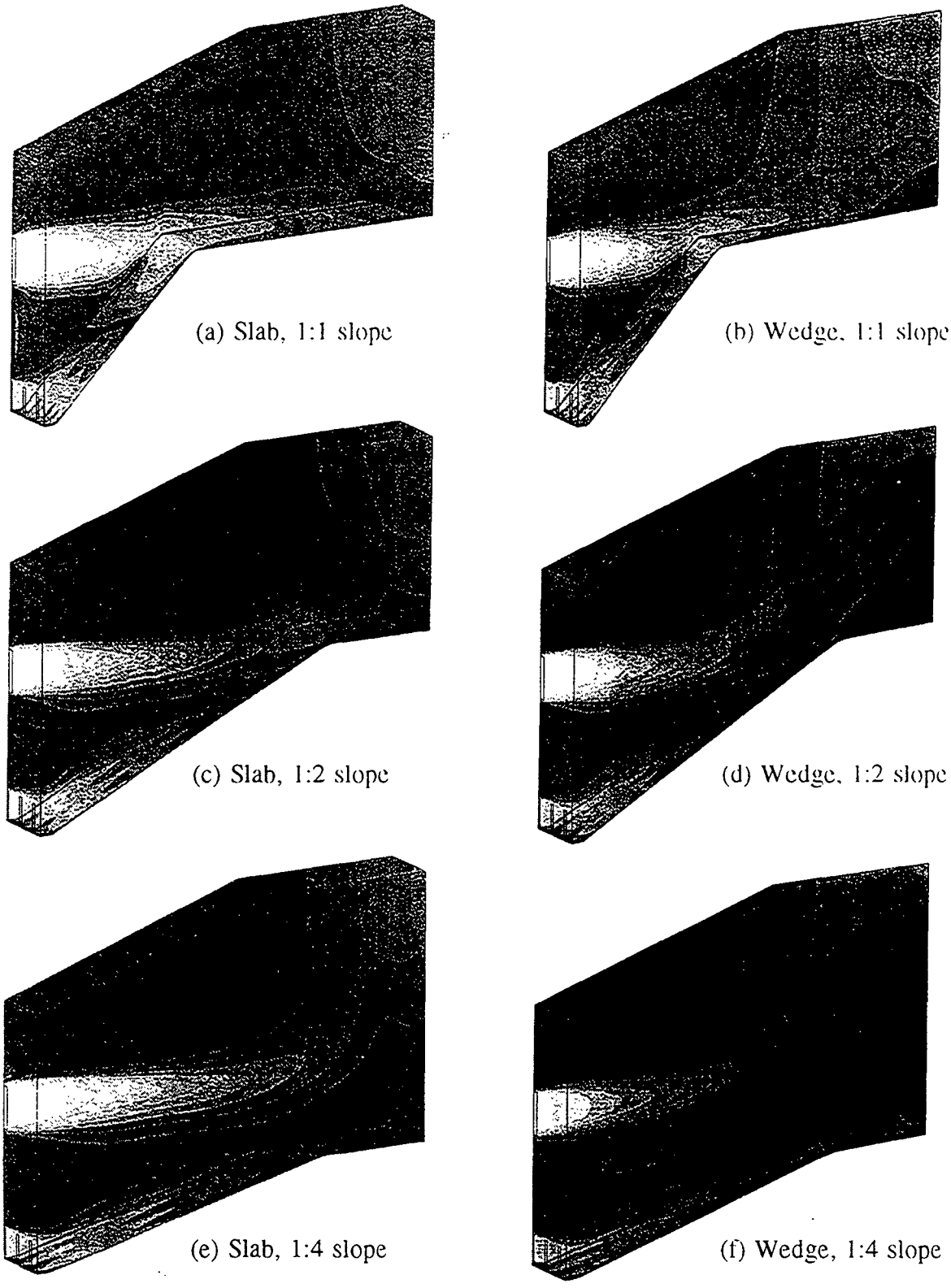

Figure 3. Flow patterns on boundary surfaces in different models.
Gray scale = 0 - 80 m/s (dark - bright).

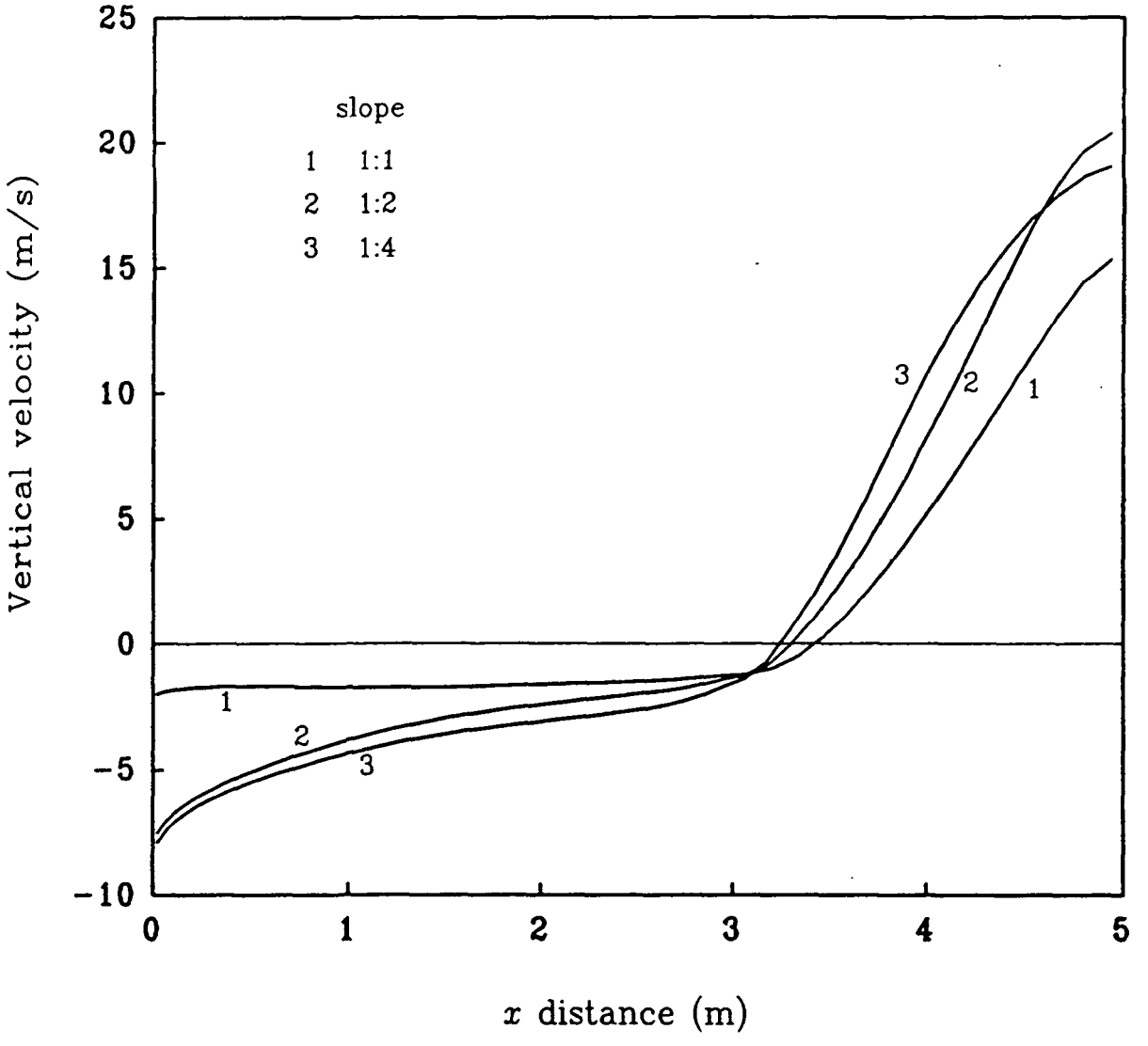

Figure 4. Average vertical velocity distributions at the upper boundaries in the slab models.

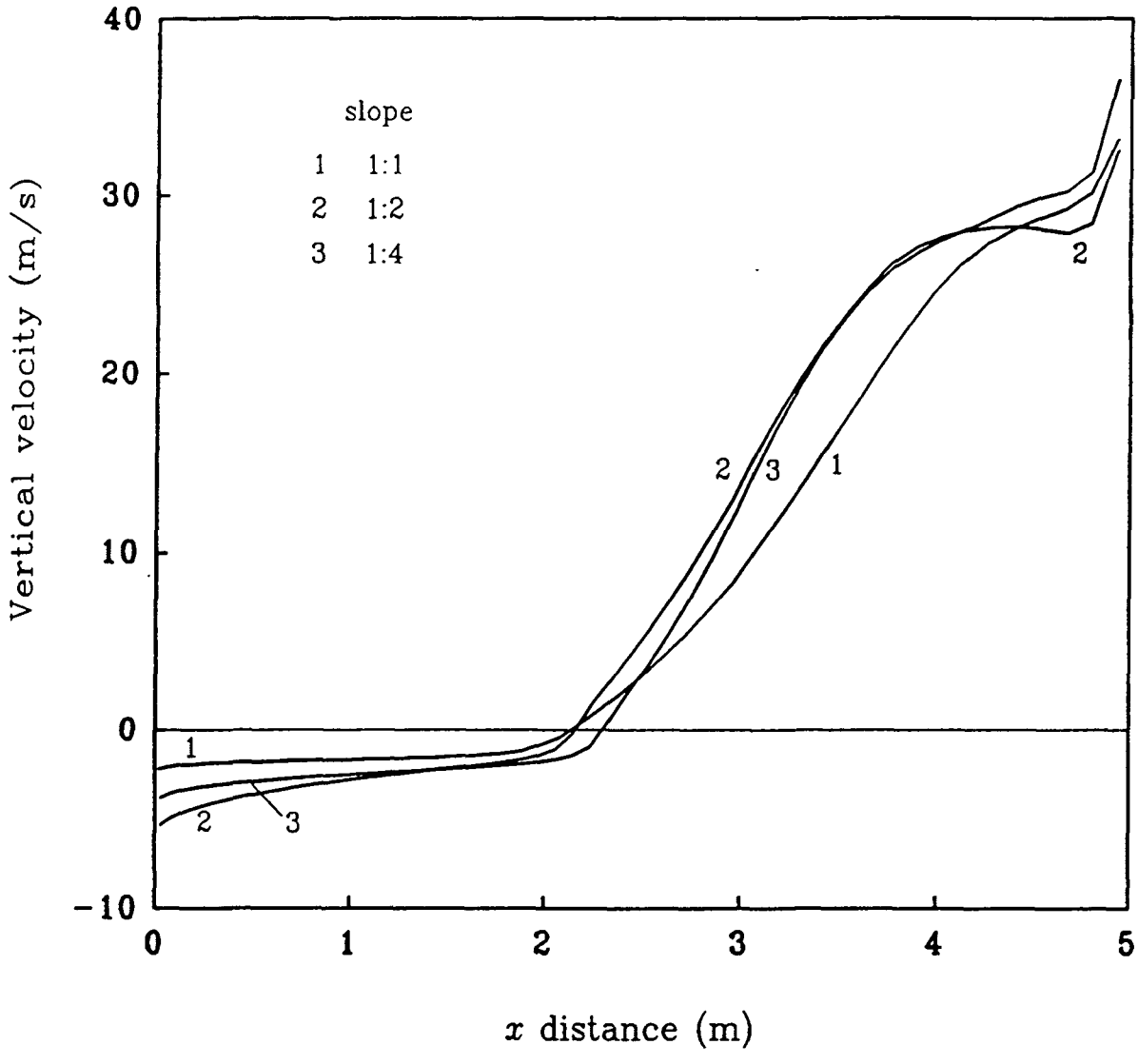

Figure 5. Average vertical velocity distributions at the upper boundaries in the wedge models.

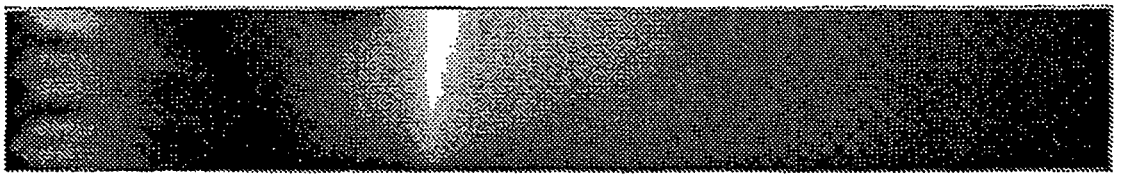

(a) Slab, 1:1 slope

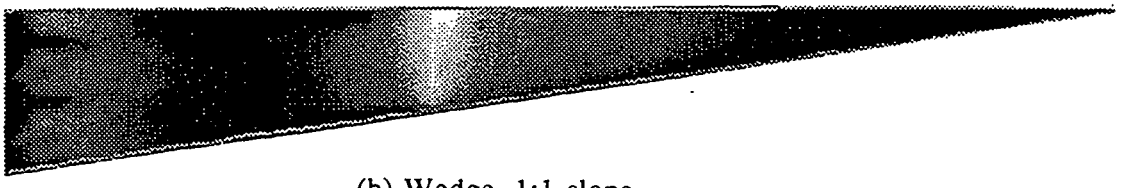

(b) Wedge, 1:1 slope

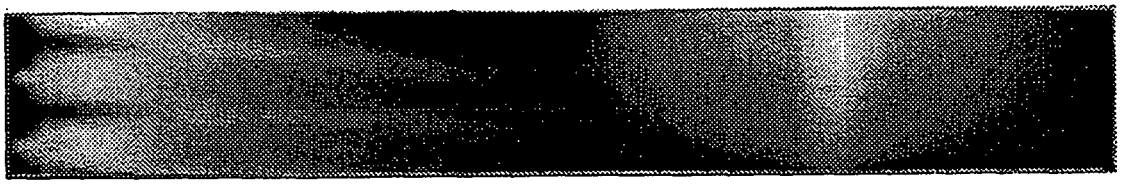

(c) Slab, 1:2 slope

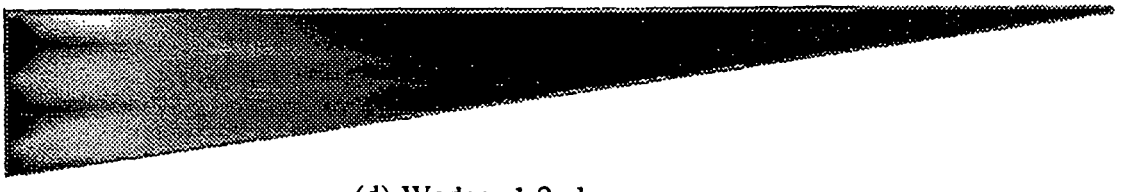

(d) Wedge, 1:2 slope

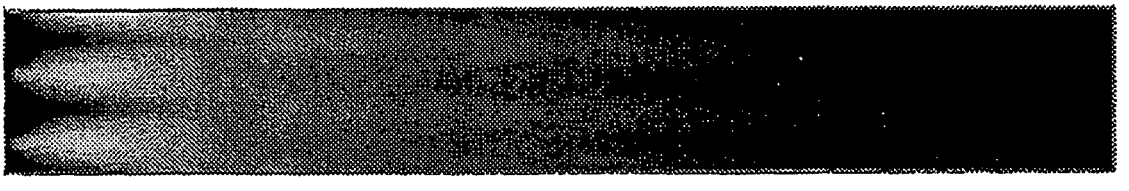

(e) Slab, 1:4 slope

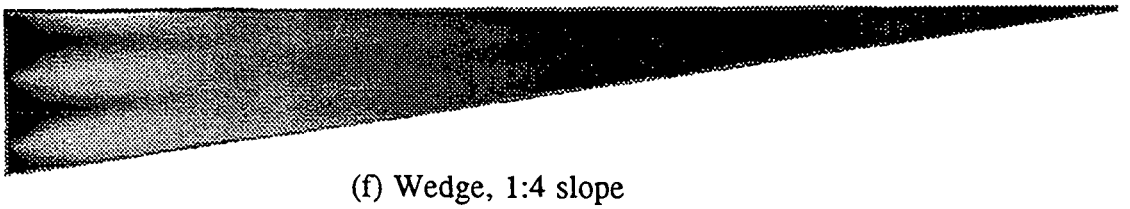

(f) Wedge, 1:4 slope

Figure 6. Plan views of shear stress distribution patterns on the char bed surfaces. Gray scale = 0 - 4.04 Pa (dark - bright) for (a) and (b). Gray scale = 0 - 1.45 Pa for (c), (d), (e), and (f).

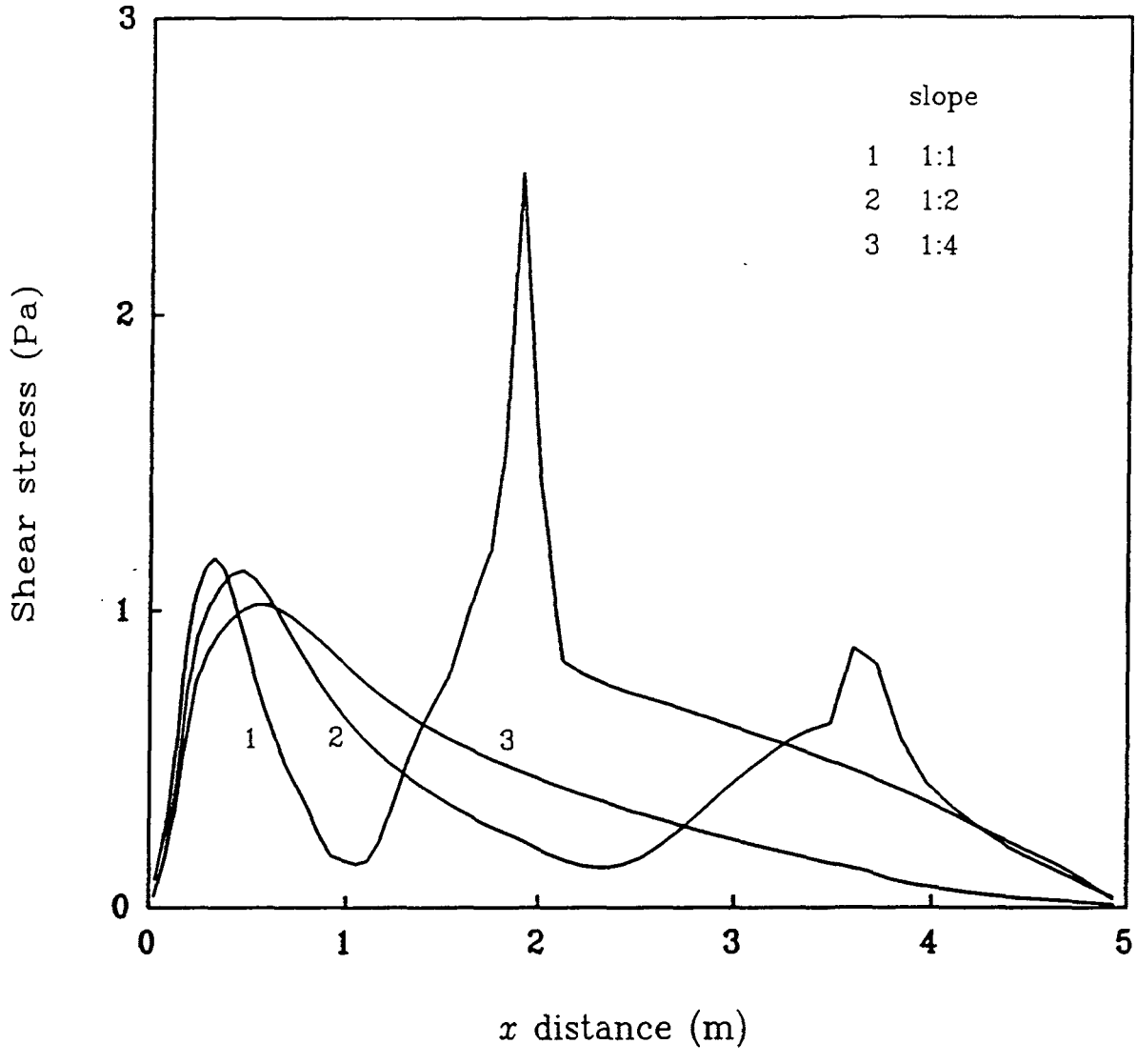

Figure 7. Average shear stress distributions on the char bed surface in the slab models.

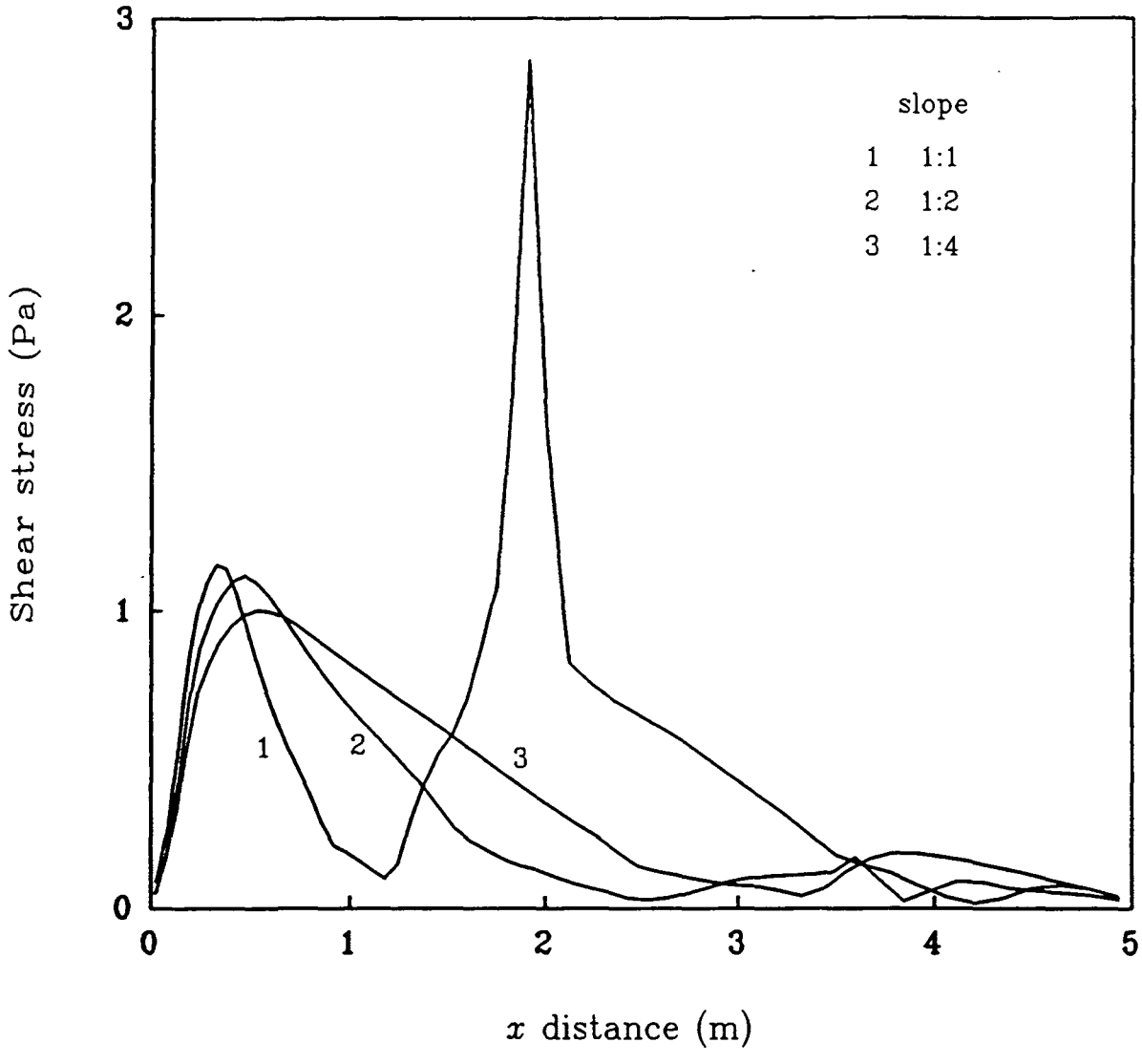

Figure 8. Average shear stress distributions on the char bed surface in the wedge models.

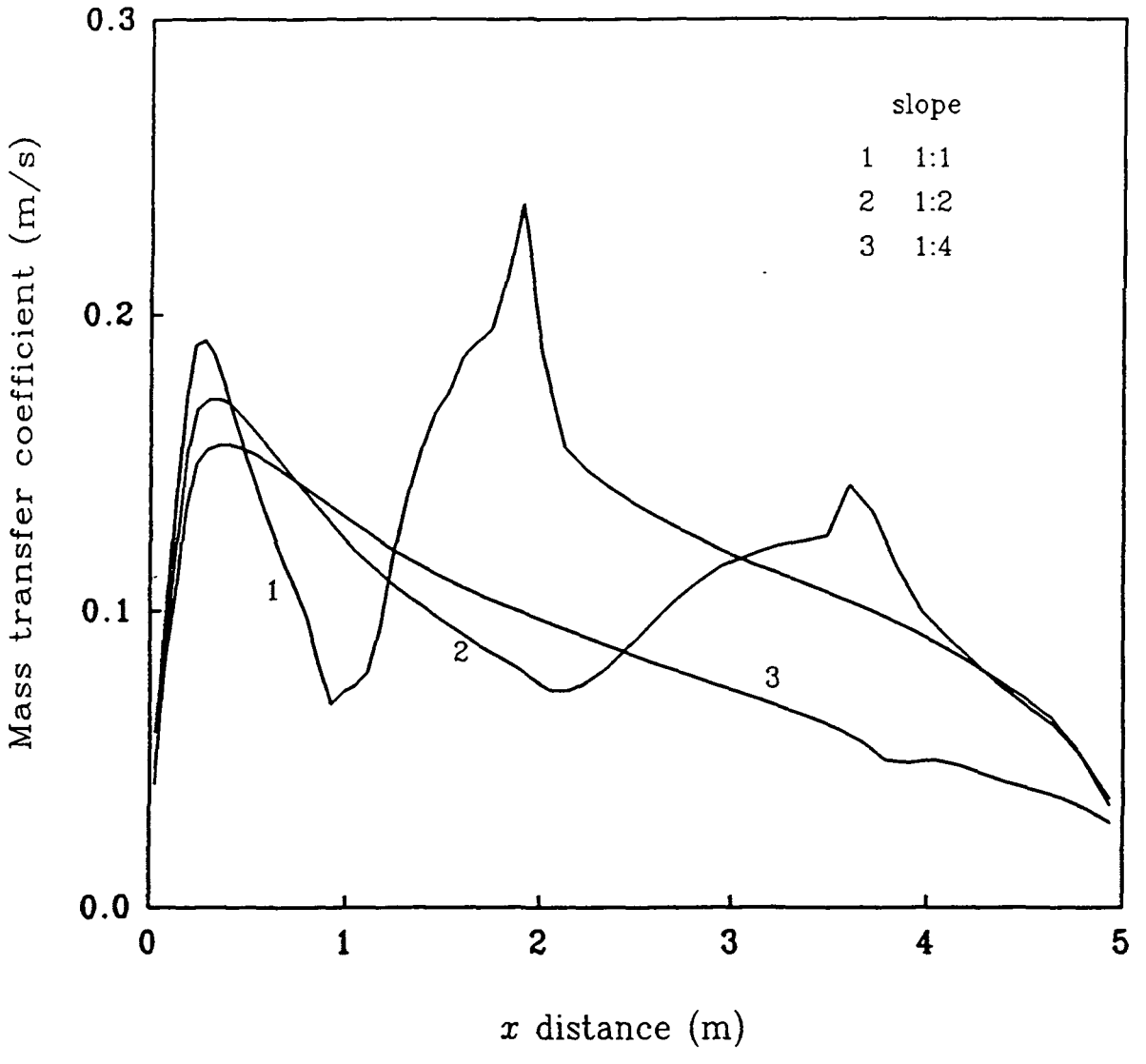

Figure 9. Average mass transfer coefficient distributions on the char bed surface in the slab models.

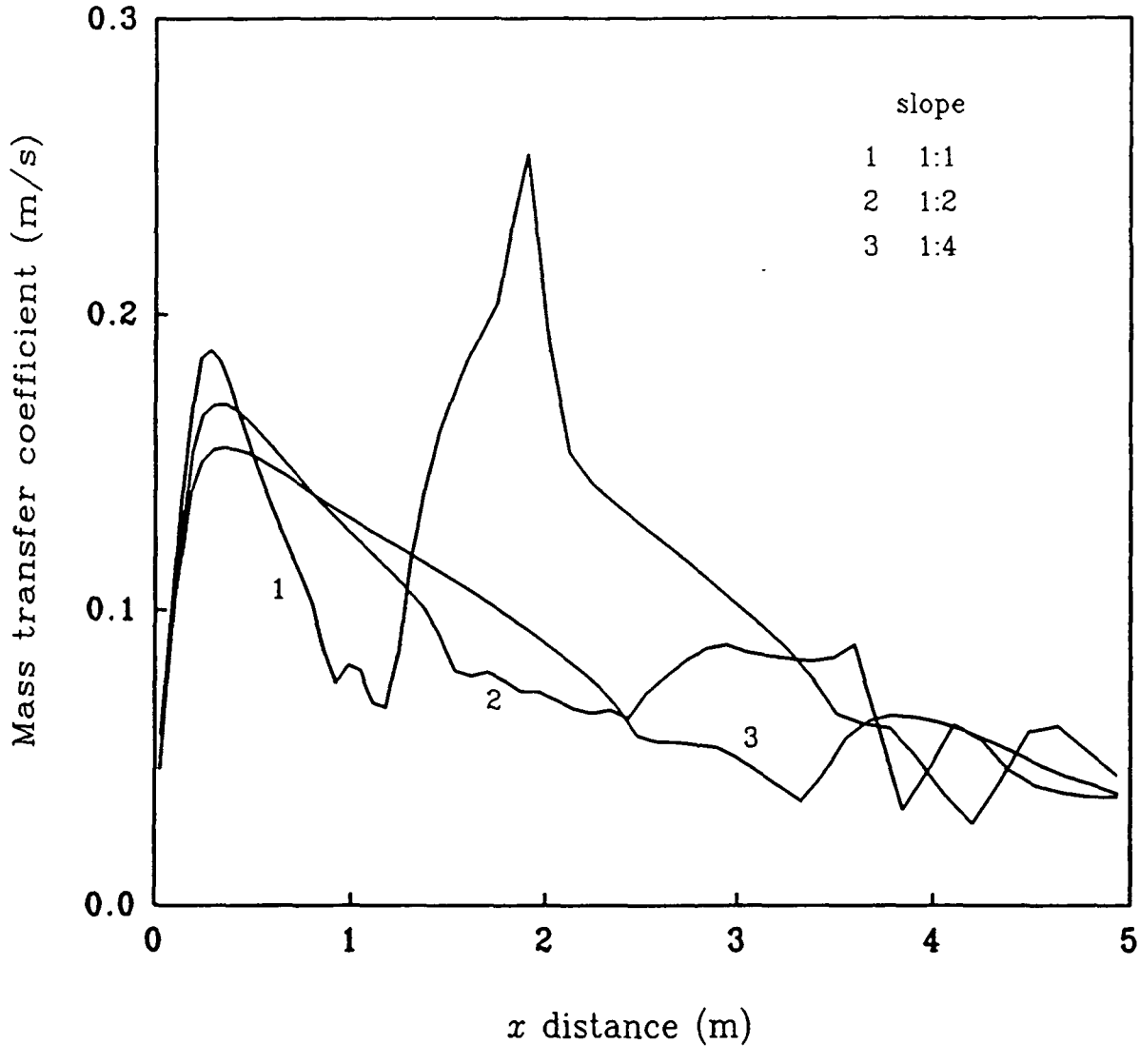

Figure 10. Average mass transfer coefficient distributions on the char bed surface in the wedge models.

CFD PREDICTIONS OF THE FLOW PATTERN AND CHAR BED MASS TRANSFER COEFFICIENTS IN A RECOVERY BOILER LOWER FURNACE

Wenrui Yang, Robert R. Horton, and Terry N. Adams

Institute of Paper Science and Technology
500 10th Street, N.W.
Atlanta, GA 30318

December 1993

ABSTRACT

A CFD study was conducted for the lower region of a recovery boiler furnace in order to study the flow patterns of air jets and their effects on the transport processes on a char bed surface. For a symmetric four-wall air system, interaction between air jets near a corner of the furnace results in a diagonal air stream that directs air flow toward the furnace center to form an upward central flow region. Air jets near the middle of a wall do not interact with perpendicular air jets directly, but they contribute to and are affected by the flow in the furnace center. For the moderately sized char bed shape examined in this study, distributions of shear stress and mass transfer coefficient indicate that char bed combustion is predominantly controlled by the primary air jets. The secondary air jets dominate the flow pattern of the main gas phase but make little direct contribution to the char bed combustion because they turn upward before reaching the char bed surface.

INTRODUCTION

Kraft black liquor recovery boilers have two main functions: combustion of the organic portion of black liquor to generate steam, and recovery of inorganic pulping chemicals. Black liquor is sprayed into the combustion zone of the boiler where it is mixed with air and undergoes four major combustion stages: evaporation, devolatilization, char burning, and inorganic reaction (1). Small particles may complete the combustion process while still in flight, whereas larger particles usually fall to the furnace floor to form a char bed and continue the combustion process there. An important inorganic reaction, sulfur reduction, takes place during black liquor combustion, and the char bed plays an important role in achieving high reduction efficiency (2).

Most of the air for char bed combustion is introduced through primary air ports located near the bottom of the boiler walls. Arrangements of the air jets can have a large influence on char bed shape since the air flow pattern determines the rate of oxygen transfer to the surface, which is often the rate-limiting step in char combustion. In turn, the shape of the char bed can affect the overall air flow pattern in the furnace by deflecting air jets that impinge on the char bed. Interaction between air jets and the char bed is a complicated process. Small-scale physical models and full-scale furnace observations are not likely to yield useful data in this area because the transport processes on the char bed surface are hard to measure or observe (3). Computational fluid dynamics (CFD) offers an attractive alternative for studying the air-jet/char-bed interaction (4-6), as well as flow and combustion in the gas phase (7-15) in recovery boilers.

A comprehensive study of a char bed requires sophisticated models to describe combustion of black liquor particles in flight, transport processes on the char bed surface, chemical reactions in the bed, and development of the shape of the char bed, in addition to a CFD solver. Before these models are developed, isothermal simulations of char bed phenomena can be conducted to increase our understanding of the complicated processes, facilitate the modeling work, and possibly provide suggestions for improving boiler operation

and design.

In a previous study of char beds, slices of the lower furnace region have been simulated using symmetry boundary conditions (6). The slice models were useful in obtaining detailed flow patterns of isolated air jets, but they could not provide an overall picture of air jet interactions, especially interactions between perpendicular jets near the corners of a furnace. In this study, a simulation is carried out in a larger region involving one quarter of the lower furnace. Symmetry conditions are still used at the central planes of the furnace. Flow patterns of interacting air jets as well as interaction between air jets and char bed are investigated. The results offer an opportunity to verify the use of the slice models in studies of air-jet/char-bed interaction.

DESCRIPTION OF LOWER FURNACE MODEL

This paper reports on an isothermal CFD simulation that is carried out for the lower region of a recovery furnace. An isobaric boundary at the liquor gun level separates the computational region from the upper furnace. The furnace is assumed to be symmetric about two orthonormal, vertical planes; thus, only one quarter of the lower furnace region is described in the model. Figure 1 shows the geometry of the model. The horizontal cross section of the model is 5×5 m^2. The char bed has a smooth surface that is described by a curvilinear body-fitted-coordinate (BFC) grid (16). The air ports have been properly enlarged to compensate for the isothermal condition simulated here so that the volumetric flow rate in the furnace is comparable with combusting conditions. The primary air velocity is 50 m/s, and the secondary air velocity is 80 m/s. The distribution of air flow between the primary and secondary is 48% for the primary air ports and 52% for the secondary air ports. In a full-furnace simulation, additional air would typically be introduced at the tertiary level.

The CFD code used in this work is FLUENT version 4.11 (17) installed on an IBM RISC/600-550 computer. The computational region is represented by a BFC grid of nearly 150,000 cells (68×68×32). The number of cells is not enough to provide a completely grid-

independent solution, especially for the primary air jets; however, the grid is sufficient for predicting major flow features properly. The κ-ε turbulence model is used in the simulation.

RESULTS AND DISCUSSION

Velocity Distribution

Flow patterns near the char bed surface and on two symmetry planes are shown in Figure 2. Due to the symmetric air port arrangement, the velocity distribution is symmetric about the vertical diagonal plane of the furnace. The primary air jets impinge on and flow along the char bed surface. Air jets near the corner of the walls penetrate shorter distances than those away from the corner due to interaction with air jets on the adjacent wall. The secondary air jets penetrate farther into the furnace. As they approach the furnace center, the secondary jets turn upward due to the action of a high pressure region above the center of the char bed, resulting in an upward high velocity flow in the center, and a low velocity recirculation region directly above the center of the char bed.

The primary air jets make a small contribution to the main gas phase flow pattern, but they dominate the flow near the char bed surface. The secondary jets dominate the flow pattern of the main gas phase with small contributions to the flow near the char bed surface.

Figure 3 shows a plan view of velocity vectors at the primary air port level. Perpendicular air jets near the corner of the furnace interact with each other, forming an air stream along the diagonal region. Air jets away from the diagonal region are less affected by the air jets from the adjacent wall. The situation is similar for the secondary air jets, as shown in Figure 4. The vectors in Figures 3 and 4 are not on flat horizontal planes, but rather on curved surfaces that follow the BFC grid lines.

In a previous study, slab and wedge-shaped models were used to study a slice of the char bed region (6). A slab model was believed to represent a symmetric two-wall air

system, while a wedge model could represent a symmetric four-wall air system because the effect of air flow rate was included. Careful comparison between the results of the wedge model and the present model indicates that a secondary air jet in the middle of a four-wall air system is similar to that predicted by the wedge model, except that the jet in the wedge model turns upward slightly sooner. It appears that the jets at the symmetry planes in the present model correspond to a situation somewhere between those predicted by the slab and the wedge models. An important difference between the present quarter furnace model and the slice models is that the quarter furnace model can predict direct interaction between air jets from adjacent walls, but the slice models cannot. Therefore, the quarter furnace model is more realistic than the slice models.

Interaction between Air Jets and Char Bed

Air jets provide oxygen for char bed combustion. Flow patterns of the air jets determine the rate of oxygen transfer to the char bed. At the same time, air jets may entrain and redistribute char particles. Shear stress and mass transfer coefficients are major factors affecting these processes.

Figure 6 presents a plan view of the shear stress distribution on the char bed surface. The primary air jets produce a zone of large shear stress along the base of the char bed. This is expected since the primary jets are designed to remove char quickly in this area by combustion and particle entrainment. In comparison, the secondary jets make little contribution to the shear stress distribution, mainly because the secondary jets are far from the char bed and the jets turn upward before impinging on the char bed. Consequently, the top of the char bed is covered by a relatively stagnant atmosphere. Combustion may be slow in this region allowing the char bed to grow above the secondary level in some cases.

Figure 7 shows a plan view of mass transfer coefficient distribution, which is calculated from values of local shear stress and velocity using the following relationship derived from the Chilton-Colburn analogy (19):

$$k = \frac{\tau_w}{\rho u_p} Sc^{-2/3} \qquad (1)$$

where k is the mass transfer coefficient; τ_w is the shear stress; Sc is the Schmidt number of the gas (≈0.7); and ρ is the gas density. The pattern of the mass transfer coefficient profile shows that the primary air jets would play an important role in combustion.

The above predictions of shear stress and mass transfer coefficient are only qualitative because the effects of temperature and chemical reactions are not considered. Surface roughness also needs to be carefully specified in more realistic simulations since the calculations of the transport processes are very sensitive to the surface roughness.

CONCLUSIONS

The air flow pattern in the lower furnace region and the transport processes on the char bed surface have been studied using a CFD char bed model. For a symmetric four-wall air system, interaction between perpendicular air jets results in a diagonal air flow toward the furnace center, forming a high velocity central core. Air jets near the middle of a wall do not interact with perpendicular air jets directly; however, they contribute to and are affected by the central core.

Primary air jets play a major role in char bed combustion. By impinging on the char bed surface, primary air jets provide both fresh air and rapid mass transfer to the char bed. In this study, the secondary air has a smaller impact on the char bed, partly because the central core prevents the jets from impinging on the bed surface.

ACKNOWLEDGMENT

This work was supported by the U.S. DOE under contract No. DE-FG02-90CE40936, and IPST member company funding.

REFERENCES

1. Empie, H. J. et al., "Black Liquor Combustion - Validated Recovery Boiler Modeling Capability," U.S. DOE Report No.1, Part 1, DOE/CE40936, 1991.

2. Adams, T. N. and Frederick, W. J., *Kraft Recovery Boiler Physical and Chemical Processes*, American Paper Institute, New York, 1988.

3. Blackwell, B., "Validity of Physical Flow Modeling of Kraft Recovery Boilers," *Tappi J.* **75**(9), 122 (1992).

4. Sumnicht, D. W., "A Computer Model of a Kraft Char Bed," Ph.D. Thesis, IPC, April, 1989.

5. Sutinen, J. E. and Karvinen, R., "Numerical Modeling of Char Bed Phenomena," *Proc. Int'l Chem. Recovery Conf.*, p. 79, 1992.

6. Yang, W., Horton, R. R., and Adams, T. N., "Effects of Boundary Geometries on CFD Simulations of Recovery Furnace Char Beds," *Tappi J.* in press.

7. Jones, A. K. and Grace T. M., "A Comparison of Computational and Experimental Methods for Determining the Gas Flow Patterns in the Kraft Recovery Boiler," *Proc. TAPPI Eng. Conf.*, p. 3, 1988.

8. Chapman, P. J. and Jones, A. K., "Recovery Boiler Secondary Air System Development Using Experimental and Computational Fluid Dynamics," *Proc. TAPPI Eng. Conf.*, p. 193, 1990.

9. Chapman, P. J. and Jones, A. K., "Recovery Furnace Combustion Modeling Using Computational Fluid Dynamics," *Proc. Int'l Chem. Recovery Conf.*, p. 71, 1992.

10. Vakkilainen, E. K., Adams, T. N., and Horton, R. R., "The Effect of Recovery Furnace Bullnose Designs on Upper Furnace Flow and Temperature Profiles," *Proc. Int'l Chem. Recovery Conf.*, p. 101, 1992.

11. Salcudean, M., Nowak, P., and Abdullah, Z., "Mathematical Modeling of Recovery Furnaces," *Proc. Int'l Chem. Recovery Conf.*, p. 197, 1992.

12. Abdullah, Z., Nowak, P., Salcudean, M., and Gartshore, I. S., "Investigation of Interlaced and Opposed Jet Arrangements for Recovery Furnaces," *Proc. TAPPI Eng. Conf.*, p. 103, 1992.

13. Siiskonen, P., Karvinen, R., Hyoty, P., Migaj, V. K., and Morgoun, A. V., "Combined Physical and Numerical Study of a Multilevel Air System," *Proc. Int'l Chem. Recovery Conf.*, p. 57, 1992.

14. Adams, T. N. and Horton, R. R., "The Effects of Black Liquor Spray on Gas Phase Flows in a Recovery Boiler," *Proc. TAPPI Eng. Conf.*, p. 81, 1992.

15. Karvinen, R., Hyoty, P., and Siiskonen, P., "The Effect of Dry Solids Contents on Recovery Boiler Furnace Behavior," *Tappi J.* **74**(12), 171(1991).

16. PreBFC User's Guide, Ver. 4.0, Fluent Inc., December 1991.

17. FLUENT User's Guide, Ver. 4.0, Fluent Inc., December 1991.

18. Llinares, V. Jr. and Chapman, P. J., "Combustion Engineering Update Stationary Firing, Three Level Air System Retrofit Experience," *Proc. TAPPI Eng. Conf.*, p. 629, 1989.

19. Incropera, F. P. and De Witt, D. P., *Fundamentals of Heat and Mass Transfer*, 3rd ed., John Willey & Sons, New York, 1990.

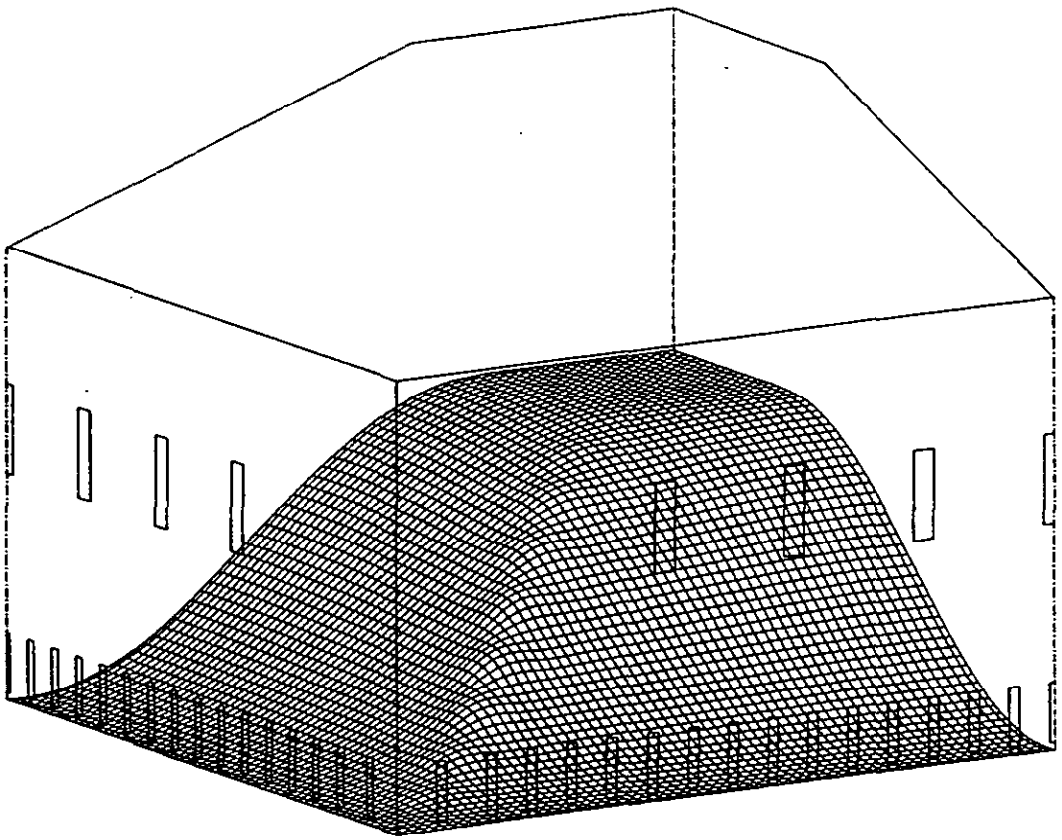

Figure 1. Geometry of the CFD char bed model.

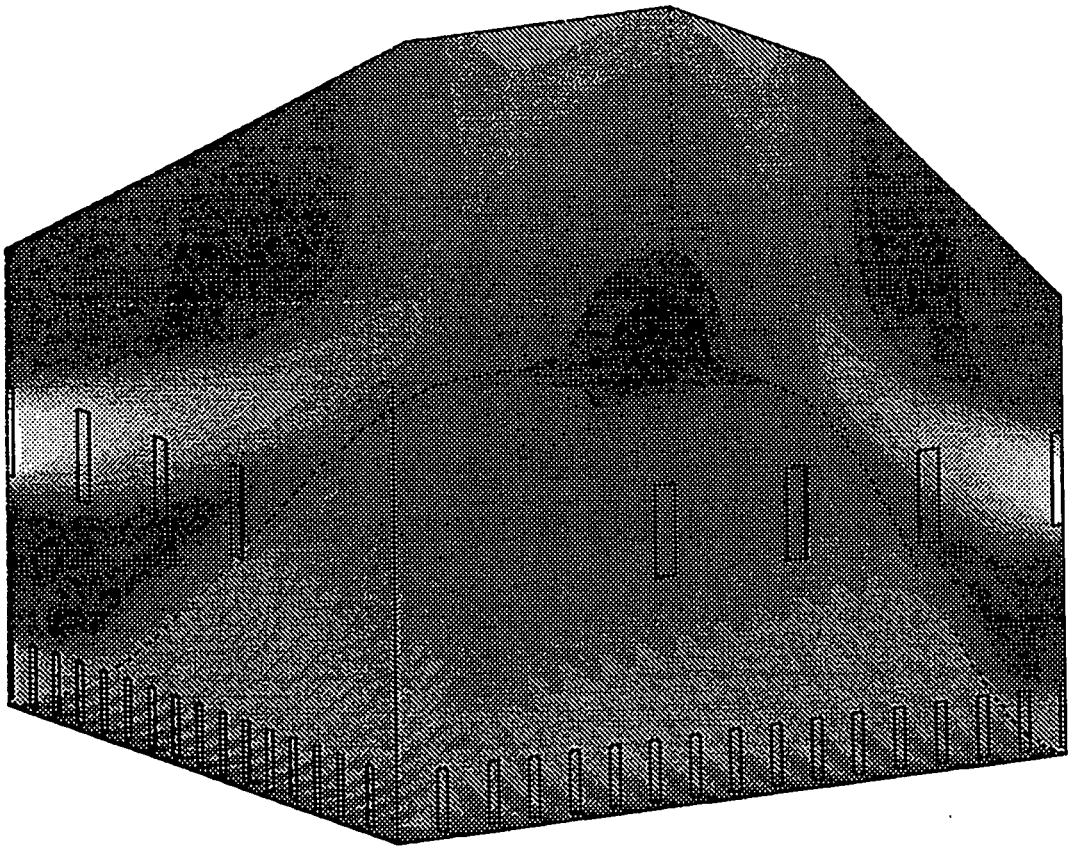

Figure 2. Velocity distributions on the symmetry planes and near the char bed surface.
Gray scale = 0 - 80 m/s (dark - bright).

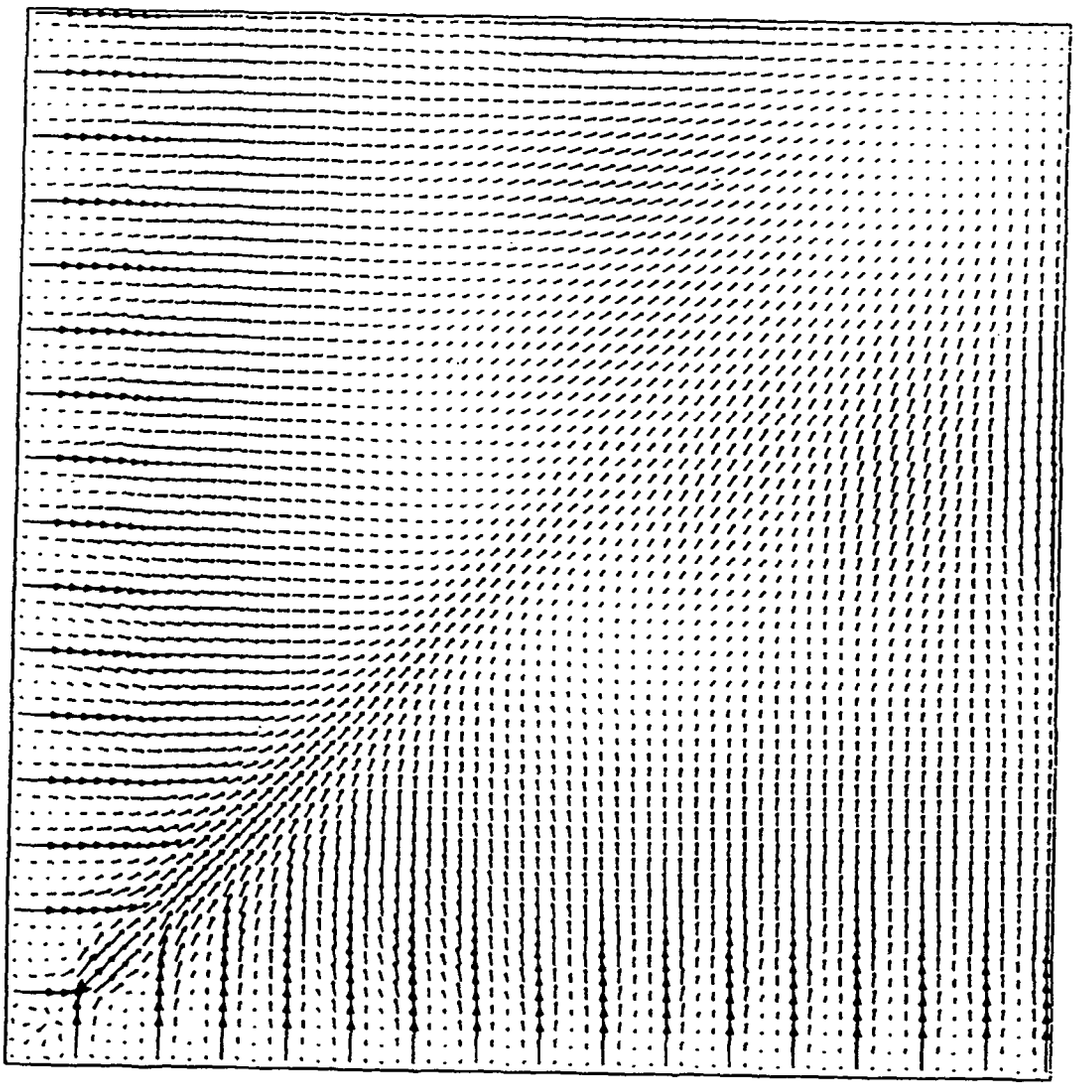

Figure 3. Velocity vectors at the primary air level.

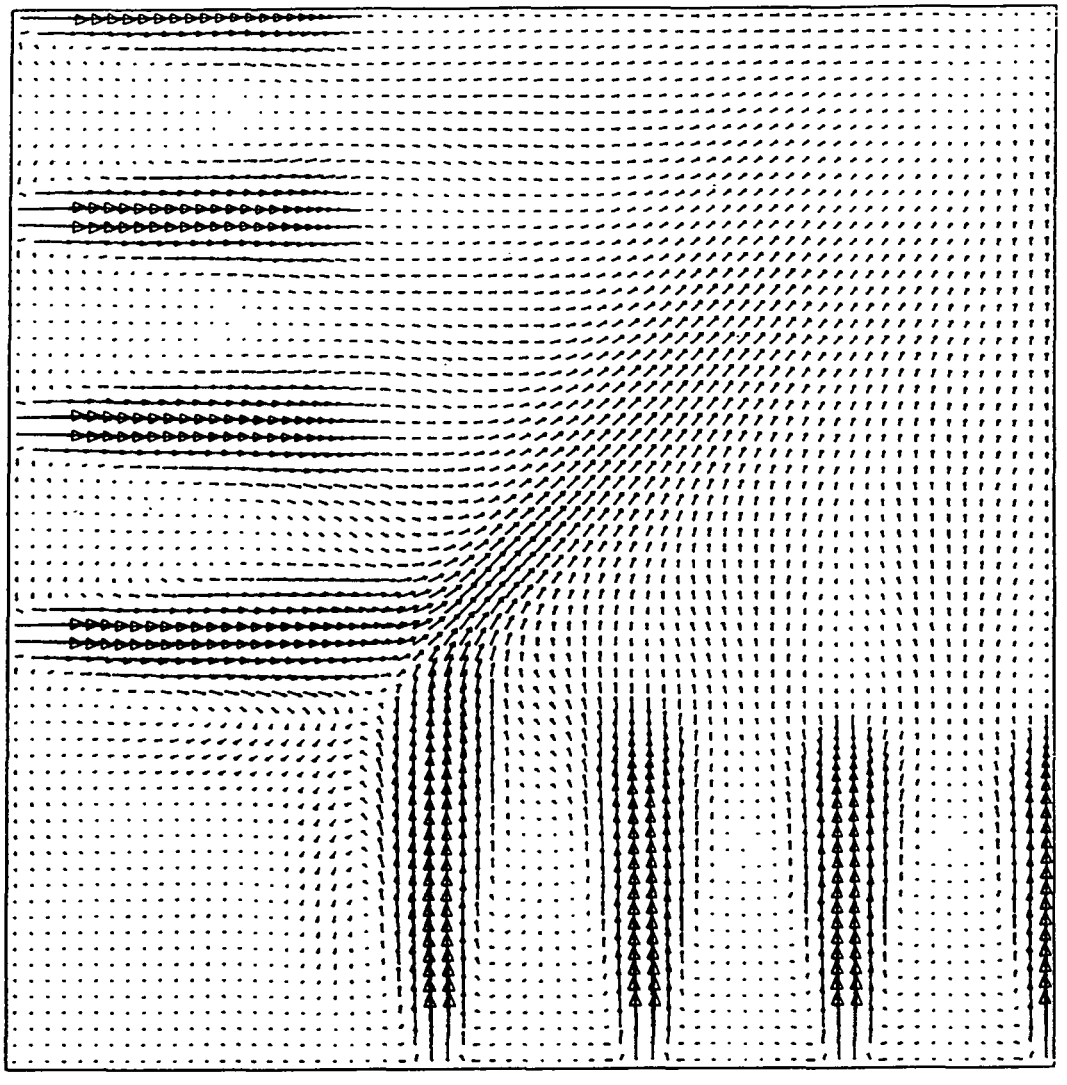

Figure 4. Velocity vectors at the secondary air level.

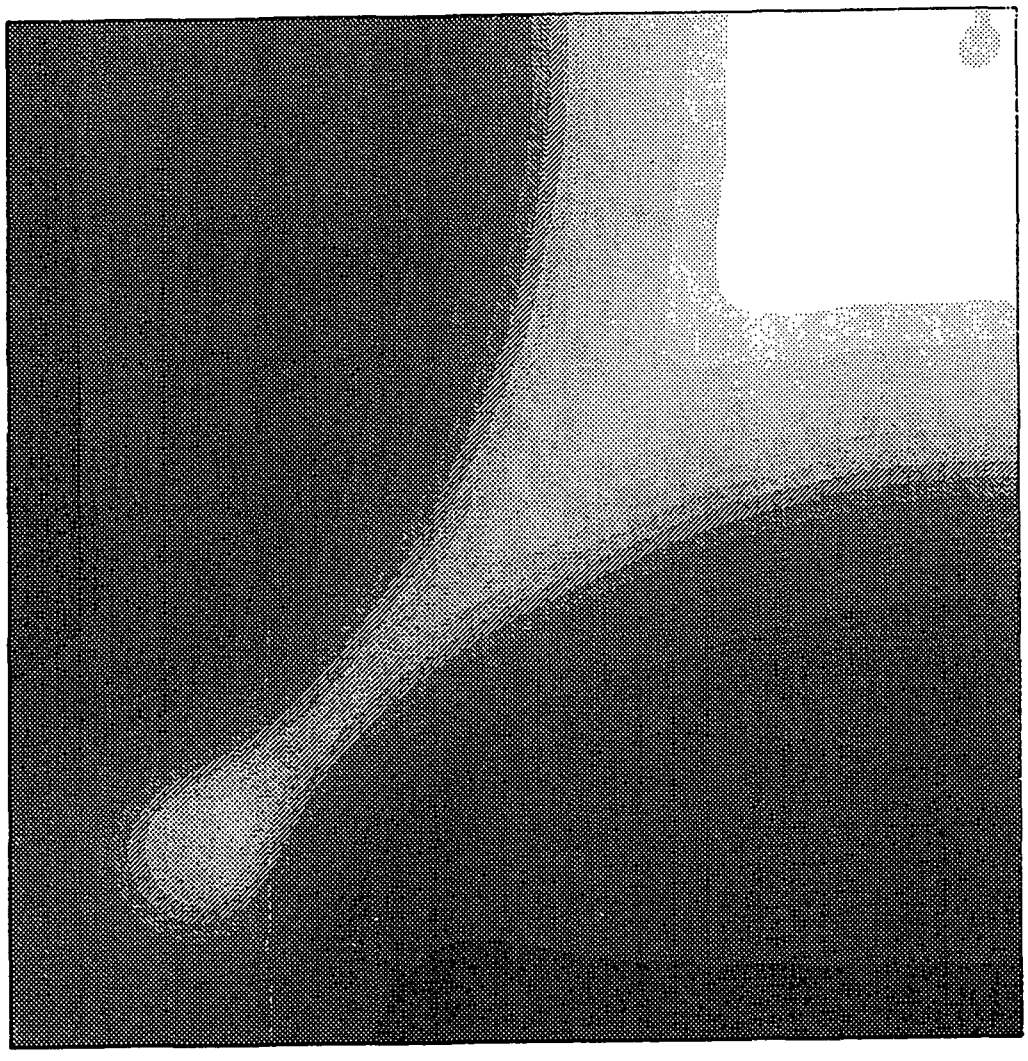

Figure 5. Vertical velocity distribution at the upper boundary. Gray scale = -15 - 30 m/s (dark - bright).

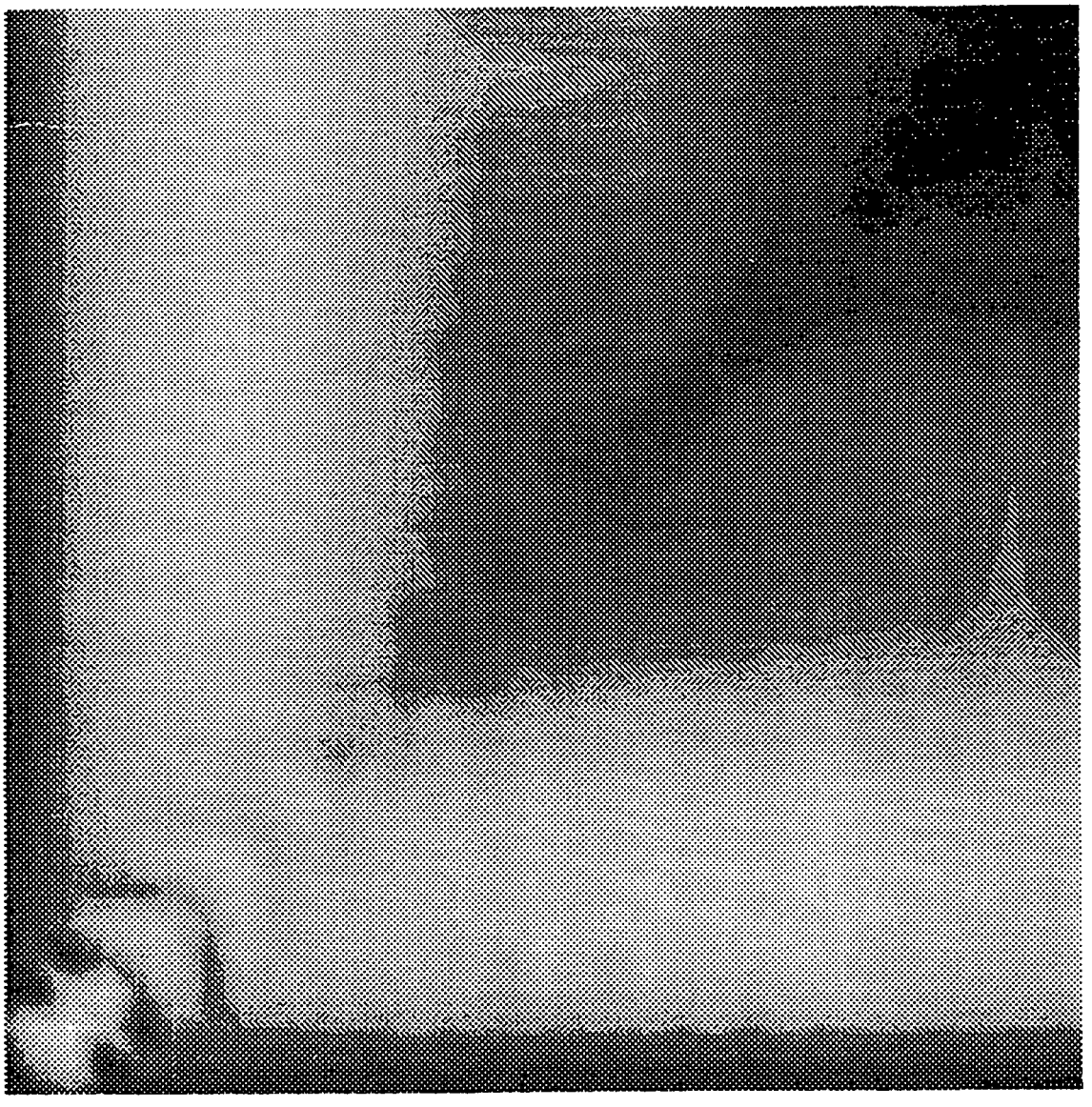

Figure 6. Shear stress distribution on the char bed surface.
Gray scale = 0 - 1.19 Pa (dark - bright).

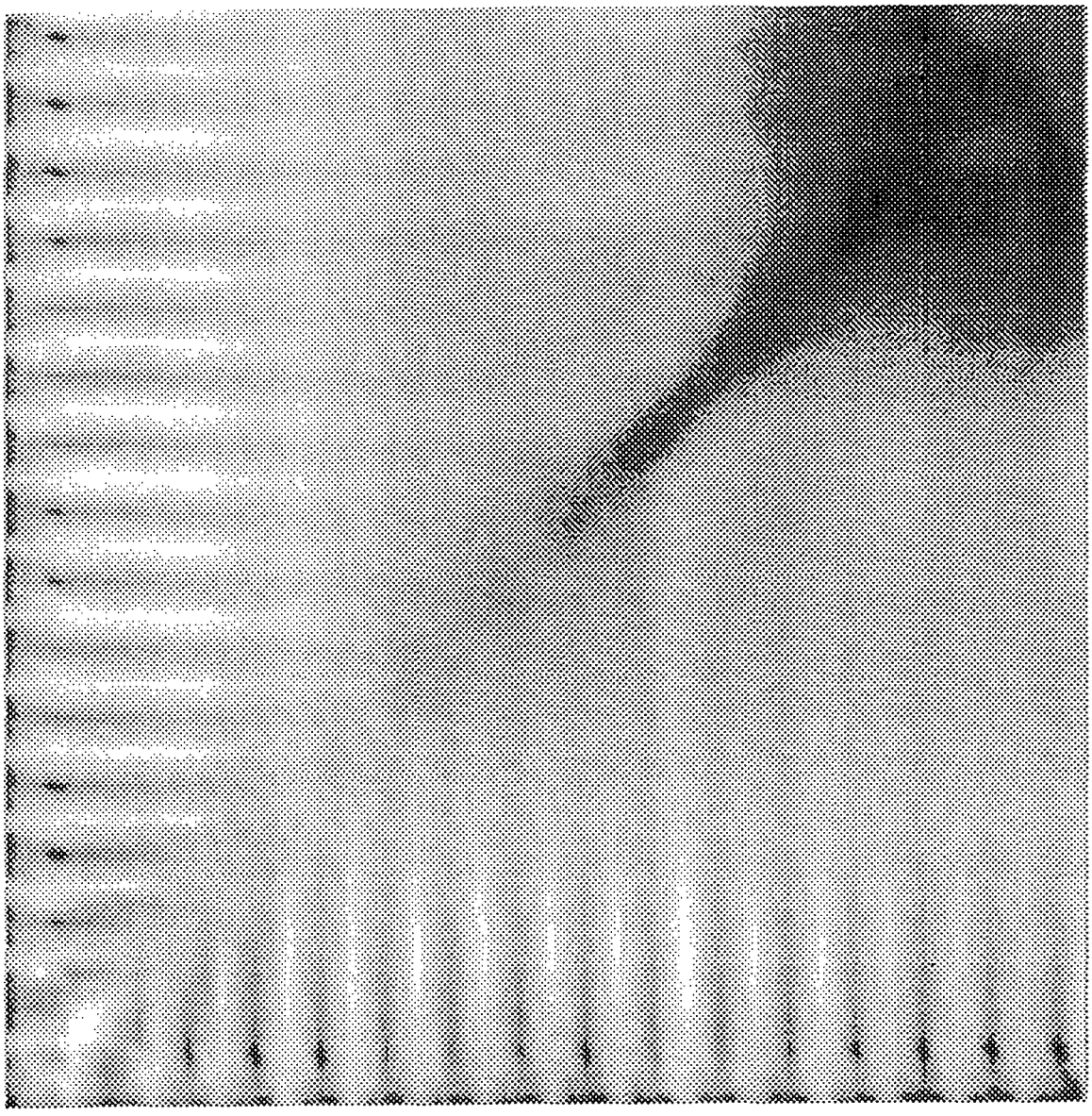

Figure 7. Distribution of mass transfer coefficient on the char bed surface. Gray scale = 0.01 - 0.16 m/s (dark - bright).

A Comparison of Fluent and Fidap

Computational Fluid Dynamics Software

by Steve Lien

Introduction

In mill operation the recovery boiler is often viewed as a black box, with little understanding of what is occurring within the boiler. Instrumentation is limited and the only control available is the flow of the feed streams into the boiler. To improve the operation of the recovery boiler a better understanding of the processes inside the boiler is needed. One approach is the development of an accurate mathematical model of the recovery boiler. The Institute of Paper Science and Technology has an ongoing project to develop a model of a Kraft recovery boiler. As a part of that project , Fidap software was investigated as a possible method for modelling the char bed section of the recovery boiler.

The creation of a mathematical model of a recovery boiler depends on the prediction of the gas flow patterns in the boiler. Although other correlations are required to give a realistic representation of black liquor combustion and other recovery boiler processes, the fluid flow model is the foundation of the entire model. Computational Fluid Dynamics (CFD) software can be used to predict fluid flow behavior.

What is CFD ?

In fluid mechanics the motion of fluids is studied by application of the principles of conservation of mass, momentum and energy. For any real problem, a set of differential equations can be derived from these principles. The solution of these equations then will describe the behavior of the fluid flow. A general form of these conservation equations (with constant viscosity), known as the Naviar-Stokes equations is often used as a starting point.

For most practical problems, an exact or analytical solution can not be determined. Therefore numerical methods such as CFD are used to provide an approximate solution to these problems. A number of commercial software codes are available, to perform CFD calculations of this type.

In computational fluid dynamics a continuum problem is converted to a discrete problem by dividing the flow region into cells in a grid structure. Two slightly different approaches are used to solve the discrete problem; Finite Difference Method (FDM) and Finite Element Method (FEM). In FDM the individual cells are used as a control volume and the difference between adjacent cell walls are used in place of the derivatives in the conservation equations.

$$\frac{\partial u_x}{\partial y} \approx \frac{u_x(\text{at } n+1) - u_x(\text{at } n)}{L}$$

Continuing this process over the entire problem region, results in a series of algebraic equations, which can solved.

In the Finite Element Method, a similar discrete grid is defined. Then values for each variable are approximated by using a shape function to interpolate between the node values. These functions are then substituted into the conservation equations to obtain a solvable solution.

Finite Element vs. Finite Difference

Several different commercial CFD software programs are available for use on a wide variety of computers. For most of the CFD Modelling work at IPST, the FDM program Fluent has been used (on an IBM RISC workstation). In addition the University of British Columbia, as part of a related project is currently developing a FDM code designed specifically for recovery boilers. To obtain information on the relative merits of FEM vs. FDM, Fluent was selected for preliminary testing of the Finite Element Method (FEM)

Listed below in Table 1 are the general differences between the two main types of CFD programs. Despite the different starting point for these two methods, the resulting program is very similar. In those areas where one technique does have a disadvantage, the software developers have worked around the limitation to provide similar capabilities.

For example, the finite element method has some additional capabilities for describing the geometry's with curved boundaries, while the FDM is best suited for rectangular coordinate. In initial versions of Fluent only rectangular or Cartesian coordinates could be used in defining the grid, but in more recent versions the use of body fitted coordinates (BFC) allows for an accurate description of curved surfaces.

Table 1 General Differences between FEM and FDM

Finite Element Method	Finite Difference Method
Properties within each cell are estimated by interpolation over the cell	Differential equation solved by using the difference across each cell
Unstructured grids provide more flexibility	More restrictive grid arrangement
Various cell types Triangles (3, 6 or 7 nodes) Quadrilaterals (4,8 or 9 node)	Cells required to be - Quadrilaterals (4 nodes)
Both linear and higher order interpolations can be used within each cell	Linear interpolation within each cell

The solution of a Fidap problem can be solved in a closely coupled manner where all of the conservation equations are solved simultaneously. For small problems (especially 2-D) this has the advantage of providing a rapid solution. However, for larger 3-D problems this becomes a disadvantage, since memory requirements increase exponentially with the number of nodes, requiring huge amounts of memory. An alternative segregated solver has been developed which reduces the amount of memory needed but increases the number of iterations required. The net result is that for large problems (such as recovery boiler models) both the memory requirements and the CPU time required to reach convergence are very similar for Fidap and Fluent.

Fidap vs. Fluent
In addition there are many other software differences between Fluent and Fidap, which are not the result of the differences in the numerical technique (Table 2). The current version of Fidap has a graphical/mouse interface, while Fluent has primarily a text based interface. Since CFD software is evolving rapidly many of these differences are also changing.

Table 2 Specific Differences between Fidap and Fluent

Fidap (Version 7.0)	Fluent (Version 4.1)
Several alternative solver methods are available	Only one solver method (Latest Version 4.23 has a multi-grid solver)
Graphical Interface	Text Based Interface
Grid Generation Algorithm	Body Fitted Coordinates
Moving Boundary Capabilities are built-in	Moving Boundary Capabilities can be achieved via user-defined subroutines
Turbulence model has built-in near wall description	Turbulence model requires higher grid density near the wall

Char Bed Problem
To test the capabilities of the Fidap in the application of char bed burning, a two-dimensional model of the DOE Black Liquor Combustion Reactor was designed and tested. Information on char bed combustion rates, in a realistic burning geometry, is a critical part of the recovery boiler model.

DOE BL Char Bed Reactor
During previous experimental work, a char bed furnace was added to the bottom of the existing in-flight reactor. This modified system allowed for the study char burning rates in a configuration comparable to the bed of a recovery boiler (i.e. one in which a horizontal air supply flows toward and then over a burning bed).

The char bed furnace consists of a metal retort, which contains the burning char and smelt, surrounded by a series of heating panels, which maintain the high temperature of the char bed system (Figure 1). A retaining insert in the retort reduces the area of the char bed to a 4 x 8 inch (10 x 20 cm) horizontal cross section.

A slot jet is located just above the surface of the retaining insert. The length of the slot is 8 inches (20 cm), the same as the width of the char bed. The width of the slot jet is adjustable to allow the jet velocity to be varied. A pre-heated gas jet (500 F- 260 C) travels out and over the surface of the char bed in a configuration similar to an actual recovery

boiler. A tray at the bottom of the char trough is connected to a variable speed drive, which allows the char bed to be to raised as the upper surface burns away.

All the char bed testing was performed in a batch mode. First black liquor is injected at the top of the flow reactor, falls through the in-flight section and collects in the hot char bed furnace. The black liquor particles that reach the char furnace are completely dry but only partially pyrolyzed. However all the particles spend a minimum of 15 minutes in the hot char bed furnace (1380 F or 750 C) under a nitrogen atmosphere, so that the material is completely pyrolyzed before the char burning is initiated. After a complete char bed has been built the black liquor flow is stopped and the char bed furnace is isolated from the in-flight reactor

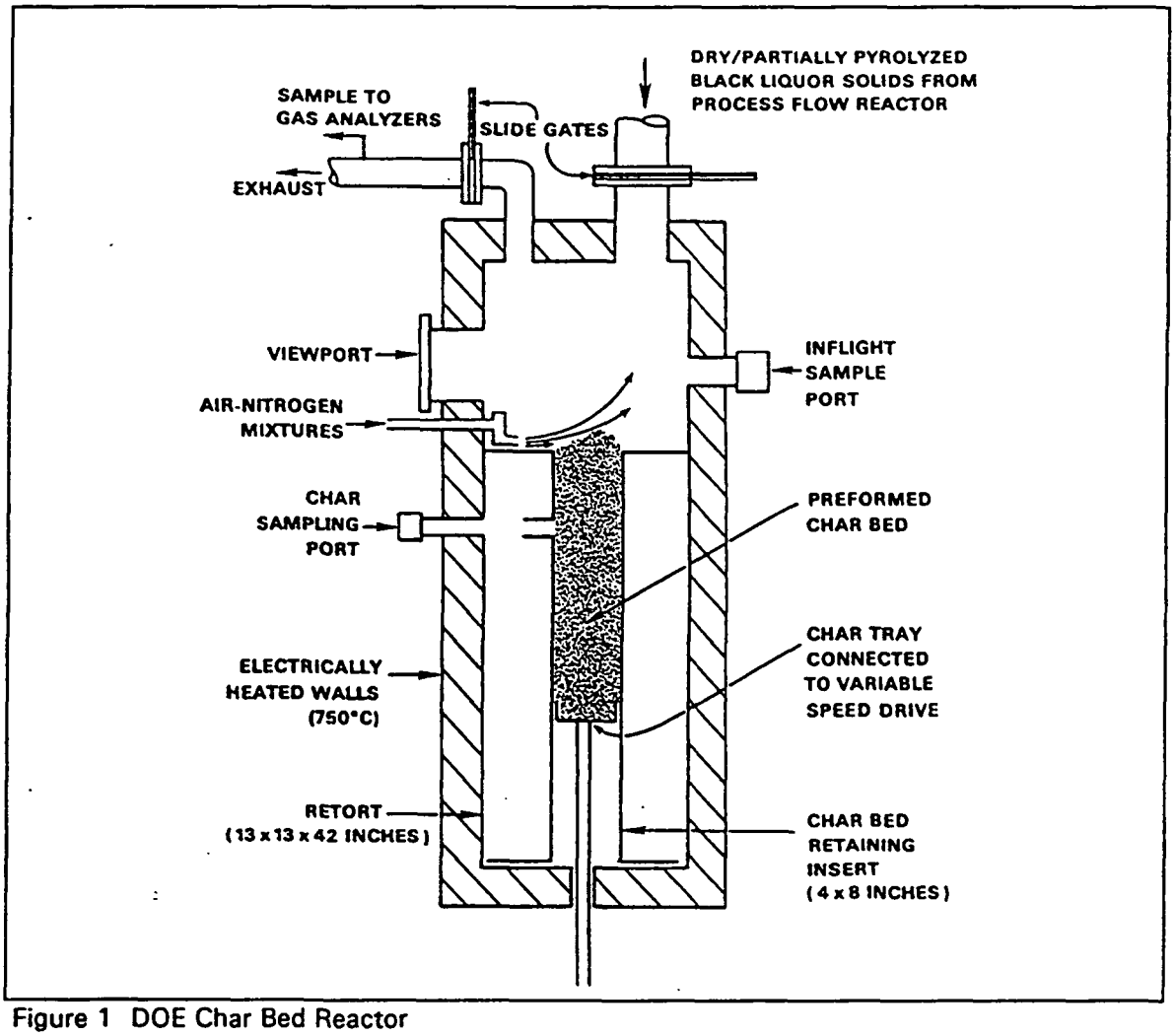

Figure 1 DOE Char Bed Reactor

The char burning is initiated by changing the gas flow from nitrogen to a mixture of air and nitrogen. As the surface of the char bed burns down, the speed of the char tray is adjusted to maintain the surface at a constant position relative to the slot jet. By measuring the outlet gas composition, the burning rate can be determined. Three thermocouples are attached to the base of the char tray , providing a temperature profile of the char bed.

Two-dimensional Model

Using the Fidap software a two-dimensional model of the char bed reactor was created. The cross section of the reactor is nearly uniform across the width of the reactor, so a 2-D model is a reasonably accurate representation of the physical situation. Only the circular outlet was modified, by using an equivalent area.

The interior region was divided into 4232 individual elements (4095 nodes) using Fidap's automated grid generation algorithm. As shown in Figure 2, more cells were used near the jet inlet (lower right corner) and near the char bed surface, since these are the regions of interest and where the highest velocities and turbulence are expected.

Using Fluent with body fitted coordinates (BFC), a similar model was developed (Figure 3). The resulting grid is more uniform but contains the roughly the same number of cells (4745 Nodes).

Both the Fluent and the Fidap models were defined to include fluid flow, temperature variation and turbulence. The boundary conditions are:

reactor wall temperature = 973 K
char bed temperature = 1273 K
inlet gas temperature = 873 K
inlet gas velocity (Ux) = - 1375 cm/sec

In addition the turbulence level at the inlet was estimated at 5% at the inlet. The turbulence model used with both software packages is based on the k-ε model, although there are differences in the way turbulence at the boundary layer is calculated. The various gas species that existed in the reactor were not included in these models (i.e. mass transfer was not a part of the models).

Results

In both Fidap and Fluent an iterative solver is used to reach the final converged result. This provides information on the gas flow patterns and the temperature profiles in the reactor.

Fluid Flow Patterns

The flow patterns and temperature profiles predicted by both of these CFD packages are very similar. A contour plot of the velocity magnitude is shown for both the Fidap case in Figure 4 and the Fluent case in Figure 5. Although there are differences in the way the data is plotted by these two programs, it is clear that the major flow patterns are virtually identical. The re-circulation pattern and the velocity profile over the char bed are very similar. The magnitude of the velocity is also nearly identical at all locations in the reactor.

The temperature profiles were also plotted and compared, and found to be in close agreement. The temperature is near 950 K over 90 % of the reactor volume. It is only in a thin boundary layer region over the char bed that gas temperatures above 1000 K are reached. Similar comparisons were also made for other calculated variables such as turbulence properties and pressure . In all cases the results were found to be in good agreement.

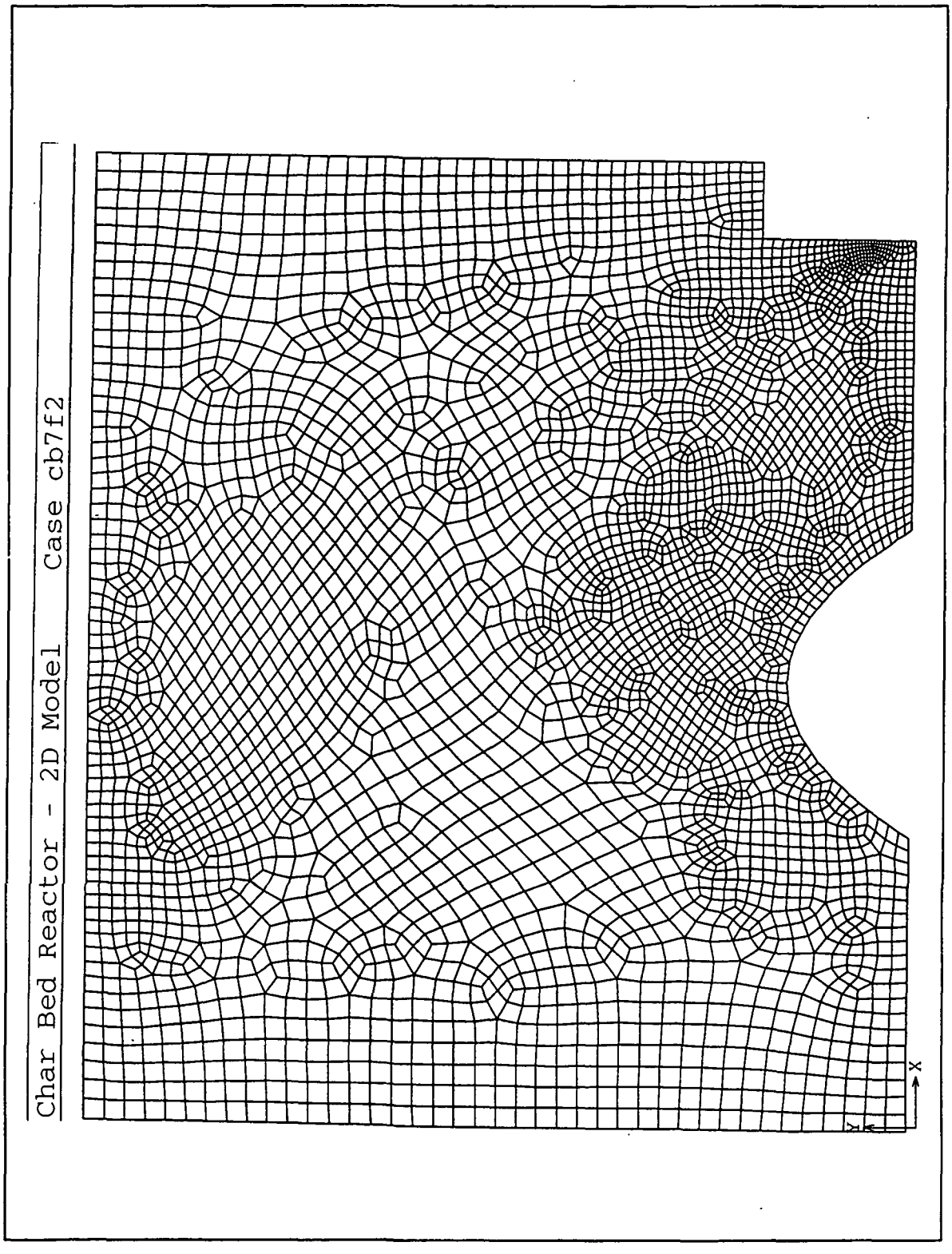

Figure 2 Grid Structure for Fidap Model of 2-D Char Bed Model.

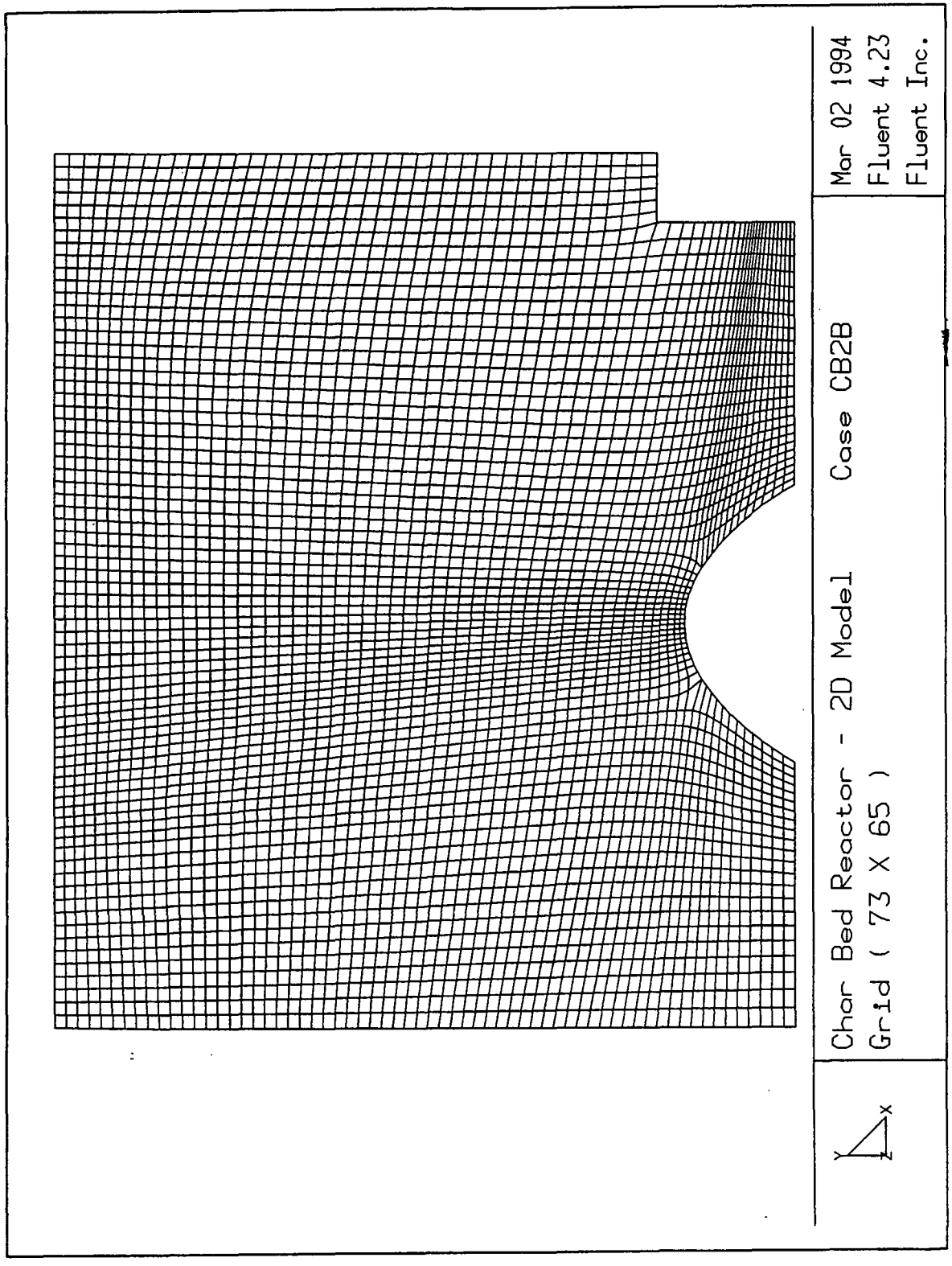

Figure 3 Grid Structure for Fluent Model of 2-D Char Bed Model.

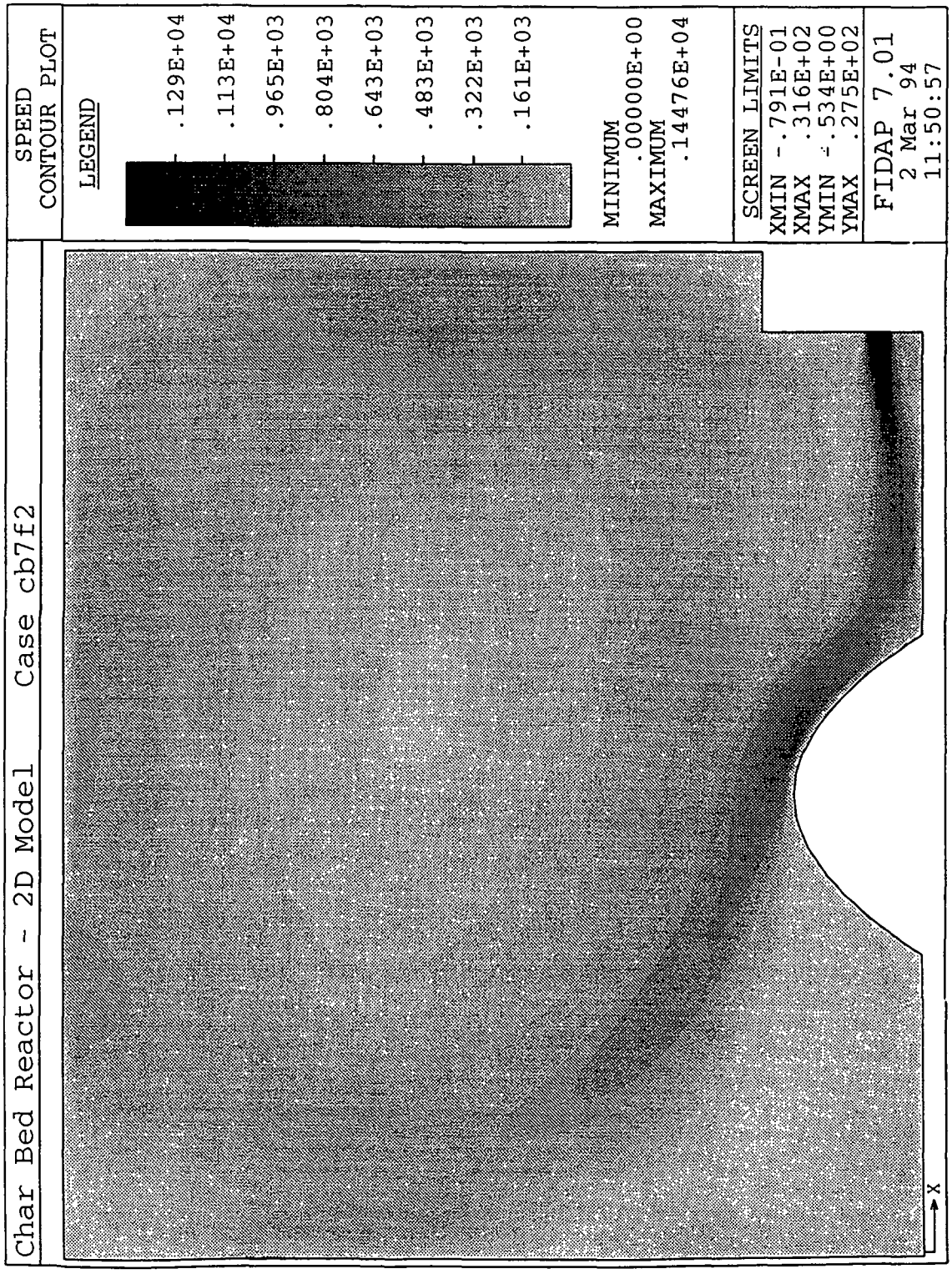

Figure 4 Gas Velocity Contours from Fidap Model (cb7f2) of 2-D Char Bed Model.

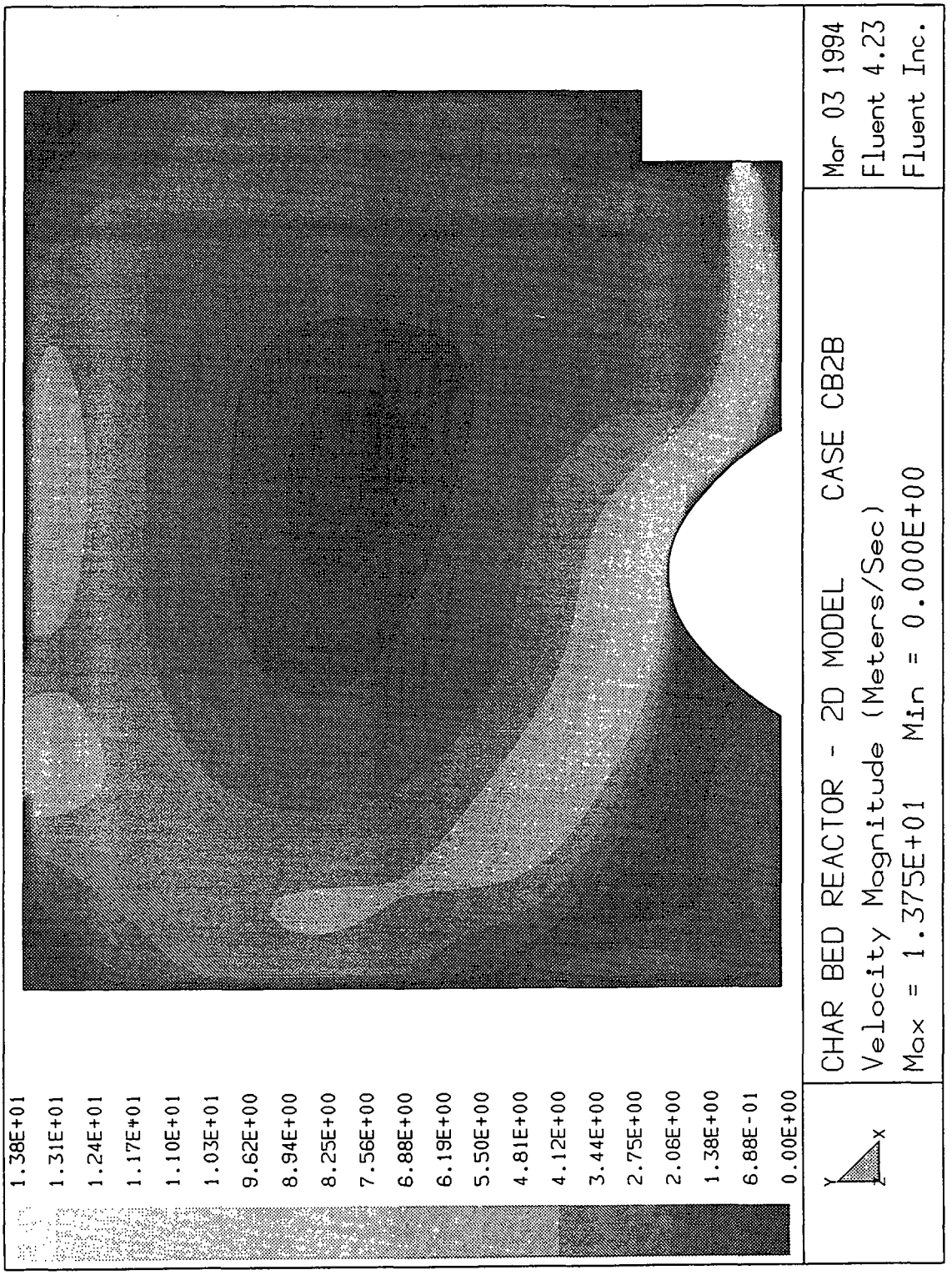

Figure 5 Gas Velocity Contours from Fluent Model (CB2B) of 2-D Char Bed Model.

Computational Results

Due to the complexity of recovery boilers, a sophisticated model is necessary to accurately describe the processes occurring in a real boiler. This also means that the model will require a large amount of computer memory and CPU time to reach a converged solution. With the current IBM RISC Workstation (model 550), a large isothermal CFD problem with 145,000 cells, requires about 50 hours to reach convergence.

Because of these computational requirements, the software used could have an important effect on the ability to solve these problems. A comparison of the computer requirements for the Fidap and Fluent char bed models are listed below in Table 3.

Table 3 Comparison of Computational Requirements

	Fluent	Fluent	Fidap	
	4.11	4.23	Seg.	Direct
CASE	CB2B	CB2B	cb7f2	cb7f1
No. of Nodes	4745	4745	4095	4095
No. DOF	6	6	6	5
Total Mem (MB)	6.24	9.50	5.80	100.07
Iterations	4729	4831	365	23
Total CPU Time (Min)	327.4	218.0	128.2	76.2
CPU-sec/Iter	4.2	4.2	21.1	198.8

Fidap has a direct solver, which can greatly reduce the computational time required, but at the cost of higher memory requirements. Although this method is useful for small problems it is not practical for large or three dimensional problems. Even for this relatively small problem it requires 100 MB, which is near the limit of the IBM RISC computer (128 MB). For large scale problems, the memory requirements increase with the number of nodes raised to the 3/2 power

When sufficient memory is available, the direct solver significantly reduces the number of iterations needed to reach convergence (from 365 to 23), but the CPU time per iteration is greater so that the net result is that the CPU time is only reduced by 40% when compared to the alternative segregated solver.

The Fidap segregated solver is similar to the Fluent solver in terms of memory and CPU requirements. The memory required for the Fidap segregated solver (5.8 MB) is less than what Fluent requires. Two versions of Fluent were tested. The older version 4.11 required 6.2 MB (very close to the Fidap segregated solver) and the new version 4.23 required 9.5 MB.

Although the new version of Fluent requires more memory it has the advantage of reduced total CPU time. Both versions required about 4800 iterations, but the new version reduces the total CPU time by 34%.

The Fidap segregated solver also requires fewer iterations (365 vs. 4831) than the Fluent version 4.23 solver to reach convergence, but each of the iterations is longer . The net result was that Fidap required only 128 minutes, compared to 218 for Fluent 4.23.

Version 4.23 of Fluent also has the capability of a multi-grid solver, which was not used on this small model. For larger models the optimized multi-griding should provide a significant improvement in performance.

Ease of Use and Other Factors

An important part of setting-up a CFD problem is the generation of an appropriate grid structure. In this area Fidap has an advantage over Fluent with a more user-friendly program. As a part of the graphical interface, Fidap uses a mouse-driven CAD type program to perform geometry/grid generation. The problem geometry is defined by selecting points which are then connected into lines, curves, and surfaces to define the physical boundaries of the problem.

The grid generation is accomplished by defining the node spacing along the edges of the geometry. Once this is done, the grid generation can be done by the software, using an automatic grid generation algorithm. This program defines an initial grid and then modifies the grid in an iterative procedure to obtain a final grid that is appropriate for CFD.

In Fluent the grid and geometry are defined by a pre-processor which is used to define the geometry and grid. The basic procedure is similar, except that the geometry is defined by entering data in a text mode. Points are used to define lines or curves, which in turn define planes or surfaces, resulting in the geometrical boundaries of the problem.

The grid generation in Fluent is performed by defining an initial Cartesian grid, which is then modified to coincide with the geometry. Although there are more restrictions on the grid shape and arrangement with Fluent, Body -fitted coordinates (BFC) do allow for curved or non-linear boundaries.

Once the grid is set-up, much more information is required to define the problem, before a solution can be found. The problem definition must include:

- equations to be solved (e.g. turbulent vs. laminar, are heat and mass transfer included)
- boundary conditions and initial conditions
- fluid properties (including viscosity, heat capacity, etc)
- solver strategy and control parameters

Problem definition is easier with Fluent and it is easier to determine if all the necessary parameters have been defined . In part this is because Fidap has more options, which provide more flexibility, but also increases the complexity of the problem setup. Fidap also includes some redundant program options to provide compatibility with older versions of their program.

Overall I found Fluent was slightly easier to use, but this is probably at least partly due to the fact that I had previous experience with Fluent. As a new user to Fidap it was difficult to adjust to their terminology.

Conclusions

Although Fluent and Fidap start from different methods for predicting fluid dynamics, the results produced for this two dimensional case are nearly identical. Both methods give similar results for velocity and temperature profiles.

There are distinct differences in the way that models are created using these programs, but neither program has a significant advantage in terms of the features we require for recovery boiler models. Fidap has a better interface for defining the geometry and grid structure, but with Fluent it is easier to set-up the material properties, initial and boundary conditions, and solver parameters. CFD software is constantly changing and improving. When one supplier provides a new feature it is quickly incorporated by the other software vendors.

For the test case, Fidap was able to reach a converged solution faster. For larger cases the multi-griding capabilities of Fluent should improve the convergence speed. The memory requirements were very close for both programs.

Fluent and Fidap have similar capabilities and there is no clear winner in this comparison. Because we have much more experience with Fluent and there is no clear reason to switch to Fidap, our model development will continue to use Fluent as the primary CFD package.

Improved In-Flight Combustion Model

Sulfate Reduction and Carbon Removal During Kraft Char Burning

Thomas M. Grace, Kaj J. Wag, Robert R. Horton, and Wm. James Frederick

ABSTRACT

This paper describes an improved model of char burning during black liquor combustion that is capable of predicting net rates of sulfate reduction to sulfide as well as carbon burnup rates. Enhancements include a proper treatment of CO_2 and H_2O gasification, reactions between oxygen and combustibles in the boundary layer, and integration of sulfate reduction and sulfide reoxidation into the char burning process. Simulations using the model show that for typical recovery boiler conditions, char burning behavior is independent of oxygen concentration up to the point of carbon depletion. Under these conditions, H_2O and CO_2 gasification reactions are primarily responsible for carbon removal. The H_2 and CO coming from the gasifying particle consume oxygen in the boundary layer and help protect against sulfide reoxidation. After carbon depletion, sulfide reoxidation occurs at a rate determined by oxygen mass transfer. The process variables having the biggest effect on char burning behaviour are initial black liquor drop diameter and temperature. There is a direct tie between char burnout times and the amount of sulfate reduction. Increasing drop size increases char burnout times and the extent of reduction. Increasing temperature gives shorter char burnout times but higher reduction. At a given temperature, any variable that shortens the char burnout time will result in proportionately less reduction. There are some indications that the model underpredicts reduction rates. There remains a need for experimental data on sulfate reduction kinetics under typical char burning conditions.

INTRODUCTION

Black liquor is a biomass fuel which is generated as a byproduct of the pulping of wood by the kraft process. It is a concentrated aqueous solution containing the spent inorganic pulping chemicals and organic substances dissolved from the wood. The inorganic (ash) content of the liquor is about half of the weight of the dissolved solids. Black liquor is burned in a recovery boiler to recover the the inorganics as a molten mixture of Na_2CO_3 and Na_2S, called smelt, and to generate steam. The Na_2S is an active pulping chemical. It is produced in the recovery furnace by the reduction of Na_2SO_4 by reaction with carbon. This process is called reduction in the kraft pulp industry.

Black liquor is sprayed into the recovery furnace as coarse drops, 1-10 mm in diameter. The drops dry and burn in suspension. The inorganic and some partially burnt organic accumulates on the furnace hearth to form a char bed. Part of the burning takes place in suspension and part on the char bed.

Black liquor burning is usually considered to take place in four stages; drying, volatiles burning, char burning, and smelt reoxidation. Char burning is a very critical step. It is a relatively slow process and takes place when the liquor particle is in a highly swollen state, typically 50-90 cm^3/g char at the onset of char burning. Thus, the rate of char burning has a large effect on the trajectories followed by the burning black liquor particles in the furnace. Slow rates of char burning can cause increased physical carryover of particles out of the furnace into the convective heat transfer sections and this can cause boiler plugging. A substantial amount of sulfate reduction also occurs during char burning.

Many of the available models of char oxidation have focused on coal chars (1,2). The model presented by Bartok and Sarofim(2) represents the current state of global modeling for char oxidation. Their model accounts for film mass transfer and intraparticle diffusion as well as the intrinsic rate of oxidation of carbon. These authors suggest that, since the rates of carbon oxidation by steam and CO_2

are much lower than that of carbon with oxygen, often only the oxidation reaction with oxygen needs to be considered in heterogeneous combustion . Char oxidation models of the type described by Bartok and Sarofim have been implemented in many reactor models for both combustors and gasifiers.

Black liquor char combustion involves two features not seen in coal chars. These are the extremely high reactivity of the chars and the importance of reducing Na_2SO_4 to Na_2S. Black liquor char carbon is several orders of magnitude more reactive than other carbons because of the catalytic effect of sodium inherent in the char(3,4). Because of this higher reactivity, the rate of carbon oxidation with oxygen is film mass transfer controlled at temperatures above 1000°C for char particles of typical size (3-20mm). One effect of this is that the rates of carbon oxidation with oxygen and water vapor, at the same O_2 and H_2O partial pressures, are similar for temperatures as low as 900°C for black liquor char particles . Since the black liquor is fired as an aqueous fuel, the concentration of H_2O in the furnace gases is high, typically 15-20%. The rate of oxidation with CO_2 is slower but definitely significant at temperatures of 1000°C and higher. Thus, all three oxidants are important in black liquor char burning.

An accurate model of char burning must deal with three process items:

1. conversion of char carbon to the gases CO and CO_2,
2. the state of reduction of the sulfur in the burning particle, and
3. the decrease in the size of the swollen char particle as the carbon is burned away.

None of the previous models of char burning have properly dealt with all of these issues. Models which have been used for black liquor drop trajectory calculations (5,6) have focused on carbon removal. Char burning was modeled as an oxygen mass transfer limited process. Chemical kinetic limitations and gasification of carbon with H_2O and CO_2 have not been handled in a rigorous manner. These models have not dealt with sulfate reduction.

The only self-consistent reduction model currently in existence is the sulfate-sulfide cycle model (7). This model assumes that all char carbon is gasified by reaction with sulfate to form sulfide. The sulfide is then reoxidized by reaction with oxygen to form sulfate. The degree of reduction of the sulfur is then determined by a balance between the competing rates of sulfate reduction and sulfide reoxidation. The sulfate-sulfide cycle model has been used to make quantitative predictions of reduction occurring during char burning in N_2 - O_2 mixtures (7). However, it was necessary to either assume very high reaction temperatures or arbitrarily increase the reaction rate constant in order to predict high amounts of reduction in typical char burning times.

This paper describes an improved model of char burning that is capable of predicting reduction changes as well as the rate of carbon removal. This model includes the following:

1. gasification of carbon by H_2O and CO_2
2. direct carbon oxidation with O_2
3. reactions between O_2 and combustibles in the boundary layer which reduce the transfer of O_2 to the particle surface
4. simultaneous sulfate reduction with carbon and sulfide reoxidation with oxygen
5. reduction computed by a sulfur balance
6. a methodology allowing parallel volatiles burning and char burning

By treating both the char gasification and sulfur oxidation/reduction reactions simultaneously, the model allows a gradual transition between char carbon removal and net sulfide reoxidation as the char carbon is depleted. Thus, this new model is applicable to both the char burning and smelt reoxidation stages and, in fact, eliminates the need to make a distinction between them.

DESCRIPTION OF CHAR BURNING MODEL

Char burning involves the reactions occurring in a smelt/char particle. Each particle is considered as a mini chemical reactor interacting with the surrounding gases. The smelt/char particle is considered to contain carbon and three inorganic compounds, Na_2CO_3, Na_2S, and Na_2SO_4. The model described herein does not include sodium vaporization reactions or sulfur release as H_2S, both of which can occur during char burning. Thus, the amount of sodium in the particle is assumed to remain constant and the total number of moles of inorganic compounds remains constant.

The chemical composition of the particle is completely specified by giving the initial values for moles of inorganic, I, and the sulfidity, S, and determining the moles of fixed carbon, C, and the reduction efficiency, E, as functions of time. Other characteristics of the burning particle, such as mass and swollen volume, can be calculated from these four quantities.

The following five reactions involving the constituents in the smelt/char are considered.

1. $C + O_2 \rightarrow CO_2$
2. $C + CO_2 \rightarrow 2\ CO$
3. $C + H_2O \rightarrow CO + H_2$
4. $C + (2\text{-}f)/4\ Na_2SO_4 \rightarrow (2\text{-}f)/4\ Na_2S + f\ CO + (1\text{-}f)\ CO_2$
5. $Na_2S + 2\ O_2 \rightarrow Na_2SO_4$

Reactions 1, 2, and 3 are heterogeneous reactions between furnace gases and char carbon. Reaction 4, the reduction reaction, is treated as a homogeneous reaction occurring in the condensed smelt/char phase. The variable stoichiometry indicated by the use of the parameter "f" is a reflection of the fact that both CO and CO_2 can be products of the sulfate-carbon reaction. Reaction 5, sulfide reoxidation, is treated as a heterogeneous reaction between gas phase oxygen and sulfide. Reactions 1 and 5 are assumed to be totally mass transfer controlled. Data supporting this assumption are contained in references (8) and (9). Reactions 2 and 3 are treated as controlled by external mass transfer,

intraparticle diffusion and chemical kinetics in series. Reaction 4 is assumed to be completely controlled by chemical kinetics.

Reduction reactions between sulfate and reducing gases such as CO or H_2 are not included in this treatment. Experimental work (10) has shown that the rates of these reactions are several orders of magnitude less than those between carbon and sulfate.

In addition to reactions occuring with smelt/char components, there are also gaseous reactions occurring in the boundary layer adjacent to the smelt/char phase. These gaseous reactions are:

6. $CO + 1/2\ O_2 \rightarrow CO_2$

7. $H_2 + 1/2\ O_2 \rightarrow H_2O$

8. $V + O_2 \rightarrow VO_2$

The CO and H_2 are produced by gasification of carbon by CO_2 and H_2O and by the sulfate-carbon reaction. "V" represents a combustible volatile produced by pyrolysis. If volatile production by pyrolysis is completed, reaction 8 can be ignored. This reaction is included to permit a gradual transition between the volatiles burning and char burning stages. Another reason for including it in this model is to allow a similar treatment of char burning chemistry in particle burning and char bed burning, since some pyrolysis is certain to be occurring in the bed.

Grace (11) showed that, when water vapor was present, the rate of oxidation of carbon in black liquor char was consistent with complete oxidation of CO in the boundary layer, limited only by the availability of oxygen. These results were based on experimental studies with kraft char beds with surface dimensions 20 cm by 10 cm. They imply that the boundary layer reactions are very fast and go to completion. The modelling work of Mitchell et al. (12) showed that very little CO is consumed in the boundary layer surrounding small (less than 100 μm) char particles. The reason for the differences in these results is not clear, but could result from the large differences in boundary layer thicknesses. In our

model, the boundary layer reactions are assumed to be very fast and to go to completion. This means that either all of the oxygen will be depleted or all of the combustibles will be combusted in the boundary layer.

The net rate of mass transfer of O_2 to the particle surface is determined by calculating the O_2 mass transfer rate in the absence of gas phase reactions and then subtracting the rate of O_2 consumption in the boundary layer. The following considerations apply.

Each CO_2 that reacts in the particle produces 2 CO which then react with one O_2 in the boundary layer. Thus each CO_2 that reacts consumes one O_2 in the boundary layer.

Each H_2O that reacts in the particle produces one H_2 and one CO which then react with one O_2 in the boundary layer. Thus each H_2O that reacts consumes one O_2 in the boundary layer.

Each V that comes off will react with one O_2 in the boundary layer.

Each CO produced by sulfate reduction consumes 1/2 O_2. The amount of O_2 consumed is then $2f/(2-f) \times R_{CS}$.

These considerations are valid as long as there is sufficient O_2 to consume all of the combustibles produced. If there is insufficient O_2, the net oxygen flux at the surface will be zero and there will be some net production of combustibles.

The net O_2 rate to the smelt/char particle is then:

$$R'_{O2} = \max (R_{O2} - R_{CO2} - R_{H2O} - R_V - 2f/(2-f) \times R_S , 0) \qquad (1)$$

The O_2 reaching the surface can react with either Na_2S or C. The relative amount of oxygen reacting with each is specified by a partition parameter, p, the fraction of O_2 reaching the surface that reacts with C. The use of an arbitrary partition parameter is necessary because there are no kinetic data on carbon burnup and sulfide oxidation occurring in parallel.

The rate of carbon burnup is then given by

$$R_C = 4/(2-f) \times R_{SO4} + R_{CO2} + R_{H2O} + p \times R'_{O2} = - d[C]/dt \qquad (2)$$

If all oxygen is consumed in the boundary layer, $R'_{O2} = 0$.

The reduction efficiency in the particle is calculated from a sulfide balance. Sulfur is assumed to be present only as sulfide and sulfate. The reduction efficiency, E, is the fraction of the sulfur that is sulfide.

$$S \times l \times dE/dt = R_{SO4} - R_S = R_{SO4} - (1-p)/2 \times R'_{O2} \qquad 0 < E < 1 \qquad (3)$$

The rate of carbon consumption then becomes

$$R_C = \max(R_{CO2} + R_{H2O} + 4/(2-f) \times S \times l \times dE/dt \, , \, R_{O2} - R_V + 2 \times S \times l \times dE/dt) \qquad (4)$$

If there is no change in the reduction state of the particle,

$$R_C = R_{O2} - R_V \text{ or } R_{CO2} + R_{H2O}, \text{ whichever is greater.} \qquad (5)$$

This is the same result as that which had been obtained earlier by Grace (11) in the treatment of bed burning when reduction state changes were neglected.

The key expressions for the char burning model are Equations 1,3, and 4. To solve them, rate equations for R_{O2}, R_{CO2}, R_{H2O}, R_V, and R_{SO4} and values for the parameters "f" and "p" are needed.

The overall rates of consumption of CO_2 and $H_2O_{(v)}$ were calculated as:

$$1/R_i = 1/R_{mi} + 1/(\eta_i R_{ci}) \quad (6)$$

where rates of consumption of gas species i under film mass transfer limited conditions were calculated as:

$$R_{mi} = k_{gi} A_p C_i \quad (7)$$

The mass transfer coefficient was estimated from:

$$Sh = k_g \mathcal{D} / D_p = 2 + 0.6\, Re^{0.8}\, Sc^{1/3} \quad (8)$$

and diffusion coefficients for the reacting gas species were estimated by the Chapman-Enskog equation using Neufeldt's correlation to estimate the diffusion collision integral (13).

The rates under chemical kinetic controlled conditions were calculated from the rate equations of Li and van Heiningen (3,4) for black liquor char:

$$R_{c,CO2} = 6.3\times10^{10}\,[C]\,P_{CO2}/(P_{CO2} + 3.4\,P_{CO})\,\exp(-30070/T) \quad (9)$$

$$R_{c,H2O} = 2.56\times10^{9}\,[C]\,P_{H2O}/(P_{H2O} + 1.42\,P_{H2})\,\exp(-25300/T) \quad (10)$$

The rate limiting effect of interparticle diffusion was accounted for with a Thiele modulus-based effectiveness factor:

$$\eta_i = \tanh(M_{Ti})/M_{Ti} \quad (11)$$

where:

$$M_{Ti} = D/6\ (k_i/\delta_i)^{1/2} \quad (12)$$

and

$$k_i = R_{ci}/(V_p C_i) \quad (13)$$

The overall rate of consumption of O_2 was assumed to be limited by the rate of film mass transfer and was calculated from Equation 7.

The reduction rate equation was taken from Cameron and Grace (14), whose data were obtained under conditions where there was a continuous smelt phase containing a small concentration of suspended carbon particles. This would be expected to be applicable toward the end of the char burning stage as the carbon becomes depleted. Its applicability to the earlier stages when the inorganic is imbedded in a carbon matrix may be questioned. However, these are the only quantitative sulfate reduction kinetic data available for use at temperatures above 780°C.

$$R_{SO4} = 1310\ [SO4]/\{0.0011\ ([C] + I) + [SO4]\}\ [C]\ e^{-14700/T} = S\ I\ (1\text{-}E) \quad (14)$$

The parameter "f" is the fraction of CO in the gas produced by the sulfate reduction reaction. Cameron's data (14) indicates that CO_2 is the major product of this reaction, and that f is probably less than 0.1. We choose to leave it in as a parameter at this point to allow sensitivity studies to be done.

There are no data available on which to base an estimate of the partition parameter "p". It was set equal to the mole fraction carbon in the particle, i.e. p = C/(C + I). This approach has the advantage that all of the O_2 will react with sulfide as the carbon becomes depleted.

SENSITIVITY TESTS OF MODEL

The model was used for a series of simulations to illustrate the effect of process variables on char burning. A base case set of model parameters was chosen to reflect typical conditions in a recovery boiler. They are:

Initial Drop Diameter = 4.0 mm
Temperature = 1300°K
O_2 = 5%
H_2O = 15%
CO_2 = 10%
H_2 = 2%
CO = 2%.

The initial char particle diameter was assumed to be three times the initial black liquor drop diameter for all of the simulations. The sulfate reduction reaction was assumed to produce only CO_2.

The gas mass transfer coefficients depend on the Reynolds number, Re, which is proportional to the product of the particle diameter and the relative velocity of the gas past the particle. Black liquor drops swell greatly during pyrolysis and then contract as the carbon is burnt away during char burning. The changing diameter, particle density and relative velocity must be accounted for in determining Re.

In a complete computational fluid dynamics based recovery furnace model the trajectories of individual particles are calculated as they respond to fluid drag and gravity. Reynolds number calculations are an inherent part of such models. For this paper, Re was estimated by assuming that, during char burning, the particles are entrained in the gas and the relative velocity will be close to the terminal velocity of the particle. Typically, Re decreases by about 15-20% as char burning proceeds, since decreasing diameter and increasing terminal velocity offset each other. Thus an assumption of constant Re during

char burning is reasonable. Using a diameter swelling factor of 3 during pyrolysis and the assumption that the char particle was at terminal velocity and standard correlations for drag on a sphere were used to develop an empirical expression for Re.

$$Re = 13.6 \times (\text{Initial Diameter})^{2.05} \quad (15)$$

Figure 1 shows the typical behavior during char burning. The mass of char carbon decreases with time as the carbon is converted to gases. The total mass of the char particle drops off and goes through a minimum as the carbon is depleted and then increases as sulfide is reoxidized to sulfate. The reduction efficiency, which characterizes the state of the sulfur in the particle rises during char burning, reaches a maximum at about the point of carbon depletion, and then falls off at a constant rate because of sulfide reoxidation. The particle diameter decreases greatly as burning proceeds and reaches the diameter of a smelt drop as the carbon is depleted.

Char burning can be characterized by two parameters: the time for 99% char carbon burnup, t_{99}, and the maximum increase in reduction efficiency, ΔE. The effect of process variables on these two quantities can provide considerable insight into the nature of black liquor combustion in a recovery boiler. The two most important process variables are the initial black liquor drop diameter and the temperature. Figure 2 shows the effect of drop diameter and temperature on t_{99} and ΔE. The spacing between points indicates that at a given temperature, both t_{99} and ΔE increase with increasing drop diameter in a nearly linear manner. As temperature increases, the gain in reduction increases in an exponential manner, while the time for carbon burnout shortens at a slower rate. It is evident that bigger drops contribute much more to reduction than do smaller drops. It is also apparent that high temperature is more important than drop size in getting good reduction.

Figure 2 also shows that, at a given temperature, the relation between reduction gain and char burnout time is nearly linear. This is to be expected. The reduction reaction takes place homogeneously

throughout the particle at a rate dependent on carbon concentration but independent of the external gas environment. The longer the time allowed for this to occur, the more reduction takes place. At a given temperature, any variable that shortens the char burnout time will result in less reduction. The effect of temperature on the sulfate reduction kinetics is so great that higher temperature results in more reduction even though it also shortens char burnout times.

The effect of gas composition on char burning was examined by making changes in gas concentrations around the base case conditions and determining the effects on t_{99} and ΔE. H_2O and CO_2 were varied by ±5%, O_2 by ±3% and H_2 and CO by ±2% on an absolute basis. The average rates of change over this range are summarized in Table 1. Both H_2O and CO_2 showed non-linear behavior, with low concentrations giving about 50% greater changes than high concentrations.

Increasing H_2O and CO_2 concentrations increases carbon gasification rates which shorten burning times and result in less reduction. H_2O has a larger effect than CO_2. Both H_2 and CO suppress gasification rates slightly and this increases burning times and gives more reduction. The effects are not very large.

The O_2 concentration, over the range from 2 to 8%, has no effect on burning times and maximum reduction gain at temperatures of 1300°K or higher, and only a minor effect at 1200°K. This apparently surprising result can be readily explained. At the conditions that are typical for char burning in a recovery furnace, gasification by H_2O and CO_2 is responsible for carbon removal. The combustible CO and H_2 coming from the particle consume the O_2 in the boundary and effectively prevent it from reaching the particle itself until the carbon is nearly depleted. The effects of oxygen concentration are very apparent after the carbon is depleted. Rates of reduction loss by sulfide reoxidation are 4.3, 10.8, and 17.2 %/sec for oxygen concentrations of 2, 5, and 8% respectively.

VALIDITY OF MODEL

There are three elements of the char burning model predictions that need to be validated. These are char burning rates (burnout times), the suppression of oxidation by combustible gasification products, and reduction efficiency gains. There are no experimental data available giving both burning times and sulfur reduction during char burning in mixed O_2, H_2O and CO_2 atmospheres which could be used to validate the complete model. There are data available on each of these individual elements that can establish model validity.

There are some data (7) on the weight changes occurring when a char particle was burned in air which show the decrease to a minimimum as carbon is burnt out and then the weight regain characteristic of sulfide oxidation. However, the total weight loss is greater than can be accounted for by carbon removal alone, apparently because of cocurrent sodium evolution. Rate equations to handle this effect are not yet available. Another problem with these data is that the model predicts that temperature has a very large effect, particularly on reduction, and the temperature of the burning particles were not measured. In an oxidizing environment, particle temperatures can exceed furnace temperatures by up to 400°K (8).

Frederick (15,16) has measured char burning times for different temperatures and gas compositions in a quiescent, thermal radiation-dominated environment and has been able to successfully predict these times with a char burning model using essentially the same treatment of mass transfer and chemical kinetics that have been incorporated in the current char burning model.

Table 2 shows rate data for carbon oxidation obtained by Grace (11) in a laboratory study of char bed burning. These data show that rates of carbon release by direct oxidation and gasification were additive in the absence of water vapor (which catalyzes CO oxidation). However, carbon release rates for O_2 - H_2O mixtures were no greater than for dry O_2 alone and the rates for O_2 - CO_2 - H_2O mixtures were less than for O_2 - CO_2. Sutinen et al. (17) were able to predict these carbon oxidation rates within ±

7% on average using a char bed burning model very similar to the one described here. We believe this is strong evidence that reactions between O_2 and combustibles close to the char burning surface decrease or eliminate the O_2 flux at the surface and that a similar effect takes place during char particle burning.

The ability of the model to predict reduction is dominated by the reliability and accuracy of the sulfate reduction kinetic model. The sulfate reduction rate model has little effect on carbon burnout rates but it has a big effect on reduction (e.g. if the sulfate reduction rate constant is doubled, the base case value for t_{99} is lowered from 3.205 to 3.11 seconds while ΔE_R is nearly doubled from 17.73% to 33.92%).

High reduction efficiencies in the recovery furnace are generally easy to obtain, and it appears that the current model is underpredicting reduction efficiency. However, there are currently no data available which would provide a firm basis for increasing the reduction rates. Cameron's (14) results, which are the source of the rate equation used in the model, were obtained under conditions of very low carbon concentrations in a mass of molten inorganic smelt. The char carbon was produced by pyrolyzing black liquor and then crushing the char before adding it to the smelt. Some loss in char carbon reactivity may have occurred during these steps. Thorman and Macur (18) obtained reduction rate data with much larger quantities of char carbon suspended in molten smelt. However, they found that the measured reduction rates depended on the amount of stirring in their reactor, and the rates were generally lower than those predicted by Cameron. Li and van Heiningen (19) obtained data on sulfate reduction at low temperatures where the sulfate is in the solid phase. The applicability of these data to the temperature region of interest is questionable.

CONCLUSIONS

1. The model appears to underpredict sulfate reduction. The capability to predict reduction is dominated by the reliability and accuracy of the sulfate reduction kinetic model. There is a need for good rate data on sulfate reduction under the conditions applicable to kraft char burning.

2. Gasification of char carbon by reaction with H_2O and CO_2 is the most important means for carbon release under typical recovery furnace conditions. Sulfate reduction is responsible for only a minor part of the carbon release. Direct carbon oxidation by reaction with O_2 is insignificant because O_2 is prevented from reaching the particle surface until the carbon is depleted due to reaction with H_2 and CO coming from the particle.

3. Under the normal range of recovery furnace conditions, the rate of carbon burnup is not enhanced by increased O_2 concentrations. Consumption of O_2 by combustible products of gasification reactions prevents direct oxidation of the char carbon.

4. The H_2 and CO from char carbon gasification by H_2O and CO_2 provide a protective effect to preserve reduction, since they prevent O_2 from reaching the char surface where it could oxidize sulfide until the carbon is depleted. This is significant in obtaining high reductions.

5. New experimental data are needed to fully validate the char burning model. These experiments should include mixed gas atmospheres and measurement of the sulfur reduction state at intermediate times dring char burning.

NOMENCLATURE

A_p	external surface area of char particle, cm^2
C_i	concentration of species i in bulk gas, $mols/m^3$
[C]	moles of fixed carbon in the particle at any time, mols
D	char particle diameter, cm
$\mathcal{D}$	diffusivity of gases, cm^2/sec
E	reduction efficiency = $Na_2S/\{Na_2S + Na_2SO_4\}$ at any time
f	fraction of CO in the gas produced by the sulfate-carbon reaction
I	mole inorganic in the particle, mols Na_2, (assumed constant)
k_g	film mass transfer coefficients for reacting gases, cm/sec
k_i	apparent first order rate constant for carbon gasification reaction
M_T	Thiele modulus
P_i	partial pressure of gases
p	fraction of the O_2 reaching the surface that reacts with fixed carbon
R_{O2}	rate of mass transfer of O_2 to the particle that would occur if there were no gas phase reactions in the boundary layer, mol O_2/sec
R'_{O2}	net rate of O_2 transfer to the particle after reactions with combustibles in the boundary layer, mol O_2/sec
R_{CO2}	rate of CO_2 reaction with fixed carbon in the particle, mol CO_2/sec
R_{H2O}	rate of H_2O reaction with char carbon in the particle, mol H_2O/sec
R_V	rate of flow of pyrolysis volatiles from the particle, mol V/sec
R_{SO4}	rate of reaction between C and Na_2SO_4 , mol Na_2SO_4/sec
R_S	rate of oxidation of Na_2S to Na_2SO_4, mol Na_2S/sec
$R_{m,i}$	rate of gas transport, mols/sec
Re	Reynolds number, UD/v, dimensionless
S	sulfidity of the inorganic = moles sulfur per mole inorganic
Sc	Schmidt number, $\upsilon/\mathcal{D}$, dimensionless
Sh	Sherwood number, $kD/\mathcal{D}$, dimensionless
T	temperature, °K
[SO4]	sulfate concentration = S × I × (1 - E)
t	time, sec
U	relative velocity between gas and char particle, cm/sec
η	effectiveness factor to account for the effects of intraparticle diffusion.
υ	kinematic viscosity of gas

ACKNOWLEDGEMENTS

This work was supported by the United States Department of Energy through the Office of Industrial Technology. Support was also provided by the American Forest and Paper Association's Recovery Boiler Committee and the Institute of Paper Science and Technology.

REFERENCES

1. Smoot, L.D. and Smith, P.J., *Coal Combustion and Gasification*, Plenum, New York (1985)
2. Bartok, W. and Sarofim, A.F. *Fossil Fuel Combustion*, John Wiley and Sons, New York (1991)
3. Li, J. and van Heiningen, A.R.P., *Ind. Eng. Chem. Res.* 29(9):1776-1785 (1990)
4. Li, J. and van Heiningen, A.R.P., *Ind. Eng. Chem. Res.* 30(7):1594-1601 (1991)
5. Walsh, A.R. and Grace, T.M., *J. of Pulp & Paper Science* 15(3):J84-J89 (1989)
6. Jones, A.K. and Chapman, P.J., *Tappi J.*, 76(7):195-202 (1993)
7. Grace, T.M., Cameron, J.H. and Clay, D.T., *Tappi J.* 69(10):108-113 (1986)
8. Frederick, W.J. and Hupa, M., *Combustion Chemistry Research Group Report 93-3*, Abo Akademi University, Turku, Finland (1993); also to be pulished as a U.S. Department of Energy Report
9. Adams. T.N. and Frederick, W.J., *Kraft Recovery Boiler Physical and Chemical Processes*, American Forestry and Paper Institute, New York, NY (1988) p.131
10. Sjoberg, M. and Cameron, J.H., *AIChE Symposium Series*, 239(80):35-40 (1984)
11. Grace, T.M., Lien, S.J. and Brown, C.A., *Proceedings of 1992 International Chemical Recovery Conference*, TAPPI, Atlanta, GA p.539-550 (1992)
12. Mitchell, R.E., Kee, R.J., Glarborg, P. and Coltrin, M.E., *Twenty-Third Symposium (International) on Combustion*, The Combustion Institute, p 1169 (1991)
13. Reid, R.C., Prausnitz, J.M. and Poling, B.E., *The Properties of Gases and Liquids*, Fourth ed., McGraw-Hill Book Company, New York (1987)
14. Cameron, J.H. and Grace, T.M., *Ind. Eng. Chem. Fundam.* 24(4):443-449 (1985)
15. Frederick, W.J., *U.S. DOE Report DOE/CE/40637-T8 (DE90012712)* (1990)

16. Frederick, W.J., Kulas, K.C., Clay, D.T., Hupa, M. and Noopila, T., *Proc. 1989 International Chemical Recovery Conference*, CPPA, Montreal, Que. (1989)

17. Sutinen, J., Karvinen, R. and Frederick, W.J., *Coupling of Phenomena ina Char Bed to the Gas Field of a Lower Recovery Furnace*, in press.

18. Thorman, R.P. and Macur, T.S., *Proceedings of 1985 International Chemical Recovery Conference*, TAPPI, Atlanta, GA , p.451-458 (1985)

19. Li, J. and van Heiningen, A.R.P., *Proceedings of 1992 International Chemical Recovery Conference*, TAPPI, Atlanta, GA p.531-538 (1992)

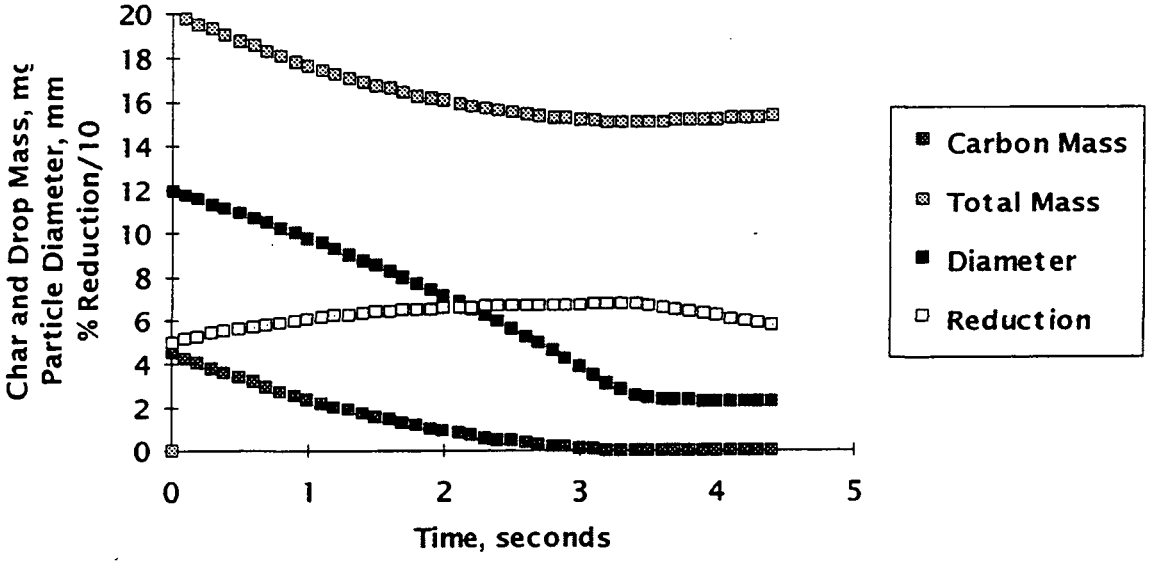

Figure 1. Typical Char Burning Behavior.

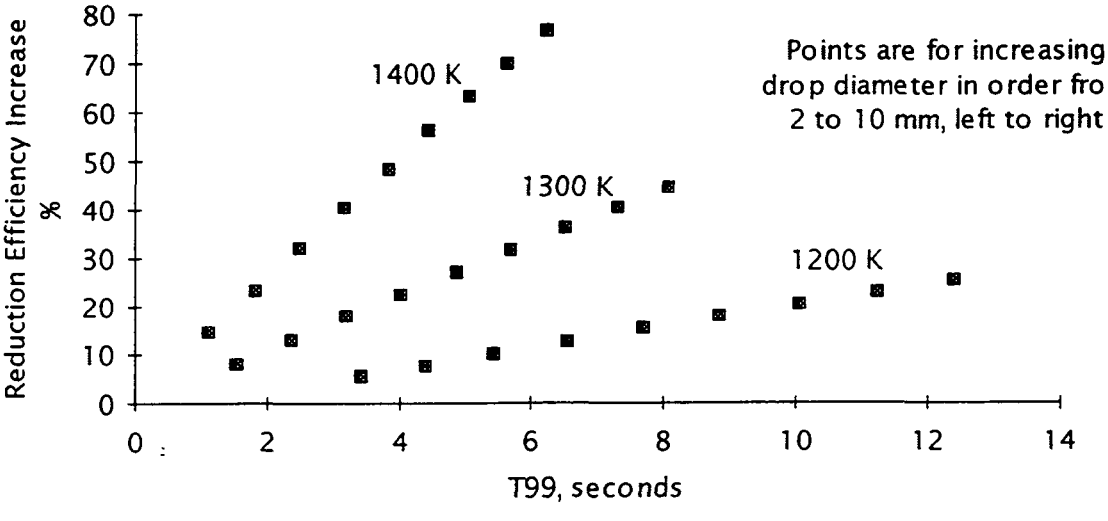

Figure 2. Effect of Initial Drop Diameter and Temperature on Maximum Reduction and Char Burnup Time.

Table 1. Effect of Gas Composition on Char Burning

Temperature, °K	Gas Changed	dt_{99}/dX, sec/%	dE/dX, % / %
1200	H_2O	-0.191	-0.39
	CO_2	-0.122	-0.25
	O_2	-0.048	-0.10
1300	H_2O	-0.128	-0.73
	CO_2	-0.088	-0.49
	H_2	+0.033	+0.13
	CO	+0.041	+0.17
	O_2	0	0
1400	H_2O	-0.103	-1.31
	CO_2	-0.072	-0.91
	H_2	+0.013	+0.13
	CO	+0.015	+0.15
	O_2	0	0

Table 2
Effect of CO_2 and H_2O on Char Bed Burning

O_2 %	H_2O %	CO_2 %	Carbon Flux gmol/sec/cm^2	$CO/(CO+CO_2)$	Temperature °C
14	0	0	24.35×10^{-6}	0.504	961
14	0	10	32.45×10^{-6}	0.638	932
14	10	0	24.86×10^{-6}	0.011	990
14	10	10	28.09×10^{-6}	0.0	967

Application of the Recovery Boiler Model

COMPARISON OF SIMULATION RESULTS AND FIELD MEASUREMENTS OF AN OPERATING RECOVERY BOILER

Robert R. Horton
Assistant Professor
Institute of Paper
Science and Tech.
500 10th St. NW
Atlanta, GA 30318

Esa K. Vakkilainen
Sr. Research Manager
Recovery Processes
Ahlstrom Corp.
SF-78201 Varkaus
Finland

ABSTRACT

A recovery boiler was operated using two sizes of black liquor firing nozzles while maintaining the same boiler load in each case. Temperature measurements were made using pyrometers to establish a vertical temperature profile within the furnace for both cases. The boiler was then simulated for both conditions using a computer-based model of the furnace to predict general combustion behavior. Simulations showed that differences in reduction efficiency for the two firing conditions can be attributed to greater amounts of organics striking the bed region for the case with larger nozzles. A simplified energy balance was used to predict heat release. The heat release profile was then compared to the mill temperature data showing good agreement and providing qualitative validation for the modeling technique.

INTRODUCTION

The purpose of this study was to use current recovery furnace modeling capabilities to explain observations of mill trials for two different firing modes of an operating boiler. One black liquor firing scheme used 15 guns with smaller nozzles (3/4" nominal ID), the other had 11 guns with larger nozzles (1" nominal ID). An effort was made to maintain the same load in both cases, yet significantly higher reduction efficiency was observed for the larger nozzle case, and pyrometry measurements showed a different temperature profile. Traditional recovery boiler design calculations cannot clearly explain these observations, so it was of interest to simulate black liquor combustion in the furnace using an advanced three-dimensional model.

There are numerous references in the literature to recovery boiler model development and simulation results (1-11). This is the first comparison of simulation results with boiler mill trials for different black liquor firing schemes. Recently, researchers have proposed a black liquor combustion model based on laboratory combustion experiments which includes both fundamental heat and mass transfer theory as well as empirically determined model parameters (12). This model is the basis for the recovery boiler simulation used in this work.

This paper first describes the mill trials and results for the Kaukas Boiler at both firing conditions. The computational modeling methodology is then described followed by a comparison of simulation results and mill data.

RECOVERY BOILER FIELD TESTING

The boiler studied in this work was the Ahlstrom 2700 tds/day recovery boiler at the Kaukas, Finland mill. The two operating conditions were 15 smaller 3/4" splash-plate nozzles and 11 larger 1" splash-plate nozzles operated at flow rates that yielded the same overall load to the boiler. Black liquor properties and firing conditions were very similar in both cases.

The pulp mill and boiler manufacturer jointly conducted full-load recovery boiler testing using the two different nozzles to determine which size gave the better performance at design loads. During testing thorough measurements were taken to document boiler operation for the two different firing strategies. Pyrometry measurements were taken at the air port levels and at the bullnose to determine the approximate vertical temperature profiles for both cases. In addition, standard recovery boiler heat and material balance calculations were done to compute the "expected" exit flue gas temperatures.

Approximate boiler dimensions and air distribution levels for the unit are given in Table 1.

Table 1. Air Distribution and Boiler Dimensions

Base Dimensions (m)	12.5 x 12.5
Height to Bullnose (m)	35
Liquor Gun Level (m)	6
Primary Air (%)	32
Secondary Air (%)	51
Tertiary Air (%)	17

Data showing average operating conditions for both mill trials is shown in Table 2. Mean droplet diameter was calculated based on the work of Empie et al. (13)

Table 2. Operating Conditions for the Two Mill Trials

	Case A	Case B
Number of Liquor Guns	15	11
Nozzle Orifice ID (mm)	22	27
Black Liquor Flow (kgds/s)	29.3	29.1
Firing Temperature (°C)	123.5	124.0
Firing Solids (%)	71.6	73.1
Mean Droplet Size (mm)*	2.62	3.25

* Calculated

The locations of black liquor guns are shown for Case A and Case B in Figures 1 and 2.

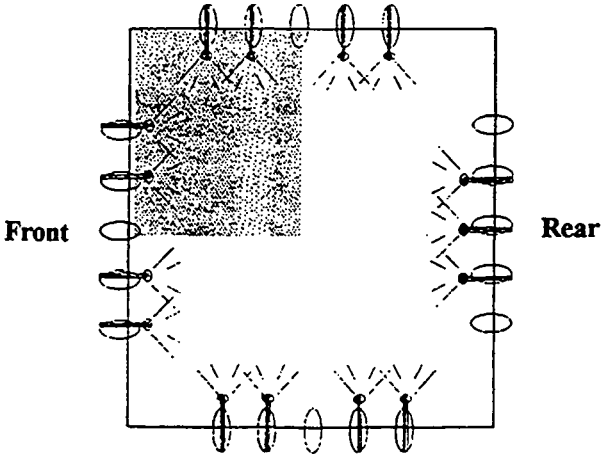

Figure 1. Black Liquor Gun Locations for Case A (15 Gun).

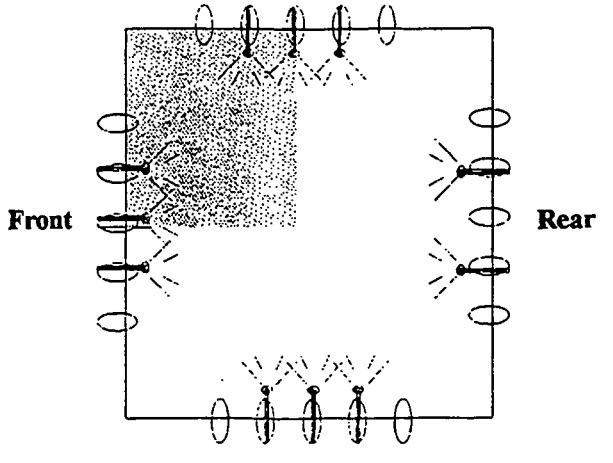

Figure 2. Black Liquor Gun Locations for Case B (11 Gun).

A standard industrial pyrometer was used to measure temperatures at the secondary, tertiary, and bullnose levels to establish an approximate temperature profile for both cases. From previous work (14) it is estimated that the temperature measurements with this pyrometer represent gas at distances roughly two meters into the furnace. Although the measurements are inaccurate for single absolute temperature measurements, they provide a good estimate of differences between the two mill trials. Pyrometry measurements and reduction efficiencies for the two cases are shown in Table 3.

Table 3. Mill Trial Results and Measurements

	Case A	Case B
Secondary Level Temp. (°C)	1012	1099
Tertiary Level Temp. (°C)	942	996
Bullnose Level Temp. (°C)	896	948
Reduction Efficiency (%)	92	96

These results show that a higher reduction efficiency was achieved in Case B by using fewer guns with larger nozzles. Standard recovery boiler heat transfer calculations based on similar combustion profiles predicted equal temperatures at the bullnose level. This is inconsistent with the pyrometry results unless a different heat release pattern with combustion higher in the furnace existed in Case B. This scenario would be counterintuitive since the mean droplet size was larger in Case B. A full three-dimensional simulation was desirable to explain higher exit furnace temperatures with larger black liquor drop sizes accompanied by greater reduction efficiency.

MODELING THE BOILER

Computer modeling of the Kaukas recovery boiler was done in two stages: 1) computational fluid dynamics (CFD) flow-field model, and 2) black liquor in-flight combustion model. The first part of the model focused on obtaining a flow pattern for the gases in the furnace. The second part involved predicting combustion behavior for the two firing conditions of 15 smaller nozzles (Case A) and 11 larger nozzles (Case B). The same flow field was used for both combustion simulations. The two main issues that we wanted to examine in the modeling effort were: 1) explain why improved reduction efficiency was observed in Case B, and 2) explain how the exit flue gas temperature could be higher for Case B at the same time.

CFD Flow Model

The initial phase of modeling was an isothermal CFD model of the gas flow in the furnace combustion zone below the bullnose. This modeling work was done at Ahlstrom Machinery in Varkaus, Finland, using FLUENT, ver. 4.01, on an HP Apollo workstation. Two planes of symmetry were used so that maximum resolution of grid nodes was available to describe individual secondary and tertiary air ports. This resulted in a flow field description of one quarter of the furnace. A nonuniformly spaced, Cartesian grid was specified, and an appropriate step bed was used as a boundary at the base of the furnace geometry.

The predicted flow field is characterized by velocity magnitude contours and vector plots in Figures 3-7. Figure 3 shows secondary level air jet penetration using velocity magnitude contours. A similar plot shows air jets at the tertiary level in Figure 4. It is evident from these figures that there is considerable interaction of the secondary air jets. Figures 5 and 6 show velocity vectors at the secondary and tertiary levels which show swirl patterns in the flow field. Figure 7 shows velocity vectors at the liquor gun level which indicates that a central core has developed where highest upward flow components are in the center of the furnace. Upward velocities dissipate with distance up the furnace.

The CFD results presented here will have limited accuracy. Some of the recognized limitations in this study are: isothermal flow, k-e turbulence model, step bed vs. smooth bed, large aspect ratios for some cells, and only a partial simulation of the overall boiler geometry. However, for the purposes of this study, only an approximation of the true flow field is needed since we are looking for differences in black liquor combustion due to a variation in firing practice. Our assumption is that the CFD-generated flow field is a reasonable approximation of the actual flow and that only minimal differences in the gas phase flow exist between firing with either 15 guns or 11 guns.

Black Liquor Combustion Model

In-flight black liquor combustion behavior was simulated at the Institute of Paper Science and Technology on an IBM RS-6550 workstation. The flow field predictions were imported into an independent full furnace geometry and were fixed for combustion calculations. Combustion simulations were done by projecting the CFD flow field predictions of a quarter furnace to a full furnace geometry through mirror images to allow asymmetric placement of liquor guns. The simulated gun arrangements followed the locations used in mill tests.

The black liquor combustion model used in this work is based on descriptions of the four stages of black liquor combustion: 1) drying, 2) pyrolysis, 3) char burning, and 4) inorganic smelt reactions. Heat and mass transfer relationships are used to predict the rates at which each of the combustion stages occur. Heat transfer calculations are based on a single, film resistance model for the individual black liquor drops. The trajectories of drops are determined by a force balance using a coefficient of drag relationship and are influenced by swelling characteristics of the black liquor and gas flow patterns within the furnace. These trajectories dictate where mass and energy are exchanged between the gas and droplet phases and whether the droplets become entrained or fall to the char bed.

Black liquor mass flow as a function of angle within the spray sheet was specified according to a parabolic distribution (15). Gun firing angle into the furnace was at a slight downward angle of 10° with respect to horizontal.

SIMULATION RESULTS

The in-flight black liquor combustion model predicts mass transfer rates in three-dimensional space for three stages of black liquor combustion: 1) evaporation, 2) pyrolysis, and 3) char burning. The model also predicts where black liquor mass, including inorganic portions, strikes the furnace boundaries, i.e. walls, bed and carryover.

Improved Reduction Efficiency

The biggest difference between the two firing patterns was the black liquor mass striking the bed. Tables 4 and 5 summarize the fate of black liquor in the two cases. Almost twice as much uncombusted organic volatiles and char mass lands on the bed in the Case B (11 larger nozzles). In addition, more inorganic material landed on the walls in Case A. These simulation results help to explain the higher reduction efficiencies observed in the mill trials in the case of larger nozzles. It is recognized that some uncombusted char is needed for good bed operation to help reduce sulfate to sulfide. If we combine the pyrolysis and char masses into a single organics term, roughly 82% of the organics burned in-flight in Case A versus about 70% burned in-flight in Case B. About 13% of the organic mass landed on the bed in Case A and versus about 27% to the bed in Case B. The remainder in each case landed on walls.

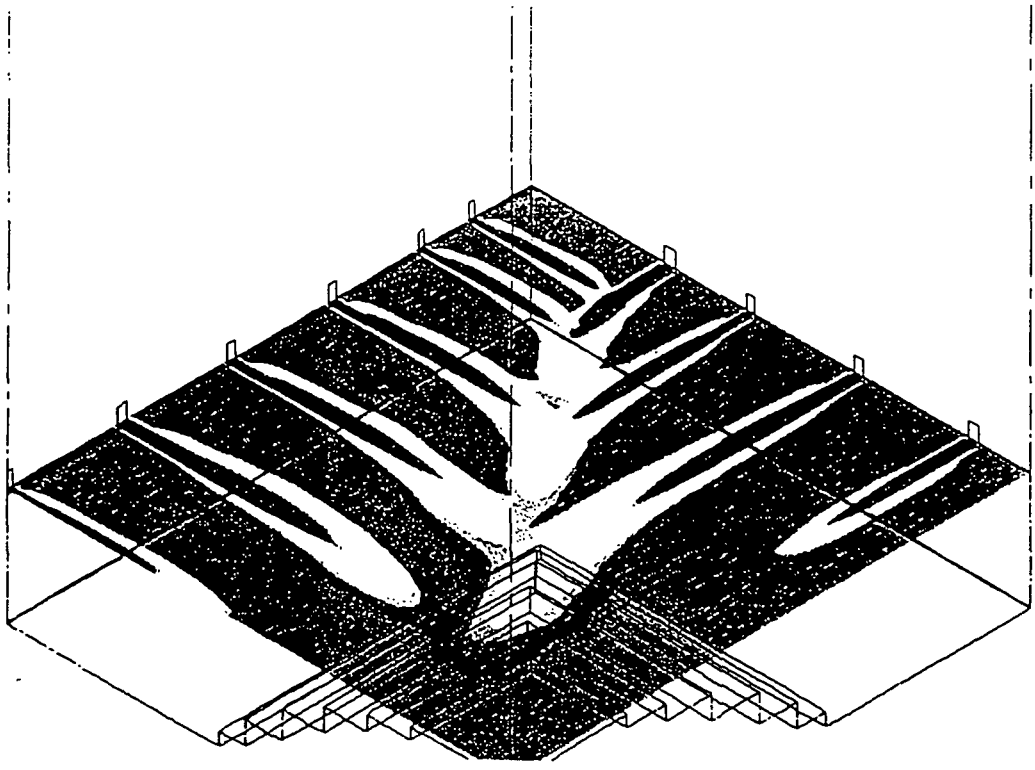

Figure 3. Velocity Magnitute Contours of the Quarter Furnace Geometry at the Secondary Air Port Level.

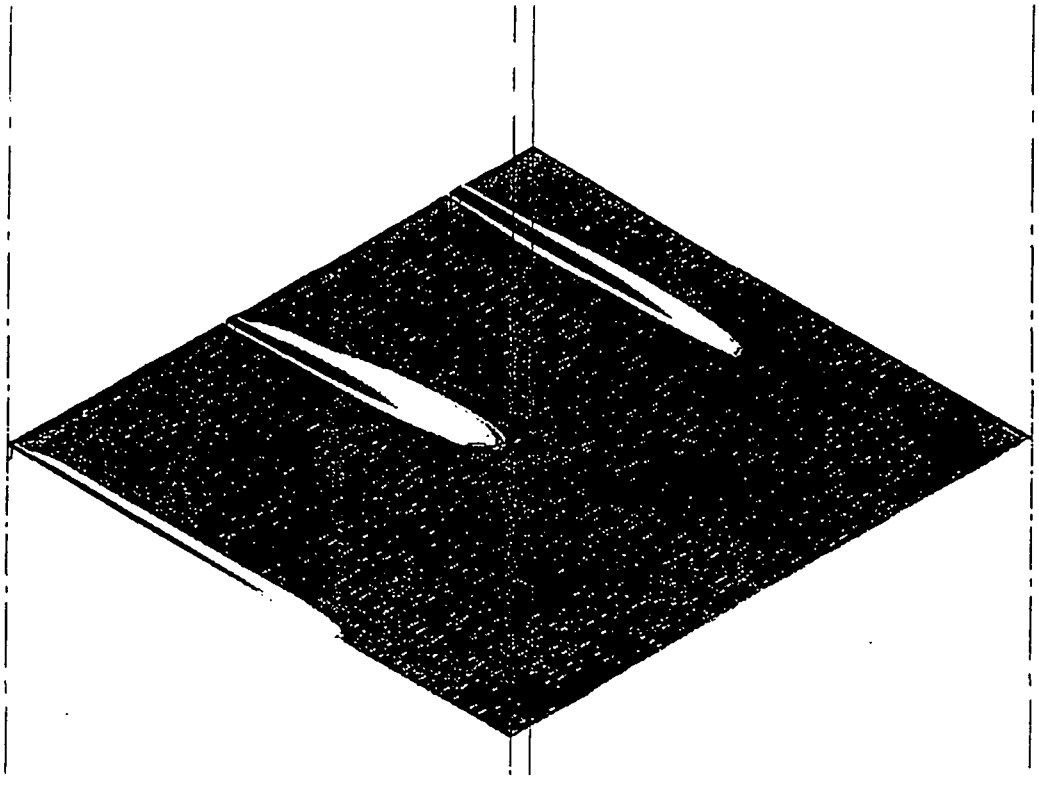

Figure 4. Velocity Magnitute Contours of the Quarter Furnace Geometry at the Tertiary Air Port Level.

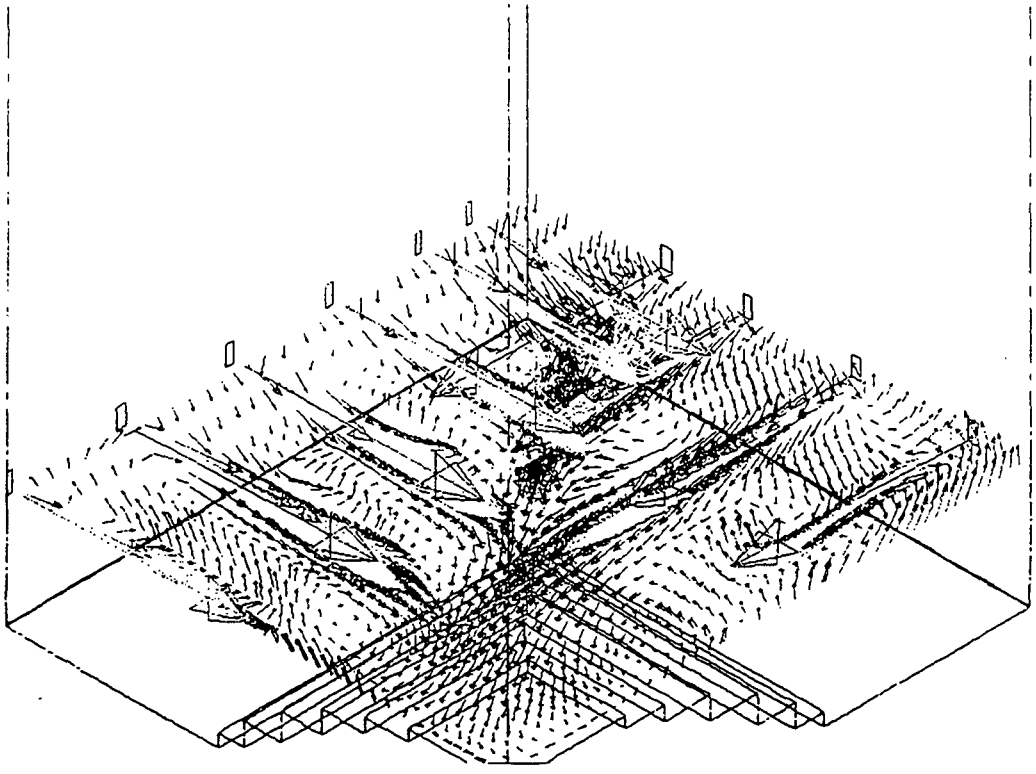

Figure 5. Velocity Vectors at the Secondary Level.

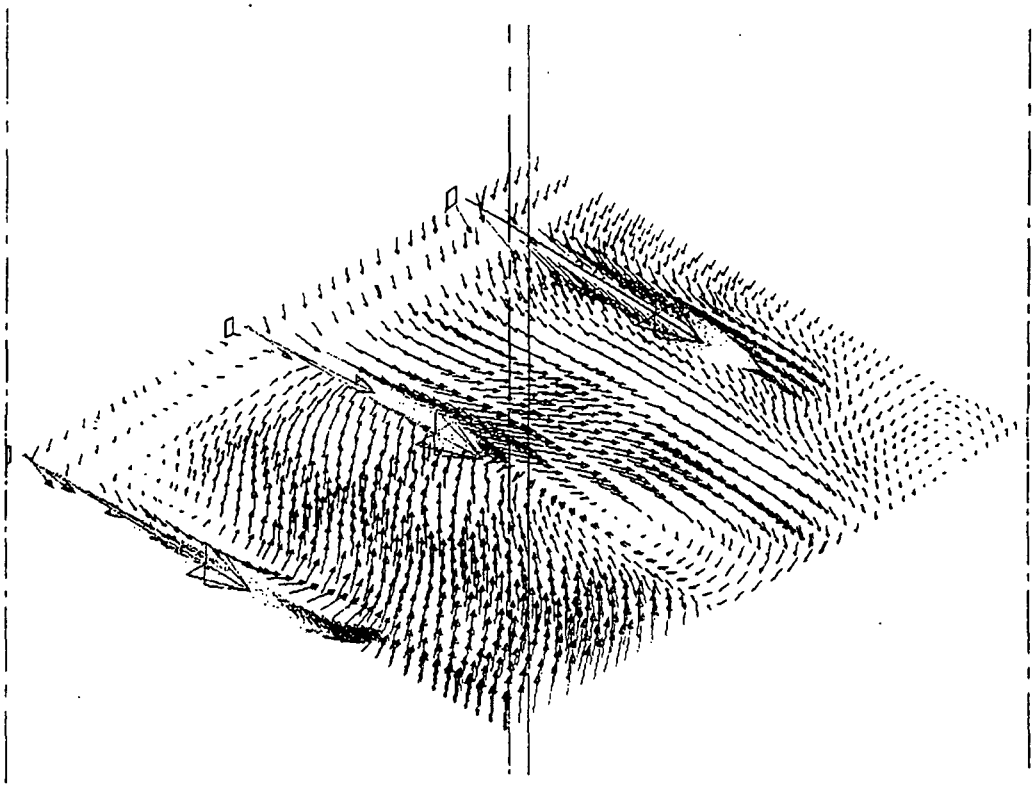

Figure 6. Velocity Vectors at the Tertiary Level.

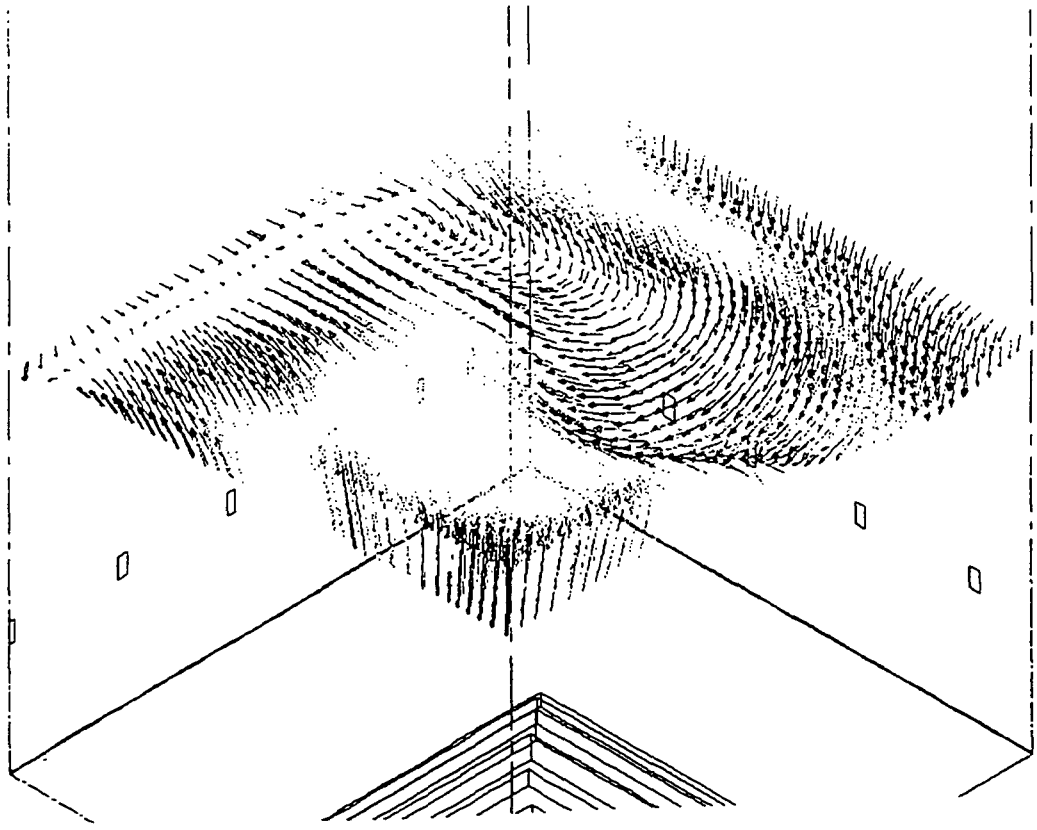

Figure 7. Velocity Vectors at the Liquor Gun Level.

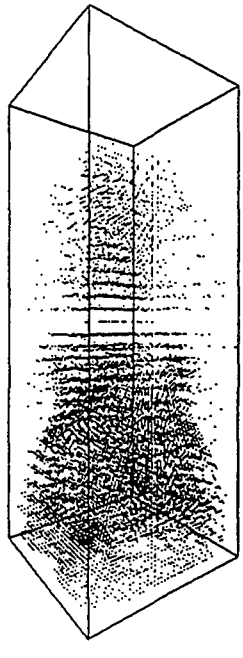

Figure 8. Char Combustion Locations for Case A.

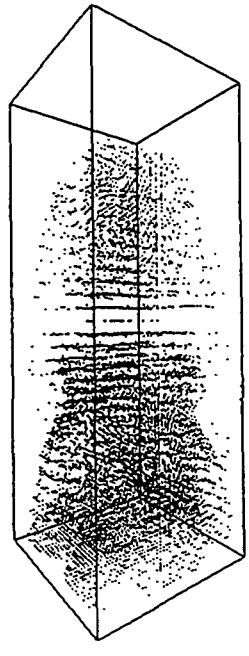

Figure 9. Char Combustion Locations for Case B.

Table 4. Final Fates of Black Liquor Mass in Case A.

	Water	Pyrolysis	Char	Smelt	Organic (total)
In-flight	0.98	0.85	0.70	0	0.82
Hit Walls	0.009	0.05	0.07	0.29	0.05
Carried Out	0	0	0	0.006	0
Hit Bull Nose	0	0	0	0.001	0
Hit Char Bed	0.01	0.10	0.23	0.70	0.13

Table 5 . Final Fates of Black Liquor Mass in Case B.

	Water	Pyrolysis	Char	Smelt	Organic (total)
In-flight	0.96	0.73	0.53	0	0.70
Hit Walls	0.006	0.03	0.06	0.22	0.04
Carried Out	0	0	0	0.004	0
Hit Bull Nose	0	0	0	0.0008	0
Hit Char Bed	0.04	0.24	0.41	0.77	0.27

Temperature Profile Differences

Figures 8 and 9 show three-dimensional views of mass transfer locations for evaporation, pyrolysis, and char burning for the 15 gun and 11, gun cases respectively. These graphics show that combustion patterns were qualitatively similar for both cases.

To give a better indication of heat release in the furnace, total organic mass release during both the pyrolysis and char burning stages was summed on a fractional mass basis. The resulting profiles of black liquor organic mass transfer are compared in Figure 10 for the two cases. The bimodal nature of the combustion pattern makes it hard to predict how temperature would be effected at the gun level. However, there was more combustion activity predicted higher in the furnace for the case with larger nozzles which would help to explain a persisting higher temperature for the case with larger mean drop size. Differences in gun locations may have contributed to the change in combustion profile.

Additional Insight

The Kaukas recovery boiler is a relatively large, modern boiler with a distance of 35 m from bed to bullnose. Because of this high furnace combustion zone, very little physical carryover was predicted in either the 15 gun or 11 gun simulations. The mill has experienced very little fouling, so this also qualitatively supports the model's predictions of minimal carryover.

CONCLUSIONS

Recovery boiler modeling techniques allowed a better understanding of observations made during mill trials.

Reduction efficiency improvement for the boiler firing with larger nozzles was shown to be the result of larger droplets and more uncombusted black liquor char directly to the bed.

A change in temperature profile resulted in higher temperatures for the exiting flue gas and was due to more combustion activity higher in the furnace for the larger nozzles.

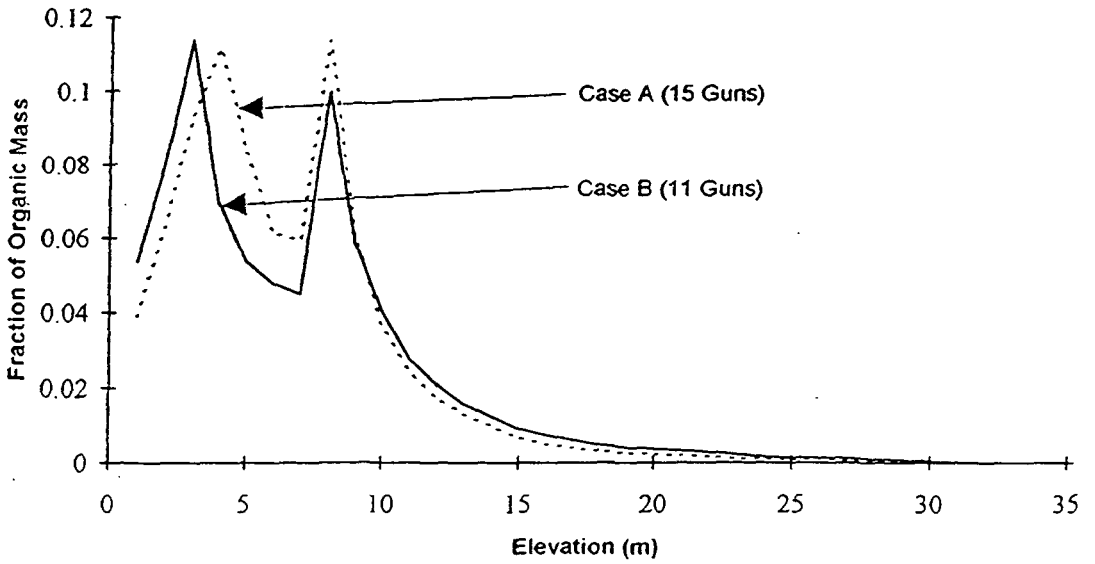

Figure 10. Release of Black Liquor Organic Mass versus Elevation in the Furnace.

LITERATURE CITED

1. Williams, T. and Galtung, F., "A Mathematical Model of a Recovery Furnace," Proceedings ISA/75, Milwaukee, WI, 1975.

2. Merriam, R., Kraft, *ver. 2.0* - Computer Model of a Kraft Recovery Furnace, A. D. Little, Inc., Cambridge, MA, 1980.

3. Shiang, N. and Edwards, L., "Kraft Recovery Furnace Capacity and Efficiency Improvement," TAPPI Int. Rec. Conf., 1985.

4. Shick, P., "Predictive Simulation of Recovery Furnace Processes on a Microcomputer," Kraft Recovery Operations Seminar, Orlando, FL., 1986.

5. Grace, T., Walsh, A., Jones, A., Sumnicht, D., and Farrington, T., "Three-Dimensional Mathematical Model of the Kraft Recovery Furnace," TAPPI Int. Chem. Rec. Conf., 1989.

6. Walsh, A. and Grace T., "TRAC: A Computer Model to Analyze the Trajectory and Combustion Behavior of Black Liquor Droplets," JPPS, vol. 15, no. 3, pp. 84-89, 1989.

7. Karvinen, R., Hyoty, P., and Siiskonen, P., "The Effect of Dry Solids Content on Recovery Boiler Furnace Behavior," TAPPI J., vol. 74, no. 12, pp. 171-177, 1991.

8. Frederick, W., "Combustion Processes in Black Liquor Recovery: Analysis and Interpretation of Combustion Rate Data and an Engineering Design Model," U. S. Dept. of Energy Report DOE/CE/40637-T8 (DOE90012712), 1990.

9. Chapman, P.., Janik, S., and Jones, A., "Visualization of the Recovery Boiler Flow Fields Predicted by Computational Fluid Dynamics," TAPPI J., vol. 75, no. 3., pp. 133-138, 1992.

10. Horton, R., Slayton, D., Grace, T., and Adams, T., "Sensitivity Studies of In-flight Black Liquor Combustion Using a Three-Dimensional Computer Model," AIChE Annual Meeting, Miami Beach, 1992.

11. Abdullah, Z., Salcudean, M., Nowak, P., and Gartshore, I., "Investigation of Interlaced and Opposed Jet Arrangements for Recovery Furnaces," TAPPI Engr. Conf. Proc., 1992.

12. Adams, T., Empie, H., Frederick, W., Grace, T., Horton, R., Huppa, M., Lee, S., Lien, S., Hichols, K., Thompson, L., Verrill, C., and Veverka, P., "Black Liquor Combustion-Validated Recovery Boiler Model," Report No. 2, U. S. DOE Contract No. DE-FG02-90CE40936, Dec. 1992.

13. Empie, H. L., S. J. Lien, W. R. Yang, and T. N. Adams, "Spraying Characteristics of Commercial Black Liquor Nozzles," TAPPI Int. Chem. Rec. Conf. Proc., Seattle, 1992.

14. Launo, T., "Recovery Boiler Exit Temperature," Masters Thesis, Lappeenranta University of Technology, 1989.

15. Horton, R. R., T. N. Adams, and T. M. Grace, "The Effects of Black Liquor Spray Parameters on Combustion Behavior in Recovery Furnace Simulations," TAPPI Int. Chem. Rec. Conf. Proc., Seattle, 1992.

ACKNOWLEDGMENTS

Funding for the development of the recovery boiler model at IPST came from member companies and the U. S. Department of Energy under contract DE-FG02-90CE40936. Mill trial data and modeling support was provided by Ahlstrom Corporation. The authors wish to acknowledge the assistance of mill personnel in the Kaukas trials.

Proposals
Submitted
to the
U.S. Department of Energy

PULSATING GASIFICATION OF BLACK LIQUOR

by

Dr. Thomas M. Grace and Dr. Robert R. Horton
Institute of Paper Science and Technology

and

Dr. Ben T. Zinn and Dr. J. I. Jagoda
Georgia Institute of Technology

A Research Proposal to
the U. S. Department of Energy
NOPI Number DE-NP-02-93CH10566

Research, Development, and Demonstration
of Advanced Technologies for the
Pulp and Paper Industry

PROJECT OVERVIEW

Objective

This proposal describes a four-phase project whose goal is the development of a novel black liquor gasifier. The proposed gasifier will utilize recently developed tunable pulse combustor technology to improve the efficiency and yield of a direct-fired black liquor gasifier. The first phase of the project will determine whether a high intensity, resonant acoustic field will permit a nearly complete gasification of black liquor in a short residence time reactor at temperatures below the ash melting point. The second and third phases will address critical issues of gasifier design and prove the feasibility of acoustic resonance enhanced black liquor gasification at the pilot scale. The fourth and final phase will cover engineering, construction and demonstration of a prototype pulsating black liquor gasification reactor at a mill site.

Rationale for Proposed Work

There is currently intense interest in the development of new, commercially attractive black liquor gasification technologies. These are expected to replace the existing Tomlinson recovery boiler technology in the next 10 to 15 years in the kraft pulp industry. Black liquor gasifiers have the potential for allowing lower capital cost installations that are modular in nature. They also are capable of providing a fuel for combined-cycle power generation, which could permit significantly greater amounts of electrical energy to be produced from the fuel value of the black liquor.

One type of improved black liquor gasification process would be a short-residence-time, partial combustion reactor operating at temperatures below the ash melting temperature and at oxygen consumption ratios well under 50% of the stoichiometric value. This would produce a gas with a greater heating value and allow the use of dry separation technology for removing the inorganic from the product gas, eliminating an energy consuming quench step.

Conversion of the organic matierial in black liquor to gases actually consists of two separate steps: 1) pyrolysis (thermal decomposition) which produces combustible volatiles and a char residue, and 2) char gasification in which the char carbon remaining after pyrolysis reacts with O_2, H_2O, or CO_2 to form CO. The key to the new gasification technology described above is the ability to achieve a very high degree of conversion of black liquor carbon to gases during pyrolysis while minimizing the amount of char carbon formed. Gasification of char carbon is kinetically limited at low temperatures and reaction rates are relatively low. The need to overcome these kinetic limitations is the reason that existing short-residence-time gasification technologies operate at high temperature (well above the ash melting point).

There is a good probability that intense acoustic fields, such as may be generated by recently developed tunable pulse combustors [1,2], can increase the degree of carbon conversion to gases during pyrolysis at relatively low temperatures. It is well known that the excitation of high intensity sound is accompanied by increases in the rates of mass, heat transfer and mixing within the system [3-6]. It is expected that similar increases in the rates of transport processes will occur within acoustically excited gasifiers. It is quite possible that such increases in the rates of heat and mass transfer to and from pyrolyzing black liquor particles will increase the rates of gas-forming fragmentation reactions relative to rates of the char-producing condensation reactions. This would significantly increase the fraction of black liquor carbon converted to gas.

Black liquor gasification is an endothermic process that is maintained by energy supplied by another source such as partial combustion of the black liquor within the gasifier. Gasification of black liquor particles in an entrained flow gasifier requires that these particles be heated by convection from the surrounding gases. There exists considerable evidence suggesting that this could be enhanced by exciting large amplitude pulsations within the gasifier. Furthermore, the increases in the rates of mixing and mass transfer in the vicinity of the black liquor particles will increase the rate at which compounds formed by gasification will be removed from the vicinity of the particles, which will further increase the rate of formation of these compounds by the gasification process.

The only known practical approach for exciting large amplitude pulsations within a large scale gasifier is by resonant driving [1,2] of acoustic oscillations within the gasifier with an appropriate acoustic driver. Such a driver must be retrofitted to the gasifier and operated at a frequency of one of the natural acoustic modes of the gasifier. Since these frequencies are generally not known in advance, because of the complex geometry of the gasifier and non-uniformity of the properties inside, the condition of resonant driving must be determined empirically on site. One or more pressure transducers attached to the gasifier walls are used to determine the variation in the amplitude of the gasifier pulsations in response to changes in the frequency of the tunable pulse combustor. Resonant driving occurs at frequencies that produce maximum amplitude pulsations within the gasifier. It has been shown that resonant driving increases the rates and thermal efficiencies of water spray evaporation [2,7], metal heating [6] and limestone calcining [2], which,like gasification, are controlled by rates of mass, momentum and heat transfer.

In summary, it is expected that application of the above described resonant driving technology to an entrained flow gasifier will improve both the partial combustion and gasification processes. Most importantly, it may permit operating the gasifier at lower temperatures, which will prevent melting of inorganic species, while increasing the energy output of the process.

Summary of R&D Plan

The proposed project is divided into the following four phases.

> Phase I : Feasibility Investigation. Demonstrate that intense acoustic oscillations can produce practically complete gasification of black liquor in a short residence time reactor at temperatures below the ash melting point. Acquire and interpret fundamental data on the effect of various acoustic waves and related process variables on carbon conversion during black liquor pyrolysis/gasification.
>
> Phase II : Engineering Development. Acquire additional data to assist in designing a pilot scale gasifier. Develop preliminary process concepts, identify critical gasifier reactor design issues, and design the pilot unit for Phase III testing.
>
> Phase III : Proof-of-Principle Testing. Prove out reactor design concepts and other aspects of the technology at a pilot-scale level. Construct a pilot unit and test critical elements of the new technology. Provide the framework for demonstrating a commercial prototype.
>
> Phase IV : Demonstration of Commercial Prototype. Demonstrate a prototype pulsating black liquor gasification unit at a mill site.

The Phase I effort is aimed at obtaining the fundamental information on the effect of high intensity acoustic fields on black liquor gasification. This information is needed to establish the validity of enhanced gasification. Phase II research will provide information necessary to further develop reactor pilot scale design concepts in Phase III.

Black liquor particles entrained in a hot flow will be passed through a tube gasifier simulator in which controlled acoustic fields can be excited. Tests will be conducted with and without pulsations in the gasifier and the volatiles and collected solid residues generated by the gasification/pyrolysis process will be chemically analyzed. Tests will be repeated with pulsations having different amplitudes and frequencies, different particle diameters, and different test section temperatures and velocities (which will determine the residence time of the particles in the gasification section). Analysis of the measured data will determine the effect of the pulsations' amplitude and frequency, and operating conditions on the gasification process. Specific attention will be paid to obtaining closed material balances for the key elements in black liquor over the test setup, which will be essential for ensuring the reliability of the measured data.

Most of the Phase I studies will be carried out with soda-process black liquor, which is much easier to handle in the laboratory than kraft-process black liquor. This will allow the proposed efforts to focus on pyrolysis and carbon conversion reactions without the complications associated with sulfur compounds and reactions. A limited number of tests will be conducted

with kraft black liquors in order to determine whether the origin (i.e., soda or kraft pulping) of the black liquor may significantly affect the behavior of the organics and char carbon during the proposed pulsating gasification process. Phase II will investigate wet black liquor feeds and will examine more closely the ash by-product and sulfur chemistry for kraft black liquors.

Overall Schedule

The proposed project is divided into four phases.

Phase I : Feasibility Investigation.

Phase II : Engineering Development.

Phase III : Proof-of-Principle Testing.

Phase IV : Demonstration of Commercial Prototype

Phases I and II will each require one year to complete. This will result in the specification of the technical requirements for a pilot unit design to be used in Phase III. Phase III will require one and a half years. It will involve the construction and operation of a gasifier pilot unit, and further development of the pulsating gasifier process. In addition, some of the Phase III efforts will be devoted to finding domestic industrial partners for commercial demonstration of the proposed pulsating gasifier concept under Phase IV.

The Evolution of Fuel Nitrogen During Black Liquor Pyrolysis

Denise Martin
Ph.D. Candidate

Dr. Earl W. Malcolm(primary advisor)

A490
Chemical & Biological Sciences Division

Institute of Paper Science & Technology
Atlanta, Georgia

March 24, 1994

The Evolution of Fuel Nitrogen During Black Liquor Pyrolysis

Introduction

Concern for ambient air quality has forced the pulp and paper industry to monitor and reduce emissions which contribute to air pollution. The oxides of nitrogen, NO_X, are of particular interest in the emissions from the combustion of black liquor during kraft recovery boiler operations. NO_X includes the species of nitric oxide, NO, nitrogen dioxide, NO_2, and nitrous oxide, N_2O. NO accounts for 95 % of the measured emissions and as such is the focus of most NO_X investigations.

The NO_X formation mechanisms are also based on NO and include thermal, prompt, and fuel NO formation. Thermal NO is generated by the oxidation of atmospheric molecular nitrogen at high temperatures. The Zeldovich mechanism, characterized by equations 1-3, describes the oxidation reactions which occur.[1]

$$O + N_2 \leftrightarrow NO + N \qquad \text{(Eq. 1)}$$
$$N + O_2 \leftrightarrow NO + O \qquad \text{(Eq. 2)}$$
$$N + OH \leftrightarrow NO + H \qquad \text{(Eq. 3)}$$

Prompt NO occurs during the very rapid reactions of hydrocarbon fragments with atmospheric molecular nitrogen. These reactions (Eqs. 4 and 5) only occur during incomplete combustion and represent a very small portion of the total NO formed.[2]

$$CH + N_2 \leftrightarrow HCN + N \qquad \text{(Eq. 4)}$$
$$CH_2 + N_2 \leftrightarrow HCN + NH \qquad \text{(Eq. 5)}$$

Fuel NO is formed from the oxidation of the nitrogen in the fuel. The reaction mechanism involves literally hundreds of reactions but is often simplified to that given in equation 6. The nitrogen in the fuel is released into the gas phase forming intermediate species such as HCN and NH_i. These species are then oxidized to NO or reduced to N_2 depending on the oxygen available in the system.[3]

$$\text{Fuel-N} \rightarrow HCN \rightarrow NH_i \rightarrow NO \text{ or } N_2 \qquad \text{(Eq. 6)}$$

While full details of the fuel NO formation mechanism are unknown, several simplified trends have been noted in various combustion systems. The conversion of fuel nitrogen to NO increases with decreased fuel nitrogen content and the formation of NO increases with increased fuel nitrogen content. Thus, as the fuel nitrogen content increases, more NO is formed; however, the conversion of the fuel nitrogen to NO is lower.

The temperatures for black liquor combustion during recovery boiler operation are to low to generate a significant amount of thermal NO. Therefore, the measured emissions likely occur from the fuel NO formation mechanism. While the fuel nitrogen content in black liquor is very low, approximately 0.1 % N based on dry liquor solids, a conversion of about 20 % could represent the majority of the NO that is measured. Conversions of fuel nitrogen in black liquor have been measured to be about 20-80 % during various laboratory and commercial tests. Therefore, the major source of NO emissions during black liquor combustion is likely the oxidation of the fuel nitrogen. A better understanding of this formation process with regard to liquor characteristics and operational parameters is desirable.

The primary objective of the current study is to evaluate the effects of pyrolysis temperature, heating rate, black liquor solids level and the structure of the major black liquor nitrogen compounds on the evolution of NO_X precursors during black liquor pyrolysis as it relates to the formation of fuel NO during recovery boiler operations. The experimental approach for the investigation is three-fold. First, evaluation of the nitrogen components in the liquor and the liquor composition are evaluated. Second, process parameters, as previously indicated, are evaluated for effects on black liquor nitrogen release during inert pyrolysis. Third, the results from one and two above will be used to create a mechanistic or global kinetic representation of the fuel nitrogen pathway during black liquor pyrolysis. The resulting equation(s) should be applicable to the recovery boiler computer modeling project and therefore, be useful in practical situations.

Results and Discussion

The results to date have been focused on evaluation of the liquor components and work has been initiated to evaluate several parameters during pyrolysis. The liquor nitrogen content observed in five different concentrated kraft black liquors has been found to be less than the reported 0.1 % average. The nitrogen content of the liquors are identified in Table 1.

Table 1. Nitrogen content (% based on dry solids) for five kraft black liquors at solids from 68-75 % dry solids.

LIQUOR	% N (based on dry solids)
Pine	0.06
Pine/Birch	0.07
Eucalyptus	0.09
Southern Pine I	0.06
Southern Pine II	0.06

The structure of the nitrogen in two of the liquor samples was also evaluated. Nitrogen was observed in the Southern Pine I in the form of nitrates, amines, and heterocyclic nitrogen. Similar nitrogen structures were observed in the Southern Pine II. These are identified in Table 2. While the structures of these compounds are very similar

in nature, some differences also exist in basic structure as well as in the quantities of these species. To date, a complete nitrogen balance for these components in the black liquors has not been made. This information provides the chemical structure of the nitrogen and therefore, the beginning point for potential fuel NO mechanisms.

Table 2. Nitrogen structures observed in two Southern Pine kraft black liquors.

SOUTHERN PINE I	SOUTHERN PINE II
• Nitrate (NO_3^-)	• Nitrate (NO_3^-)
• Protein (NH_3)	• Protein (NH_3)
• Amino Acids	• Amino Acids
Glutamic Acid	Glutamic Acid
Proline*	• Hetercyclic Nitrogen
Aspartic Acid	Indole*
Cystine	Pyrazine*
Valine	Pyrimidine*
Leucine	

Several points to note include the following. First, the nitrogen content is very low for kraft black liquors. In the liquors measured, the nitrogen content was less than the reported 0.1 % N average. Second, the nitrogen was present in the form of nitrate, amine, and heterocyclic ring structures suggesting various pathways for the fuel nitrogen to be released. Third, variations both in nitrogen content and in the structure of the nitrogen species do exist between liquors indicating the potential for the fuel nitrogen release to be liquor specific.

Two sets of pyrolysis experiments have been completed to date. The first involves effects of the liquor components on the decomposition of model fuel nitrogen species (nitrogen as amine and in heterocyclic ring structures). The second involved inert pyrolysis of individual droplets and measurement of the nitrogen release from 300-1000 °C at 100 and 200 °C intervals. In the first set of experiments, the effects of the anion species (sulfate, sulfide, and carbonate) on fuel nitrogen model compounds volatiles yield and decomposition onset temperature during inert pyrolysis were determined. Both sulfate and carbonate were found to have a significant effect on both of these parameters. With the addition of sodium, two trends were observed. As the amount of sodium increased in the system, the expected volatiles yield decreased. Also, the increased sodium increased the expected temperature for the onset of decomposition. This likely results from the organic nitrogen species being bound, either chemically or physically, to the sodium in the system.

The inert pyrolysis experiments were carried out for individual commercial black liquor droplets in a tube furnace. The nitrogen released during pyrolysis was measured as NO and as NH_3. The residual chars were analyzed for nitrogen and the difference between the original nitrogen content and the nitrogen accounted for as NO, NH_3, and

char nitrogen was assumed to be volatile nitrogen released to form N_2. Comparisons of the measured volatile nitrogen and of the total measured nitrogen for four commercial liquors are presented in Figures 1 and 2. Figure 1 indicates the change in the volatile nitrogen release with increasing temperature. Also, the majority of the fuel NO species appear to be released as NO under the inert pyrolysis conditions employed. In Figure 2, the volatilized nitrogen was released primarily by 500-600 °C. A summary of the nitrogen release for the four liquors tested is provided in Figure 3.

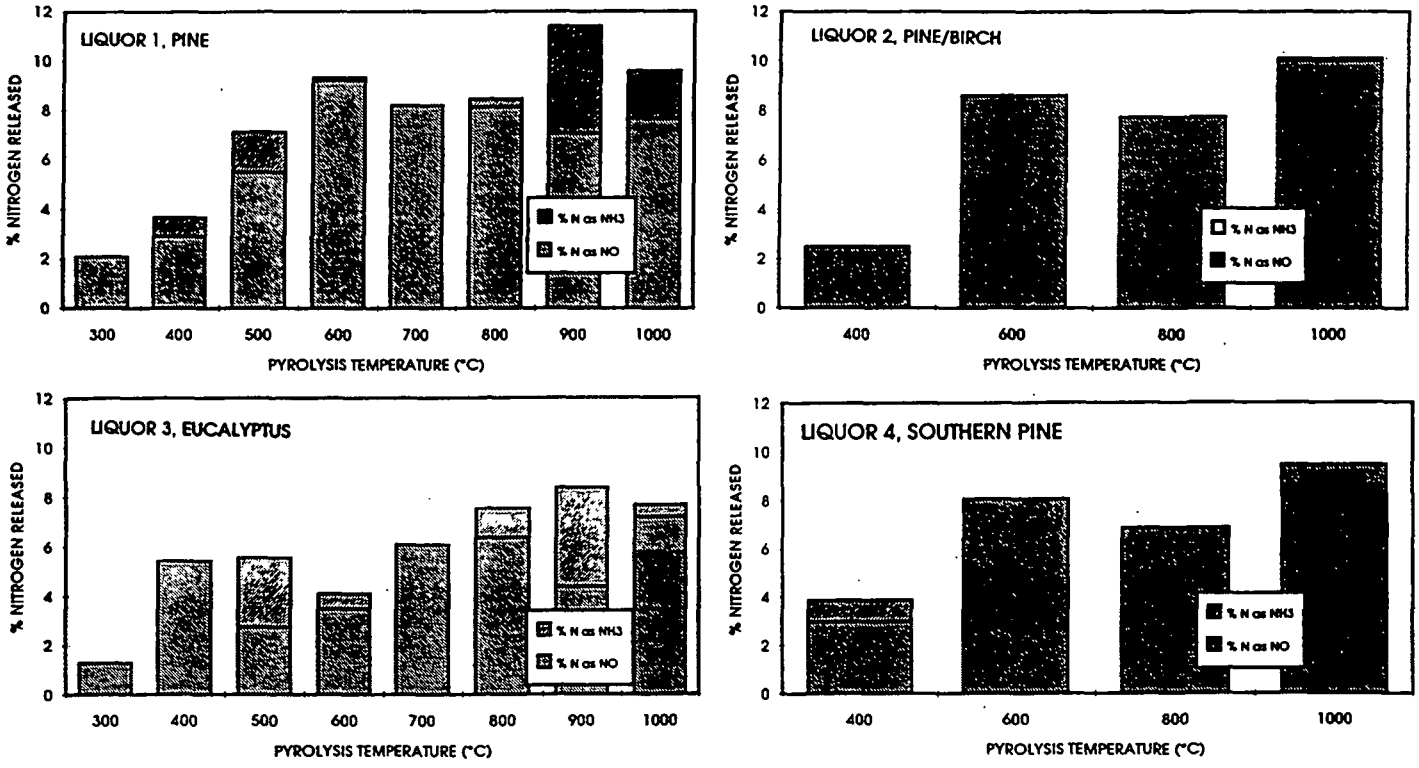

Figure 1. Nitrogen release as NO and NH_3 as measured from four commercial kraft black liquors during individual droplet pyrolysis in inert conditions.

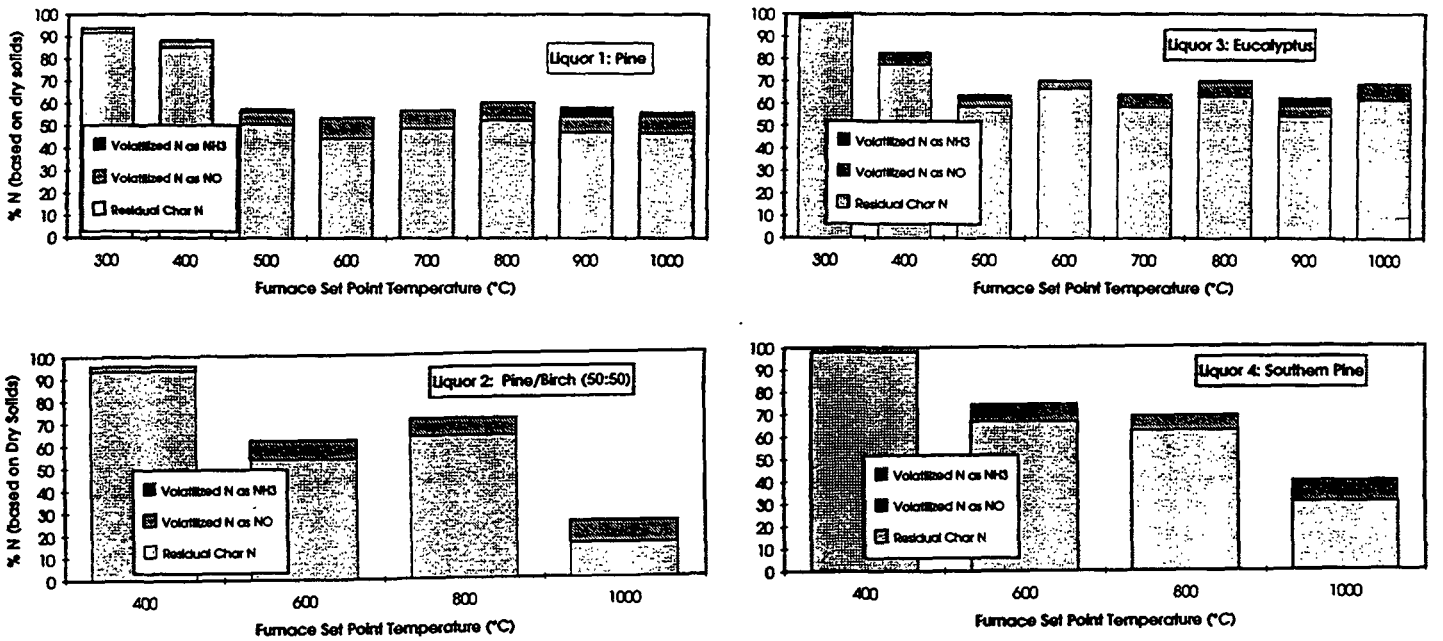

Figure 2. Total measured nitrogen for droplet pyrolysis in inert conditions for four commercial kraft black liquors.

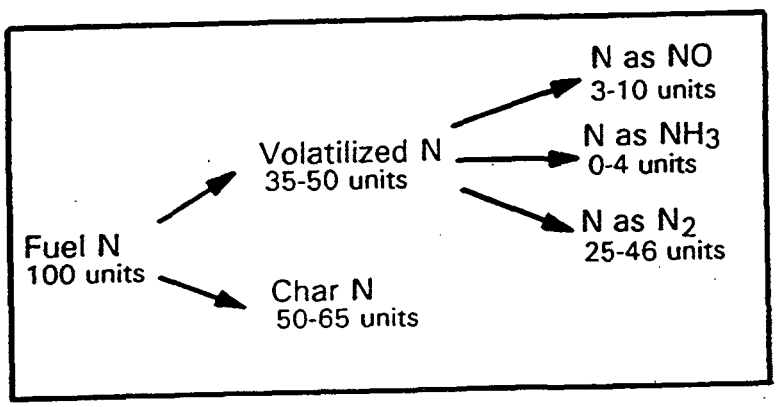

Figure 3. Summarized pathway for nitrogen release of kraft black liquor during inert pyrolysis over the temperature range from 500-900 °C.

Conclusions

To summarize the results to date, previous literature supports the formation of NO_X emissions from the nitrogen in the black liquor. As such, the need for a better understanding of the nitrogen in the black liquor as a source and its ultimate release during the combustion process is warranted.

Current investigations have shown the black liquor nitrogen content to be very low for the kraft liquors investigated, less than the reported average of 0.1 % N based on dry solids. The nitrogen has been observed as nitrates, amines, and in heterocyclic compounds indicating various pathways for the fuel NO formation. Variations in the liquor nitrogen concentration and species occur indicating these to be liquor specific.

Inert pyrolysis experiments with model systems have shown the inorganic composition to be important with regard to the onset temperature for decomposition and volatiles yield of the fuel nitrogen components. Sulfate and carbonate were significant as well as the sodium content. The initial addition of sodium to the system greatly affected the expected volatiles yield for the model fuel nitrogen compounds and also shifted the expected decomposition into a higher temperature range. These phenomena are most likely explained by a complexation which occurs between the inorganic species and the organic fuel nitrogen model compounds.

The inert pyrolysis of the commercial black liquors indicated that the volatile nitrogen is released by 500 °C. In the 500-900 °C range, approximately 35-55 % of the original liquor nitrogen is volatilized with 3-10 % as NO, 0-4 % as NH_3, and 25-46 % as N_2. The variations observed within the experimental results and with previously reported data[4] may be due to liquor variations and experimental conditions. Further investigations into these differences are needed.

Future Activities

Future experiments are planned to further investigate the effects of the liquor composition both in terms of the inorganic composition and the fuel nitrogen structure. Both synthetic and commercial black liquors will be used in the studies. Also, inert pyrolysis experiments will be done on both types of liquors. The nitrogen release will be measured at various heating rates and different pyrolysis temperatures so that a better understanding can be obtained of the generation of NO_X precursors with respect to fuel NO formation during black liquor combustion.

Literature Cited

1. Zeldovich, J. Acta Physiochimica U.R.S.S. 21(4):577-628 (1946).
2. Hayhurst, A. N.; Vince, I. M. Progress in Energy and Combustion Science. 6:35-51 (1980).
3. Bowman, C. T. in Fossil Fuel Combustion: A Source Book. Bartok, W.; Sarofim, A. F., eds. John Wiley & Sons, Inc., New York, NY (1991).
4. Aho, K.; Hupa, M.; Nikkanen, S. TAPPI Engineering Conference Proceedings, Book 1, Orlando, FL, September 1993. pp. 377-384.

The Depletion of NO_x in a Kraft Recovery Furnace

Laura M. Thompson
Ph.D. Candidate

Advisory Committee:
Dr. Jeff Colwell
Dr. Jeff Empie (primary advisor)
Dr. Lucy Sonnenberg

A490
Chemical & Biological Sciences Division

Institute of Paper Science & Technology
Atlanta, Georgia

March 24, 1994

Summary

This study investigates NO_x reactions with sodium compounds as a potential depletion mechanism which is unique to the operation of kraft recovery furnaces. Experiments have been conducted in which nitric oxide (NO) is bubbled through molten sodium carbonate. Conversions of 20-70 % have been observed over the temperature range of 860-960 °C. The rate of depletion appears to be mass transfer controlled over this temperature range. Preliminary analytical work indicates that NO is being converted to other gaseous products, such as N_2 or N_2O.

Objectives

The overall objective of this thesis is to determine if reactions of NO with sodium species provide a depletion mechanism for NO in kraft recovery furnaces. Specifically, the rate of depletion of NO will be determined for use in emissions modeling. Also, a mechanistic explanation for the depletion will be proposed.

Background

In order to predict NO_x emissions from a combustion process, one must understand both the rate of formation and the rate of depletion of the NO_x species. NO_x emissions from recovery furnaces typically account for only 25 % of the nitrogen in black liquor. At the low concentration of nitrogen in black liquor (approximately 0.1 %) a much higher conversion to NO would be expected (on the order of 80%). Also, it is understood that reactions of SO_x with sodium species provide a natural scrubbing mechanism for SO_2. The result is the formation of sodium sulfate which is captured as dust in the electrostatic precipitators. For these reasons, it seems likely that

depletion of NO is occurring in recovery furnaces and the contact of NO_x with sodium species could be a mechanism for depletion.

Experimental

An experimental apparatus has been designed in which a known concentration of nitric oxide is bubbled through molten sodium salts. This apparatus is shown below in Figure 1.

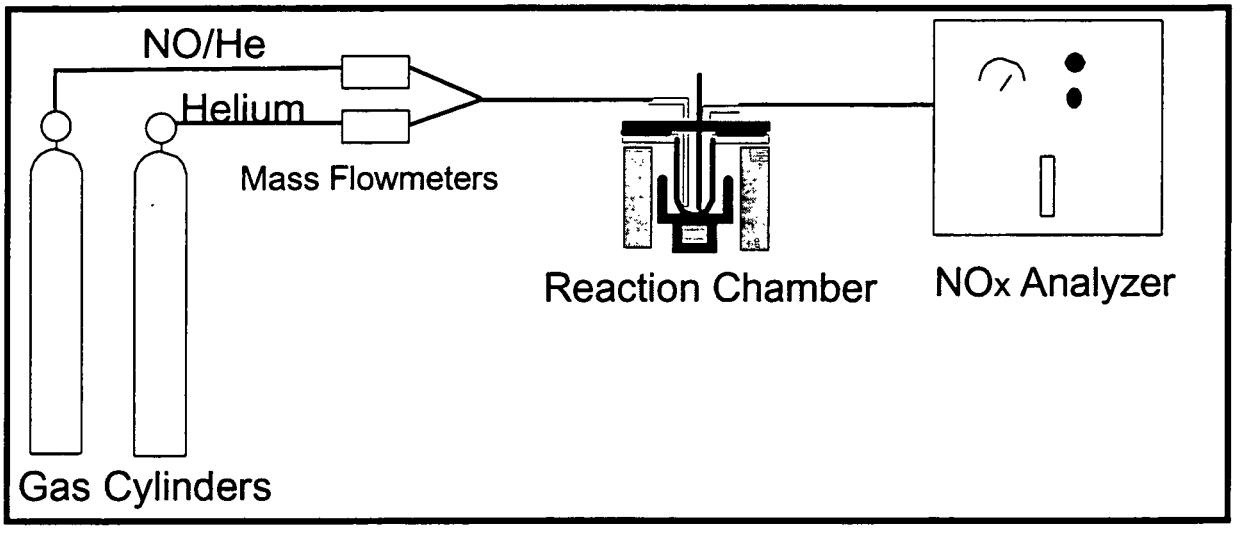

Figure 1: Experimental Apparatus

Gas is fed from pressurized cylinders through mass flow meters to the reaction chamber. The reaction vessel consists of a two inch diameter alumina crucible which contains sodium carbonate. The crucible is suspended in a tube furnace rated at 1000 °C. The gas entering the crucible flows through a 0.25 inch alumina tube and bubbles up through the bottom of the molten salt. The exit gas flows to a chemiluminescent NO_x analyzer. By measuring the concentration of NO in the off gas, it is possible to determine the rate of depletion of NO.

Results

For NO in contact with molten sodium carbonate, conversions of 20-70 % have been observed over the temperature range of 860-960 °C. The rate of depletion appears to be mass transfer controlled. Experimental data fits the expression:

(1) $-\ln(y_f/y_i) = (a/H\rho)(1/1-\varepsilon)(mk/V)$

where, y = mole fraction of NO
a = surface to volume ratio (m^2/m^3)
H = Henry's Constant (mol/m^3)
ρ = density of molten salt (kg/m^3)
ε = volume fraction of gas
m = mass of molten salt (kg)
k = mass transfer coefficient (m/s)
V = volumetric flow rate of gas (m^3/s)

The variables: H, ρ, k are dependent on temperature while the surface to volume ratio, a, and ε are dependent on the volumetric flow rate. Analysis of the nitrogen content in the residual salt does not account for the total NO lost in experimentation. This indicates conversion of NO to other gaseous products (such as N_2O, or N_2).

Future Work

Further experimentation is planned to validate the mass transfer model. Variables that will be manipulated are: the mass of salt, flow rate of gas, inlet concentration of NO and temperature. Additional analytical work is planned to close the nitrogen mass balance and identify reaction products. Specifically, samples of the off gas will be analyzed for total nitrogen. This analysis accounts for all nitrogen except N_2. By comparing the exit NO concentration to the total nitrogen, it will be possible to determine the concentration of N_2 by difference. Future work will also include experiments in which sodium sulfide (Na_2S) is added to the molten salt.

KRAFT BLACK LIQUOR DELIVERY SYSTEMS
(DOE Funded)

PROJECT 3657-2

H. Jeff Empie
Steve Lien
Don Sachs

March 24, 1994

Institute of Paper Science and Technology
500 10th Street, N.W.
Atlanta, Georgia

TECHNICAL PROGRAM REVIEW
FY 93-94

Project Title:	KRAFT BLACK LIQUOR DELIVERY SYSTEMS (DOE Funded)
Project No.:	3657-2
Division:	Chemical and Biological Sciences
Project Staff:	Jeff Empie, Steve Lien, Don Sachs
FY 93-94 Budget:	$153,000

IPST GOAL:

Increase recovery boiler capacity and operating efficiency through improved black liquor spraying technology.

OBJECTIVE:

Develop new and improved black liquor spraying nozzles that give the operator some capability to control droplet size and size distribution.

PRIOR RESULTS:

Early results were obtained on the performance of the three basic types of black liquor spray nozzles: the splashplate, the swirl cone, and the U- and V-jets. From the visual analysis of the video tapes of the spray patterns, it was apparent that the solids concentration of the black liquor had a strong effect on droplet formation. At low solids (50%), the majority of the drops were spherical, but at high solids (70%), most of the images were large, irregularly shaped drops connected to strings and filaments.

Accuracy of droplet measurements by image analysis was assessed by using ball bearings and cylinders of known diameter. Error was less than 6% for diameters greater than 2 mm; the minimum quantitatively measurable diameter was about 0.5 mm (+/- 50%). Measurement of actual black liquor drops is less precise because the background is less uniform and some particles can be out of focus.

Several drop size distribution models were tested to fit the experimental data; the best one continued to be the square root-normal distribution. It was shown that the ratio of the standard deviation to the square root of the mass median diameter has a

constant value of 0.2, and therefore only one parameter, the mass median diameter, is necessary to characterize the square root-normal distribution for black liquor sprays.

A test series with the B&W splashplate, CE swirl cone, and SS V-jet nozzles was completed, using a 3x3x3 matrix (solids of 50, 60, and 70%; viscosities of 270, 90, and 30 cP; and nozzle pressures of 15, 30, and 45 psig). Pressure vs. flow rate correlations were derived as a function of Reynolds Number. For the three tests at high viscosity and low pressure, the flow rate was too low to produce sheet breakup.

Data on droplet size distributions from a B&W splashplate nozzle and a CE swirl cone nozzle showed a weak dependence on liquor velocity and fluid physical properties. The ratio of mass median droplet diameter to nozzle diameter was related to the product of Reynolds Number and Euler Number, each raised to some experimentally determined non-integral power; similarly, Euler and Schmidt Numbers also correlated well. Both dimensionless correlations were broken down into the product of the individual physical parameters, each raised to some experimentally determined power. It was shown that the parameters which most strongly influenced mass median drop diameter were nozzle diameter, and liquor density and velocity. At high solids levels, liquor viscosity became important. When droplet diameter was empirically correlated with velocity and temperature raised to appropriate exponents, drop size was shown to decrease as either operating parameter was increased.

A study of the behavior of spray nozzles at liquor temperatures above the atmospheric boiling point was performed. Three different nozzles were tested at temperatures ranging from 200 to 270°F using 65% solids liquor. As temperature was increased, drop diameter gradually decreased until a transition temperature was reached (6-9°C above the atmospheric boiling point) where the drop size abruptly decreased by about 20%; the normalized standard deviation for the drop size distribution remained unchanged at 0.2. This effect was accompanied by a noticeable change in the physical appearance of the spray. The normally planar spray sheet became oval in cross-section, and, for a splashplate nozzle, the central plane of the sheet came off the plate at a 20 to 40 degree angle, rather than at zero degrees. These phenomena can be attributed to flashing at the nozzle.
This effect would result in a several-fold increase in the number of drops being fired into the furnace, increasing burning rates and possibly carryover rates.

Spraying tests on five different black liquors from four kraft mills were conducted to determine the effect of liquor type on droplet size and size distribution. A wide range of spraying conditions was examined with the finding that liquor type was not important at comparable viscosities; mean drop diameter depended primarily on nozzle type and diameter, pressure, temperature, and liquor viscosity.

Measurements were made of the local distribution of liquor flow in the spray pattern as a function of the angle from the sheet centerline. Results for both the

splashplate and V-jet nozzles showed the mass flow distribution to be parabolic, with the maximum mass flow at the centerline and decreasing with increasing angle. Limited analysis of drop size as a function of the angle from the sheet centerline showed no significant difference.

A series of trials was conducted at James River's Camas Mill to study black liquor sprays in a recovery furnace environment. High-speed video images of sprays were taken through a gun port on Camas' No.4 recovery boiler. Three different nozzles were operated at two levels of liquor flow and fired liquor temperature. Changing one nozzle and/or firing conditions for a short period of time did not produce significant changes in furnace operation as indicated by particulate count or lower furnace temperatures. There was evidence of liquor sheet breakup by perforation, which agrees with the findings of the present study. Differences in sheet breakup between nozzles were seen in the video images; however, it was not possible to detect variation due to firing conditions. The video images were optically too dense to determine droplet size distribution by image analysis.

Alternative commercial nozzles were surveyed, including two-phase, sonic, and rotary atomizers and full-cone nozzles with and without swirl. Most of these strive to give very fine droplets or mists, which are unsuitable for recovery boiler operation. Ultimately, three of these nozzles were tested, and only one, the Delavan Raindrop©, exhibited any noticeable difference in performance. It gave a coarser-than-normal droplet size, but did not result in a different distribution width. None of the alternative commercial nozzles demonstrated any ability to give independent control over drop size distribution.

Development of new nozzle concepts started with modified splashplate nozzles with no moving parts. Making various physical changes to the surface of the splashplate (e.g., grooves, slots) resulted in 25% smaller median drop diameters, with no change in the distribution width. One design, on which small cylindrical pegs were mounted normal to the splashplate surface around its outer periphery, also gave smaller drops, but with a larger normalized standard deviation, characteristic of a bimodal distribution. A different design specifically aimed at generating a bimodal distribution employed two different sized orifices back-to-back using opposite sides of the same splashplate. The two liquor sheets formed tended to interact during break-up, giving larger-than-normal droplets with the usual distribution width. The two orifice conditions tested were not different enough to give component median diameters far enough apart that would yield a recognizable bimodal distribution.

It is apparent that gaining any degree of control over drop size distribution is going to require some external force, independent of the viscous, momentum, and surface tension forces which fundamentally control the droplet formation process. The concept of vibratory assist should provide an independently controlled means of influencing the sheet formation/break-up process. Application of vibrations normal to the plane of the sheet gave a 15-30% increase in median diameter and distribution width using an air vibrator, but no change in either parameter using a mechanical

vibrator. Vibration in the direction of flow (i.e., pulsation) is expected to be more effective for reducing the randomness of the sheet break-up process.

SUMMARY OF RESULTS SINCE LAST REPORT:

Two nozzle designs featuring axial vibratory assist were conceptualized, fabricated, and tested with the black liquor spray apparatus. The more promising design could pulse the liquor flow by interrupting the flow at frequencies up to 270 Hz. Reliable operating characteristics were demonstrated. Results showed a weak dependence of drop size distribution width on pulsation frequency, with the distribution narrowing slightly as frequency increased. The existence of a harmonic frequency where the distribution width exhibits a local minimum is suspected, but must still be substantiated.

The second design pulsed the flow directly by +/-20% for frequencies up to 150 Hz. No dependence of median drop size or size distribution width was detected. Nozzle operating characteristics were less reliable with this design.

An alternative independent external force that can be applied to spray sheet break-up is an electrostatic one using dielectrophoresis. The non-uniform electric field applied can exert a force on the electrically neutral droplets in a direction normal to the bulk flow direction. This has potential for promoting droplet coalescence, and hence could skew the drop size distribution away from the smaller sizes. The limited data obtained did not substantiate the desired effect.

PLANNED ACTIVITY THROUGH FY 95:

*Develop and test a high frequency vibratory device to induce a pulsed liquor flow in an attempt to reduce the randomness of the liquor sheet break-up process.

*Provided that positive results are obtained with the developmental vibratory assist nozzle, select a host mill for mill scale testing of a vibratory-assisted prototype nozzle for performance comparison with existing nozzles.

*Using existing commercial nozzles, collect extensive drop size data at temperatures above the transition point.

*Obtain drop size data for a range of nozzle diameters under standard spraying conditions using conventional nozzles.

KRAFT BLACK LIQUOR DELIVERY SYSTEMS

by

Jeff Empie, Steve Lien, Richard Rumsey, and Donald Sachs

ABSTRACT

An improved spray nozzle for black liquor injection into kraft recovery boilers is expected to result from obtaining a controlled, well-defined droplet size distribution. An environmentally sound experimental spray facility capable of delivering black liquor at normal firing temperatures has been installed and operated at the Institute of Paper Science and Technology. Previous work showed that black liquor sprays have a characteristic size distribution which is determined by the fluid mechanical forces acting on the spray sheet issuing from the nozzle. Recent work has centered on applying an independently-controlled force on the sheet break-up process in an attempt to change the drop size distribution. Early results are presented which feature vibratory assist applied in the axial direction. An alternative concept employing dielectrophoresis is also explored.

EXECUTIVE SUMMARY

The research work described in this report represents the results of the fifth year of a multi-year project, now extended to a sixth, designed specifically to develop the optimum black liquor delivery system for the current recovery boiler. Black liquor obtained from normal mill operation is being used in this study.

The primary objectives of the research program have been:

*To develop laboratory equipment and methods for quantitatively studying commercial black liquor nozzle designs when spraying kraft liquors at typical operating conditions;

*To quantify droplet size distribution, velocity, and mass distribution for commercial nozzles spraying kraft liquors at typical boiler feed conditions;

*To develop techniques currently envisioned for improving the control of black liquor spray droplet size distribution with commercial nozzles; and

*To extend current liquor spraying technology by testing several fundamentally different, but commercially viable, delivery systems.

Success with this program should yield benefits in increased thermal efficiency and process productivity, as well as have potential for improvements in equipment design and process control. Coupled with the recovery boiler modeling project currently under way at IPST, the potential value of these programs to the industry is approximately $93MM/year for increased thermal efficiency and $240MM/year for increased productivity.

It is apparent from previous work that gaining any degree of control over drop size distribution is going to require some external force, independent of the viscous, momentum, and surface tension forces which naturally control the droplet formation process. The concept of vibratory assist should provide an independently controlled means of influencing the sheet formation/break-up process. Application of vibrations transverse to the plane of the sheet were reported last year to give a 15-30% increase in median diameter and distribution width using an air vibrator, but no change in either parameter using a mechanical vibrator. Vibration in the direction of flow (i.e., axial pulsation) is expected to be more effective for reducing the randomness of the sheet break-up process. Unfortunately, high frequency pulsation of flow is more difficult to accomplish experimentally and may require an "invention."

Two nozzle designs featuring axial vibratory assist were conceptualized, fabricated, and tested with the black liquor spray apparatus. The more promising design could pulse the liquor flow by interrupting the flow at frequencies up to 270 Hz. Reliable operating characteristics were demonstrated. Results showed a weak dependence of drop size distribution width on pulsation frequency, with the distribution narrowing slightly as frequency increased. The existence of a harmonic frequency where the distribution width exhibits a local minimum must still be substantiated.

The second design pulsed the flow directly by +/-20% for frequencies up to 150 Hz. No dependence of median drop size or size distribution width was detected. Nozzle operating characteristics were less reliable with this design.

An alternative independent external force that can be applied to spray sheet break-up is an electrostatic one using dielectrophoresis. The non-uniform electric field applied can exert a force on the droplets in a direction normal to the bulk flow direction. This has potential for promoting droplet coalescence, and hence could skew the drop size distribution away from the smaller sizes. The limited data obtained did not substantiate the desired effect.

MAJOR ACTIVITIES FOR YEAR SIX:

*Develop and test a high frequency vibratory device to induce a pulsed liquor flow in an attempt to reduce the randomness of the liquor sheet break-up process.

*Provided that positive results are obtained with the developmental vibratory assist nozzle, select a host mill for mill scale testing of a vibratory-assisted prototype nozzle for performance comparison with existing nozzles.

*Using existing commercial nozzles, collect improved drop size data at temperatures above the transition point.

*Obtain drop size data for a range of nozzle diameters under standard spraying conditions.

1.0 INTRODUCTION

1.1 OBJECTIVE

This research program was initiated as an applied effort to identify the optimum black liquor delivery system for the kraft recovery boiler and to present it to the industry in a timely fashion. Because it is not known what are the preferred conditions for optimum recovery boiler operation, the fundamental objective has to be to develop ways to control the formation of black liquor droplets such that, once the optimum conditions are actually known, the specified drop size and size distribution can be obtained and the optimum achieved. The recovery boiler modeling program currently under way at IPST may ultimately be the best way to establish what are the preferred operating conditions for optimum operation.

1.2 DELIVERABLES

This research effort has delivered or will deliver the following:

a) A test facility capable of quantitatively assessing the performance of commercially viable spray systems while processing kraft black liquors at typical furnace feed conditions.

b) The best commercial spray delivery system available with current technology.

c) An appraisal of the commercial viability of several fundamentally different black liquor delivery systems.

The first two items have been accomplished, and the third will be in the coming year.

1.3 BENEFITS

The objective of this program can be viewed as delivering the tools which will help to realize the benefits of several other research activities in the black liquor area. Primary among these is the fundamental recovery boiler modeling research currently underway at IPST under DOE sponsorship. This basic work will determine the optimum black liquor droplet size and velocity distribution to maximize effective use of the furnace volume. Development of a system to achieve this desired liquor distribution is the objective of the present program. Potential benefits from this applied study are the same as projected in last year's report on this project (1).

Thermal efficiency and process productivity goals are not independent. The recovery boiler is often the bottleneck in the entire pulping process. Thermal efficiency is often sacrificed for high productivity. Hence, thermal efficiency and productivity increases may not be realized simultaneously. On the other hand, the recovery boiler is the only pulp mill operation which can often claim that improved unit productivity will result in increased millwide productivity.

The in-place capital investment in recovery boiler technology is so large ($10 billion) that radical changes, expansions, and replacements will be rare for the foreseeable future. Barring a significant departure from the kraft process in the near term, the industry will be firing black liquor in conventional recovery boilers well beyond the year 2000.

1.4 ORGANIZATION

Organizational and technical responsibility for the Delivery Systems Project has remained with Dr. H. Jeff Empie, Professor, in the Chemical and Biological Sciences Division. Mr. Steven J. Lien, Associate Engineer in the Chemical Recovery Group, continues responsibility for equipment operation and data gathering/analysis. Mr. Richard S. Rumsey, a Master's Degree student at IPST, undertook a summer appointment to operate the spray facility and perform image analysis duties. Mr. Donald G. Sachs, Sr. Technician in the Chemical Recovery Group, now maintains responsibility for equipment installation and operation, as well as image analysis.

1.5 SCHEDULE

The work reported here covers the fifth year of the project. Because of the interruption caused by the 1989 move from Appleton, WI to Atlanta, GA by IPST, the project was extended by DOE so that the remaining tasks could be successfully completed.

1.6 SUMMARY OF PREVIOUS RESULTS

Early results were obtained on the performance of the three basic types of black liquor spray nozzles: the splashplate, the swirl cone, and the U- and V-jets. Video recordings of the spray pattern were made at four positions at distances of 34 to 44 inches from the nozzle. From the visual analysis of the video tape, it was apparent that the solids concentration of the black liquor had a strong effect on droplet formation. At low solids (50%), the majority of the drops were spherical, but at high solids (70%), most of the images were large, irregularly shaped drops connected to strings and filaments.

Accuracy of droplet measurements by image analysis was assessed by using ball bearings and cylinders of known diameter. Error was less than 6% for diameters greater than 2 mm; the minimum quantitatively measurable diameter was about 0.5 mm (+/- 50%). Measurement of actual black liquor drops is less precise because the background is less uniform and some particles can be out of focus.

Several drop size distribution models were tested to fit the experimental data; the best one continued to be the square root-normal distribution. It was shown that the ratio of the standard deviation to the square root of the mass median diameter has a constant value of 0.2, and therefore only one parameter is necessary to characterize the square root-normal distribution for black liquor sprays.

A test series with the B&W splashplate, CE swirl cone, and SS V-jet nozzles was completed, using a 3x3x3 matrix (solids of 50, 60, and 70%; viscosities of 270, 90, and 30 cP; and nozzle pressures of 15, 30, and 45 psig). Pressure vs. flow rate correlations were derived as a function of Reynolds Number. For the three tests at high viscosity and low pressure, the flow rate was too low to produce sheet breakup.

Data on droplet size distributions from a B&W splashplate nozzle and a CE swirl cone nozzle showed a weak dependence on liquor velocity and fluid physical properties. The ratio of mass median droplet diameter to nozzle diameter was related to the product of Reynolds Number and Euler Number, each raised to some experimentally determined non-integral power; similarly, Euler and Schmidt Numbers also correlated well. Both dimensionless correlations were broken down into a product of the individual physical parameters, each raised to some experimentally determined power. It was shown that the parameters which most strongly influenced mass median drop diameter were nozzle diameter, and liquor density and velocity. At high solids levels, liquor viscosity became important. When droplet diameter was empirically correlated with velocity and temperature raised to appropriate exponents, drop size was shown to decrease as either operating parameter was increased.

A study of the behavior of spray nozzles at liquor temperatures above the atmospheric boiling point was performed. Three different nozzles were tested at temperatures ranging from 200 to 270°F using 65% solids liquor. As temperature was increased, drop diameter gradually decreased until a transition temperature was reached (6-9°C above the atmospheric boiling point) where the drop size abruptly decreased by about 20%; the normalized standard deviation for the drop size distribution remained unchanged at 0.2. This effect was accompanied by a noticeable change in the physical appearance of the spray. The normally planar spray sheet became oval in cross-section, and, for a splashplate nozzle, the central plane of the sheet came off the plate at a 20 to 40 degree angle, rather than at zero degrees. These phenomena can be attributed to flashing at the nozzle.
This effect would result in a several-fold increase in the number of drops being fired into the furnace, increasing burning rates and possibly carryover rates.

Spraying tests on five different black liquors from four kraft mills were conducted to determine the effect of liquor type on droplet size and size distribution. A wide range of spraying conditions was examined with the finding that liquor type was not important at comparable viscosities; mean drop diameter depended primarily on nozzle type and diameter, pressure, temperature, and liquor viscosity.

Measurements were made of the local distribution of liquor flow in the spray pattern as a function of the angle from the sheet centerline. Results for both the splashplate and V-jet nozzles showed the mass flow distribution to be parabolic, with the maximum mass flow at the centerline and decreasing with increasing angle. Limited analysis of drop size as a function of the angle from the sheet centerline showed no significant difference.

A series of trials was conducted at James River's Camas Mill to study black liquor sprays in a recovery furnace environment. High-speed video images of sprays were taken through a gun port on Camas' No.4 recovery boiler. Three different nozzles were operated at two levels of liquor flow and fired liquor temperature. Changing one nozzle and/or firing conditions for a short period of time did not produce significant changes in furnace operation as indicated by particulate count or lower furnace temperatures. There was evidence of liquor sheet breakup by perforation, which agrees with the findings of the present study. Differences in sheet breakup between nozzles were seen in the video images; however, it was not possible to detect variation due to firing conditions. The video images were optically too dense to determine droplet size distribution by image analysis.

Alternative commercial nozzles were surveyed, including two-phase, sonic, and rotary atomizers and full-cone nozzles with and without swirl. Most of these strive to give very fine droplets or mists, which are unsuitable for recovery boiler operation. Ultimately, three of these nozzles were tested, and only one, the Delavan Raindrop @, exhibited any noticeable difference in performance. It gave a coarser-than-normal droplet size, but did not result in a different distribution width. None of the alternative commercial nozzles demonstrated any ability to give independent control over drop size distribution.

Development of new nozzle concepts started with modified splashplate nozzles with no moving parts. Making various physical changes to the surface of the splashplate (e.g., grooves, slots) resulted in 25% smaller median drop diameters, with no change in the distribution width. One design, on which small cylindrical pegs were mounted normal to the splashplate surface around its outer periphery, also gave smaller drops, but with a larger normalized standard deviation, characteristic of a bimodal distribution. A different design specifically aimed at generating a bimodal distribution employed two different sized orifices back-to-back using opposite sides of the same splashplate. The two liquor sheets formed tended to interact during break-up, giving larger-than-normal droplets with the usual distribution width. The two orifice conditions tested were not different enough to give component median diameters far enough apart that would yield a recognizable bimodal distribution.

It is apparent that gaining any degree of control over drop size distribution is going to require some external force, independent of the viscous, momentum, and surface tension forces which fundamentally control the droplet formation process. The concept of vibratory assist should provide an independently controlled means of influencing the sheet formation/break-up process. Application of vibrations normal to the plane of the sheet gave a 15-30% increase in median diameter and distribution width using an air vibrator, but no change in either parameter using a mechanical vibrator. Vibration in the direction of flow (i.e., pulsation) is expected to be more effective for reducing the randomness of the sheet break-up process.

2.0 EXPERIMENTAL DESIGN FOR BLACK LIQUOR SPRAYING:

The same spray facility, as reported previously in Progress Reports No. 4, 3, and 2 (1,2,3), continued to be used in this study. The system is designed so that both commercial spray nozzles, as well as new experimental designs, can be tested over a wide range of spraying conditions. The black liquor spray pattern is recorded on video tape, which is then subjected to computerized image analysis to yield drop size information.

2.1 PREVIOUS WORK:

Results of earlier work performed during years one through four of this project are described in Progress Reports No. 1-4 (4,3,2,1). A summary of this work is contained in Table 2.1.

Table 2.1 Four Year Experimental Test Plan

Year	Location	Activity
10/88-9/89	Appleton, WI	* Construction of spray facility * Preliminary testing with water, corn syrup, and black liquor * Measurement of Sheet Thickness and Sheet Velocity * Pressure vs. Flow correlations * Preliminary drop size analysi * Comparison of Flash X-ray vs. High Speed Video imaging
10/89-9/90	Atlanta, GA	* Design and Construction of environmentally acceptable black liquor spray facility
6/90	Camas, WA	* Mill Trial giving video recordings of black liquor sprays in an operating recovery boiler
10/90-9/91	Atlanta, GA	* Black Liquor Spraying - Effect of Nozzle Type, Liquor % Solids, Viscosity, and Flow Rate * Pressure vs. Flow Rate correlations * Black liquor chemical analysis and Viscosity correlations * Black Liquor Spraying - High Temperatures * Analysis of drop size and shape * Mass Flow Distribution vs. Spray Angle
10/91-9/92	Atlanta, GA	* Black Liquor Spraying - Variation of Nozzle Size and Spray Angle * Black Liquor Spraying - Effect of Liquor Type * Black Liquor Spraying - High Temperatures * Alternative Commercial Nozzles * Modified Splashplate Designs * New Nozzle Concepts - Vibratory Assist (transverse mode)
10/92-9/93	Atlanta, GA	* New Nozzle Concepts - Vibratory Assist (axial mode) * New Nozzle Concepts - Dielectrophoresis

2.2 YEAR 5 TESTING:

The experimental work during the past year centered on new nozzle design concepts based on vibratory assist (axial direction) and dielectrophoresis.

2.2.1 Vibratory Assist

A number of studies have been carried out regarding the stability of thin liquid sheets moving in a gaseous environment. Inviscid theories of two-dimensional wave

growth predict that, in the initial stages of growth, an optimum frequency exists where the growth rate is a maximum. Viscous theory, on the other hand, predicts the absence of a wave of maximum growth rate except at low velocities. Crapper, et al. (5) have claimed that dominant waves seen on a sheet must be of a frequency imposed by some external force. Hence, the role of vibratory assist is to obtain growth rates of low amplitude waves at any distance from the nozzle orifice. Crapper and Dombrowski (6) suggested that drop size may be affected by both nozzle amplitude and frequency. Since these factors may depend upon natural frequencies in the apparatus, drop sizes in industrial settings could well turn out to be different from those given by the same nozzle in the laboratory.

The effects of external vibrations on the disintegration of liquid jets have been investigated by many, with the finding that atomization can be induced only in widely separated narrow bands of frequency (7,8,9). If a sinusoidal perturbation is applied to a jet of liquid, the jet rapidly decomposes into a sequence of droplets whose diameters are determined by the wave length of the original disturbance. The wave length of the disturbance can easily be varied, and thus, in principle, the size of the droplets can be controlled (9). A similar analysis applied to droplet formation from liquid sheets showed different behavior than that exhibited by jets (10). For perturbations driven solely by capillary forces, the sheet of fluid was found to be stable for all perturbations. Hence, the technique of inducing controlled atomization with a small perturbation works only for circular jets and not for sheets.

On the other hand, it has been reported that a high amplitude acoustic signal can achieve some control over the drop size from fans, cones, cylinders, and sheets (10). An acoustically driven atomizer gave a sheet comprised of dilational waves (c.f. Fig. 2.1), which subsequently broke up into ligaments which then broke up into uniform drops; a sheet with sinuous waves (c.f. Fig.2.2) ejected small drops from the sides of the sheet.

For vibratory assist to work effectively, it must be done at the proper frequency and amplitude of vibration. Otherwise, the natural frequency of the sheet will dominate, giving a normal distribution of drop sizes. An estimate of the required vibrational frequency was calculated from wave theory, assuming that the sheet breaks up into discrete uniform bands with no interactions between adjacent bands (1). For typical values of the black liquor process parameters, a minimum vibrational frequency of 240 Hz was calculated. There is no easy way to estimate the desired amplitude because it is related to complicated stability theory.

Vibration of the liquor flow can be done either in-line with or normal to the flow. The resulting waves in the liquor sheet issuing from the nozzle should be in the dilational and sinuous modes, respectively. Conceptually, the dilational mode would be expected to give a narrower drop size distribution, since the breakup of the sheet into ligaments should occur at the points of minimum thickness. These are not randomly placed because of the vibrations imposed on the system. The subsequent breakup of ligaments into drops will still be a random event. On the other hand, the

Figure 2.1

VIBRATORY ASSIST

Dilational Wave Generation

– Wave-like Disturbances to Upper and Lower Surfaces of the Sheet Are Out of Phase

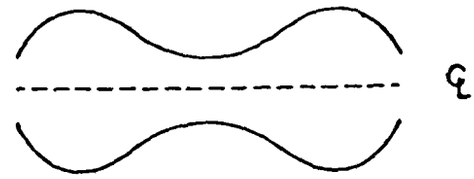

– Vibration in Direction of Liquor Flow (i.e. pulsation of Liquor flow)

Figure 2.2

VIBRATORY ASSIST

Sinuous Wave Generation

- Wave-like Disturbances to Upper and Lower Surfaces of the Sheet Are in Phase

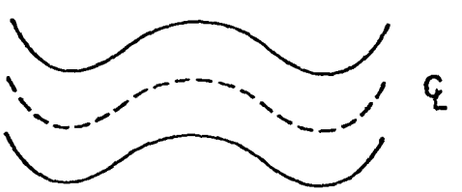

- Vibration in Direction Normal to Plane of the Sheet

sinuous wave mode maintains a constant sheet thickness, implying that sheet breakup will be a random phenomenon going to ligaments, which then randomly break up into drops.

The sinuous mode, reported earlier (1), was examined first because it is easier to accomplish experimentally. A splashplate nozzle was vibrated in a direction normal to the plane of the plate by a two-knobbed cam rotating with a motor shaft. Vibrational frequency was varied from 0 to 93 Hz. Splashplate displacements were about 0.1 and 0.2 mm. Using a black liquor flow rate of 12 gpm at 90°C and liquor viscosities ranging from 75 to 150 cP, no significant changes in median drop size or normalized standard deviation were recorded. We did, however, observe that vibrations caused the liquor sheets to break up sooner than without vibration. The higher vibrational amplitude did form liquor bands whose width decreased with increasing frequency.

An alternative mode of generating transverse waves was examined using an air-driven vibrator. Frequencies up to 130 Hz were tried with the splashplate nozzle operated at the same conditions as for the cam-driven nozzle. Results showed a significant effect on the liquor sheet, the drop size, and size distribution. Bands of liquor formed whose width was inversely proportional to the vibrational frequency. The bands broke into smaller pieces just like sheets formed with no forced vibrations, resulting in a relatively broad range of drop sizes. Relative to the zero vibration case, the median diameter for 70 to 110 Hz on average was 20% higher, and the normalized standard deviation was 24% higher. No trend was observed with increasing frequency. Hence, this did not appear to be a promising route toward obtaining a more controlled drop size distribution.

2.2.1.1 Axial Vibratory Assist - Pulsed Flow Design

The dilational wave mode was examined by imposing axial vibrations (i.e., pulses) on the liquor flow. This mode is very difficult to accomplish experimentally, as evidenced by the lack of activity reported in the literature. We conceptualized, designed, built, and tested an apparatus to mechanically pulse the liquor flow to a commercial V-jet nozzle under controlled conditions of vibrational frequency and amplitude.

With this design black liquor is fed through a pipe tee which precedes the nozzle (c.f.Fig.2.3). At the other end of the run of the tee (oppposite the nozzle) is the vibrator assembly. Between the tee and the vibrator assembly is a variable volume section which seals the vibrator from the liquor in the tee and which can vary the volume of liquor present in the tee at any instant in time. This variable volume section is a section of 3/4-inch flexible corrugated tubing. Vibration (i.e., reciprocating motion of the connector rod) is accomplished with a rotating triangular cam. A rectangular slot was machined in the rod so that the cam can rotate within it. The slot is so dimensioned that a vertex of the cam will displace the rod by a

Figure 2.3

VIBRATOR ASSEMBLY
(with CT-Flex Tubing)

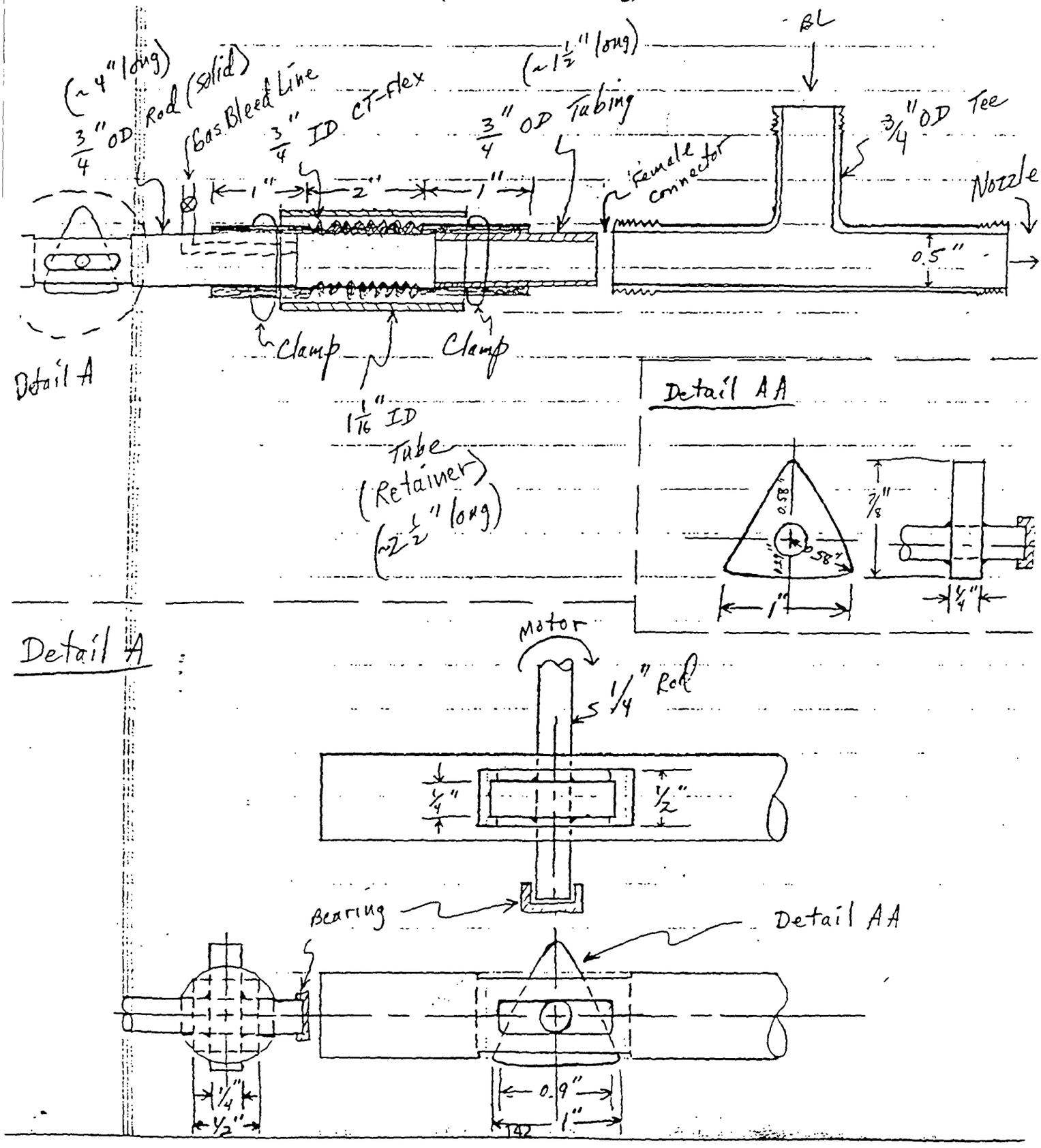

small distance, effectively giving the amplitude in flow variation. As the cam rotates, the preceding vertex pushes the rod in the opposite direction, by the same distance. This gives the negative variation in amplitude. The amplitude that is achieved is dependent upon the volume change in the variable volume section and the liquor feed rate. The speed of rotation of the cam is driven by a variable speed motor, and this determines the frequency of pulsation (vibration) of the black liquor flow.

A key feature of this method of pulsing the flow is that the operator can positively control the amplitude and frequency of vibration. One does not have to rely on a "spring constant" which most other mechanical vibratory methods do. Also, larger amplitudes can be accomplished than what are normally achieved with traditional acoustic or pneumatic vibrators.

2.2.1.2 Axial Vibratory Assist - Interrupted Flow Design

An alternative mode of achieving vibratory assist in the axial direction is to use flow interruptions rather than pulsations. This has been accomplished by using the designs depicted in Figs. 2.4 and 2.5. In both designs, continuous delivery of nozzle solids black liquor with vibratory assist in the axial direction can be accomplished by a rotating cylinder within a stationary pipe section. In both cases, the cylinder contains one or more pairs of holes that are diametrically opposed, while the outer pipe section contains two outlets, also diametrically opposed. In the first design, the sets of holes are also axially displaced.

One outlet on the outer pipe is connected to the nozzle orifice, while the other outlet is connected to a recycle line. Black liquor is fed to the inner cylinder which is rotating at a rate set by a drive motor assembly. Liquor flows out to the nozzle or to the recycle as dictated by whether or not the holes in the same axial position line up. In general, when liquor flows to the nozzle orifice, it doesn't to the recycle; and vice versa. For the design where the pairs of holes are axially displaced, an O-ring seal is placed between the cylinder and outer pipe, axially between the pairs of holes, to prevent leakage of liquor from a closed outlet to the open one. For the other design where the pairs of holes are not axially displaced, leakage through the annular space between the rotating and stationary bodies is minimized by providing a tight clearance between the bodies.

The net effect of this concept is to provide a pulsed flow to the nozzle orifice while not deadheading the black liquor pump. The frequency of pulsation is determined by the angular rotation speed provided by the drive assembly. The amplitude of pulsation is determined by the relative sizes of the holes and the liquor pressure. Additional pairs of holes could be drilled in the rotating cylinder to increase the frequency of spray interruption.

A Disclosure of Invention has been filed covering a nozzle to give a pulsed black liquor flow by the flow interruption mode described above.

Figure 2.4

AXIAL VIBRATORY ASSIST

(INTERRUPTED FLOW MODE 1)

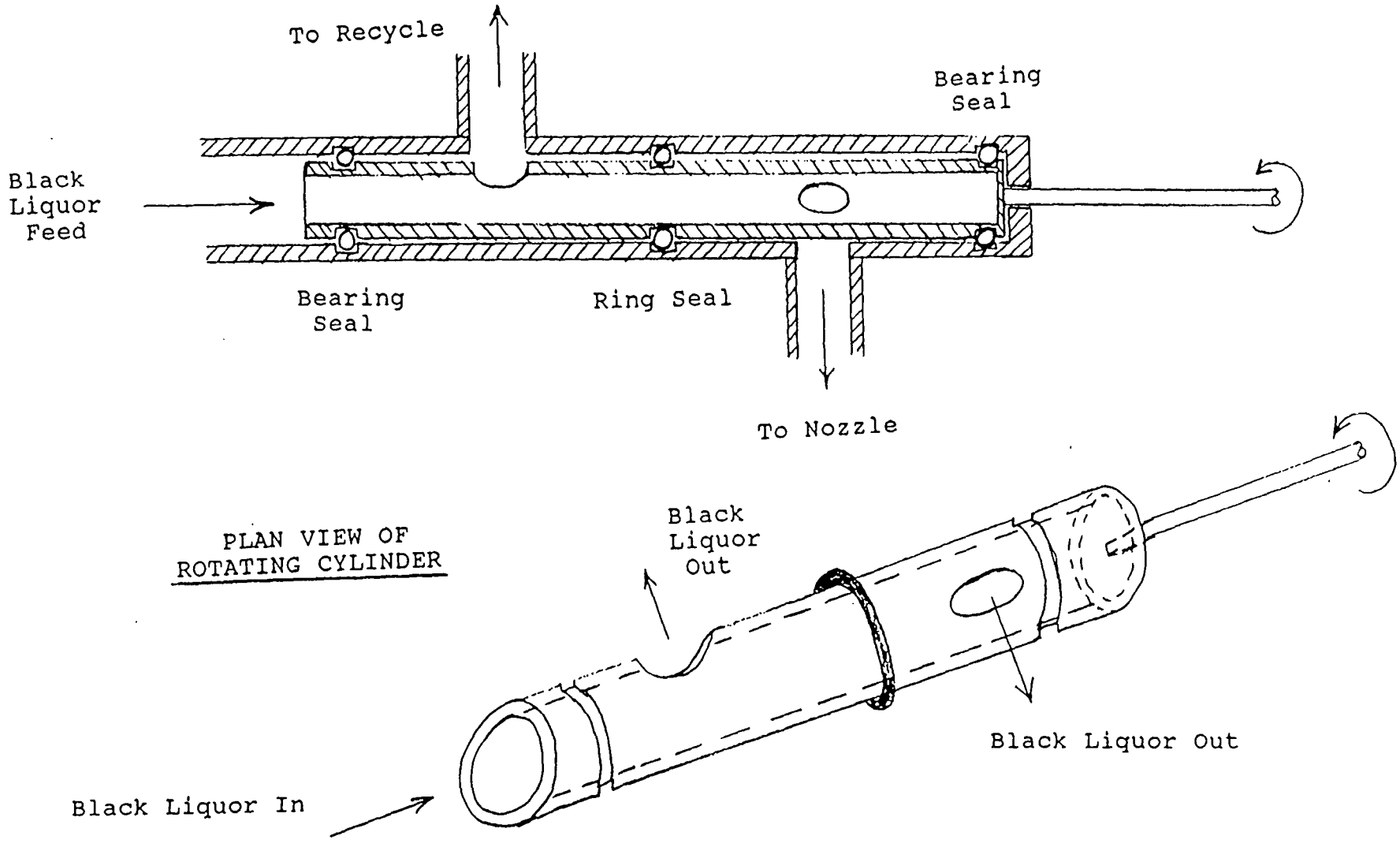

Figure 2.5

AXIAL VIBRATORY ASSIST

(Interrupted Flow Mode 2)

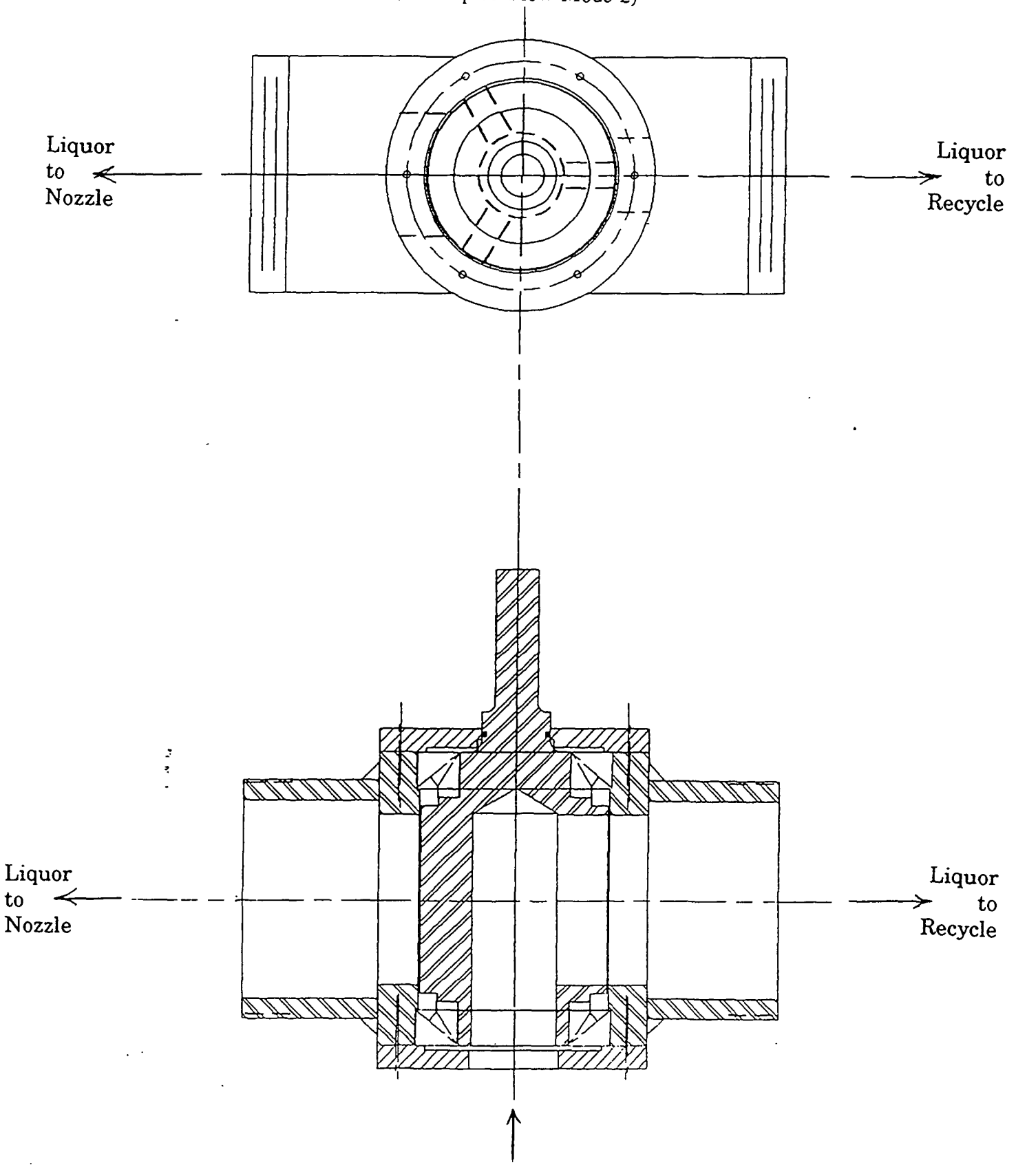

2.2.2 Dielectrophoresis

An alternative concept which has potential for influencing drop size distribution in black liquor sprays may use the phenomenon of dielectrophoresis where an electric field is positioned around the spray sheet to alter the direction of flow of the neutral, but polarizable droplets that are formed. By exerting an independently controlled force on the droplets that will be proportional to drop diameter, it may be possible to cause collisions of the smaller drops with larger ones, resulting in coalescence. This concept, if successful, should reduce the fraction of fine droplets and result in a size distribution skewed toward the larger sizes. If a drop size distribution can be achieved having a reduced percentage of the fine fraction, then entrainment/carryover rates in the recovery boiler should be decreased, thereby making room for a capacity increase. Improvements in energy recovery efficiency would also be expected from reduced sootblowing requirements.

Dielectrophoresis is the movement of an uncharged particle in a non-uniform field, by virtue of the dipole induced on the particle by the field (c.f.Fig.2.6) (11). The dielectrophoretic force on a droplet will be proportional to droplet volume, field strength, field gradient, and difference in dielectric constants between the droplet and the gas space through which it is flowing. Typically, field strengths of 10 kV/m are required for dielectrophoretic forces to be significant.

It should be noted that, ideally, there is no current flow with dielectrophoresis. Only when the spark-gap voltage (the minimum potential difference required for current to flow between electrodes of a given spacing in a given dielectric medium) is exceeded does the electric field break down and current flow. For air at 25°C and a 2.5 cm spherical electrode, a potential difference of 5 kV has a spark-gap of 0.13 cm (12). Since we intend to operate well below 385 kV/m, electrical shorting (i.e. sparking) should not occur.

Since the force of an isolated dipole is towards the higher field strength for both polarities of field, both AC and DC fields produce dielectrophoretic motion. In a DC electric field, the dielectrophoretic force is normally much lower than the electrophoretic force, but there is no net electrophoretic motion in an AC field. Hence an AC field can be used to make independent observations of dielectrophoretic effects.

Electrostatic forces have been used to encourage coalescence in emulsions since the beginning of the twentieth century (11). Coalescence is known to occur as particles or droplets moving at different velocities collide. Dielectrophoresis enhances this tendency by providing a force of attraction between two polarized droplets.

Generation of a non-uniform field can be accomplished by any number of electrode configurations. Of course, parallel plates are excluded because the resulting field is

Figure 2.6

DIELECTROPHORESIS MECHANISM

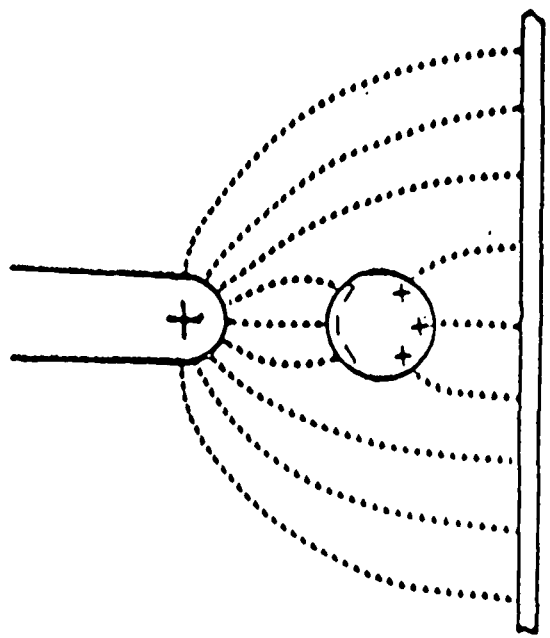

Force on a dipole in a non-uniform field. The negative end of the particle is in a higher field and therefore experiences a higher force than the positive end and there is a net translation towards the higher field.

uniform. Our initial choice of electrode configuration which could be mounted in the black liquor spraying apparatus is shown in Fig.2.7. Three electrodes, contained in each of two parallel planes, span the lateral area of the spray sheet and provide a non-uniform field for practically all of the drops that form.

With this geometry, two operating modes are possible (c.f.Fig.2.8). In the first case, the spray is placed equidistant between the two planes of electrodes. Droplet migration toward both planes is expected, in principle. Only the drops exactly equidistant from the two electrode planes will not experience a non-uniform field, and hence they will not be subject to the dielectrophoretic force. In the second arrangement, the electrode planes are both on one side of the spray sheet. The electric field lines of force are more non-uniform for all droplets, and hence should provide a stronger dielectrophoretic force on all drops in the spray.

2.3 YEAR 6 TEST PLAN

In the final year of this DOE-funded project, work will be conducted in three different areas:

* A more thorough investigation of vibratory assist using the interrupted flow mode will be undertaken. Pulsation at frequencies up to 500 Hz will determine whether or not drop size distribution can be altered by trying to reduce the randomness of the droplet formation process.

* Drop size data above the transition temperature will be extended to about 25°F above the transition value to see if the diameter dependence on temperature is the same as it is below the transition point. Mills firing high solids liquors operate at temperatures near the transition point and are interested in what potential there is in going higher.

* Although most of the work done in this study has been with commercial nozzles, usefulness has been somewhat limited because the nozzle diameters employed have been on the small end of the scale. Limited data have been obtained on the effect of diameter, but more are needed so that extrapolations to the larger diameters presently used can be made with greater confidence. The experimental apparatus limits how high in diameter we can go to about 20 mm.

* Anticipating a positive result with vibratory assist, we will use the recovery boiler model currently being developed at IPST to identify at what conditions a mill test ought to be explored. A candidate mill will be identified and plans for a mill trial will be initiated.

Figure 2.7

Nozzle - Electrode Configuration

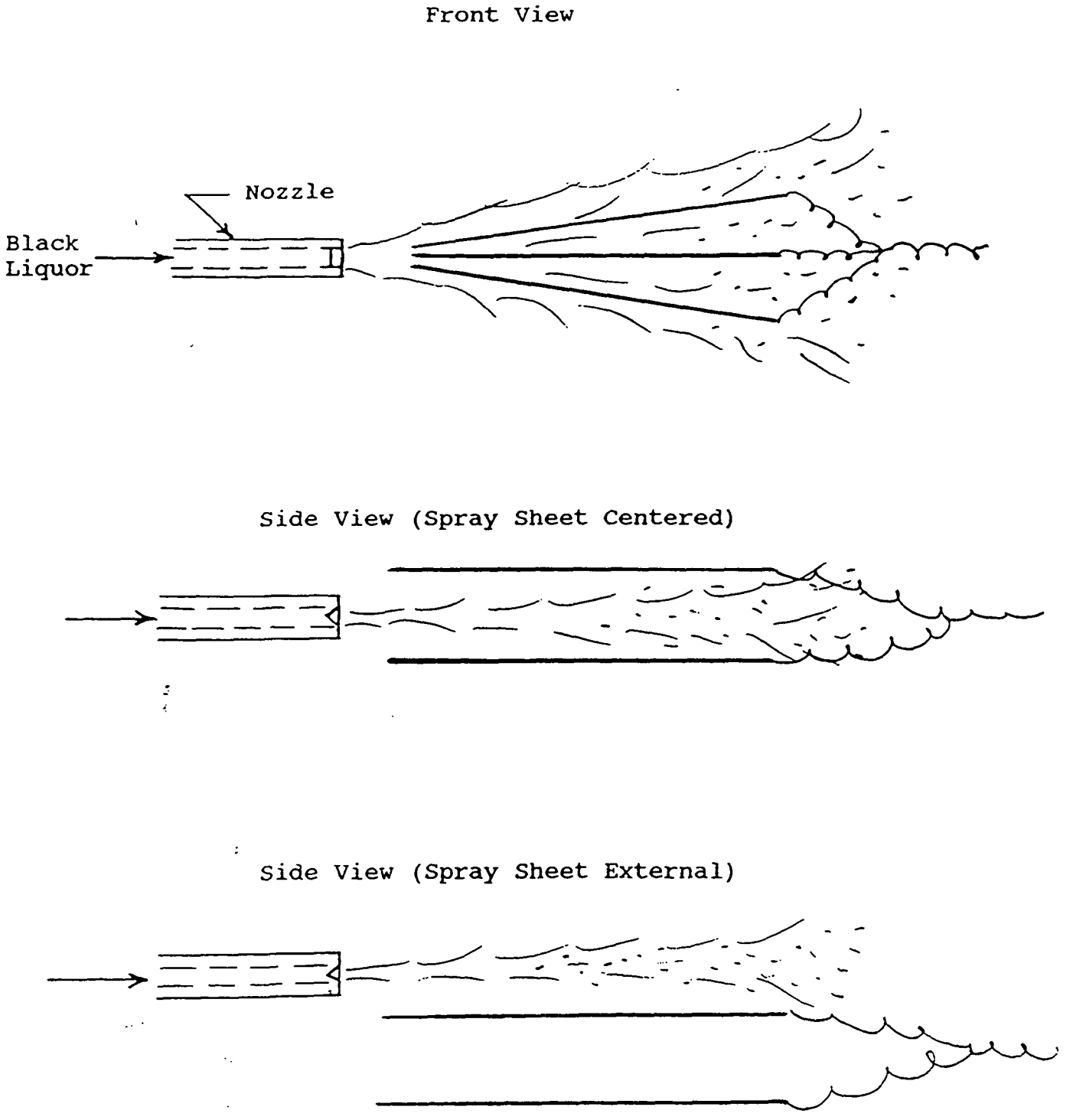

Figure 2.8

Spray Sheet - Electrode Configuration

Spray Sheet Centered

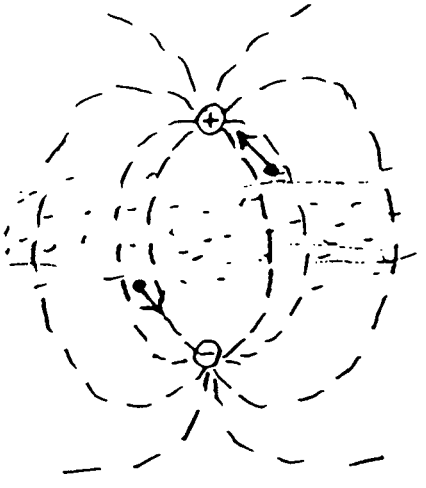

Spray Sheet External

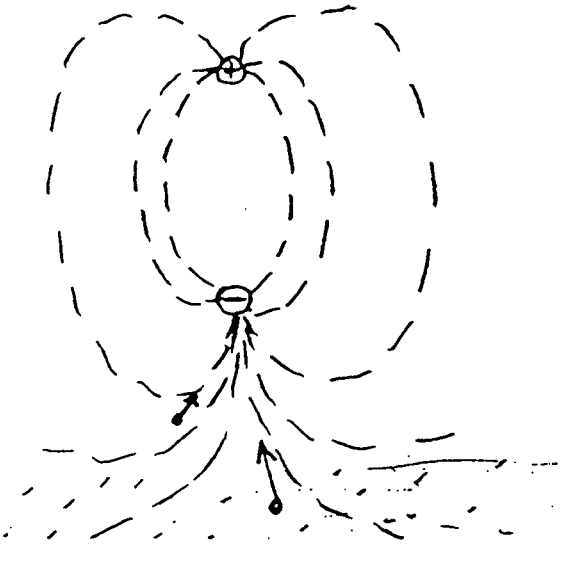

3.0 BLACK LIQUOR SPRAYING RESULTS

3.1 Axial Vibratory Assist

3.1.1 Pulsed Flow Mode

Testing with axial vibratory assist using the pulsed flow mode described above was carried out with 62% solids black liquor flowing through a 3/8-inch V-jet nozzle at 73°C and 8 gpm. Results are presented in Table 3.1. Liquor viscosities ranged from about 100 to 160 cP. Frequencies up to 147 Hz were run with a maximum variation in the liquor flow to the nozzle orifice of +/-20%.

Table 3.1 - Axial Vibratory Assist (Pulsating Flow) Results

Temp (C)	Solids (%)	Frequency (Hz)	Viscosity (cP)	Dm (mm)	8 -
74	61.6	0	107	2.96	0.265
73	61.9	18	117	2.75	0.242
74	62.2	30	117	2.56	0.239
74	62.7	79	122	2.90	0.272
72	63.0	110	152	2.64	0.269
72	63.4	122	167	2.62	0.239
73	63.4	147	164	3.00	0.261

Compared with the zero vibration case, median drop diameters and normalized standard deviations for the vibratory runs were not significantly different. If the normalized standard deviation (8) values are correlated linearly with frequency, a small positive coefficient results, implying the distribution width increases with frequency. This is counter to the result that was expected. Unfortunately, equipment limitations precluded going to greater frequencies and amplitudes of flow variation.

3.1.2 Interrupted Flow Mode

Testing with axial vibratory assist using the interrupted flow mode was carried out under similar process conditions using the same V-jet nozzle as with the pulsed flow mode. Two different designs were tested - one machined so that liquor flowed to the nozzle orifice 3/4 of the time (1/4 time going to recycle) and one machined so that liquor went to the orifice 1/4 of the time. Both were operated with pulsations ranging from zero to 30 Hz; subsequent modifications were made to the latter design so that the range of pulsation was extended up to 270 Hz.

A total of four tests were run using this mode of operation with the 1/4 on-3/4 off design. The data are summarized in the Appendix. The distribution of liquor flow between to the nozzle and to recycle is depicted in Fig.3.1; a ratio of 1:3 is evident. For each test, the median drop diameters and normalized standard deviations were correlated by linear regression according to the following general form:

$$Dm = A\,f + B$$

$$\delta = E\,f + G$$

where:

Dm = mass median diameter (mm)
f = frequency of flow interruption (Hz)
δ = normalized standard deviation (-)
A,B,E,G = experimental constants

Results are depicted in Figs. 3.2-3.9 and are summarized in Table 3.2. The important experimental constant is the value of E; if E is negative, then the width of the distribution (δ) decreases as frequency increases. All E-values were negative, but also very small. Correlation coefficients were also very low. Obviously, more work needs to be done to more completely characterize this particular nozzle design.

Table 3.2 - Frequency Dependence of Median Diameter and Distribution Width

Test No.	Black Liq. Solids (%)	Temp (C)	Visc (cP)	Freq (Hz)	Correlation Parameters A (x10E2)	B	E (x10E5)	F
64	54	82		0-29	-0.6	3.17	-120	0.204
70	51	92	120	10-32	-2.62	3.77	-55.7	0.209
72	56	47	120	30-96	0.25	2.30	- 7.8	0.184
		40	240	40-96	-3.30	5.52	-37.0	0.225
75	56	47	120	120-270	0.81	1.38	- 1.6	0.178

Vibratory motion is fundamentally characterized by periodic displacement above and below an equilibrium position and hence may exhibit harmonic motion. Further examination of the results from Test 75 suggests the remote possibility of there being a harmonic frequency where the distribution width goes through a local minimum. Arranging the Test 75 data according to increasing frequency, Fig.3.9, shows this effect at around 230 Hz where three consecutive values of δ (Tests S, L,

Figure 3.1

BLACK LIQUOR FLOW DISTRIBUTION WITH INTERRUPTED FLOW MODE

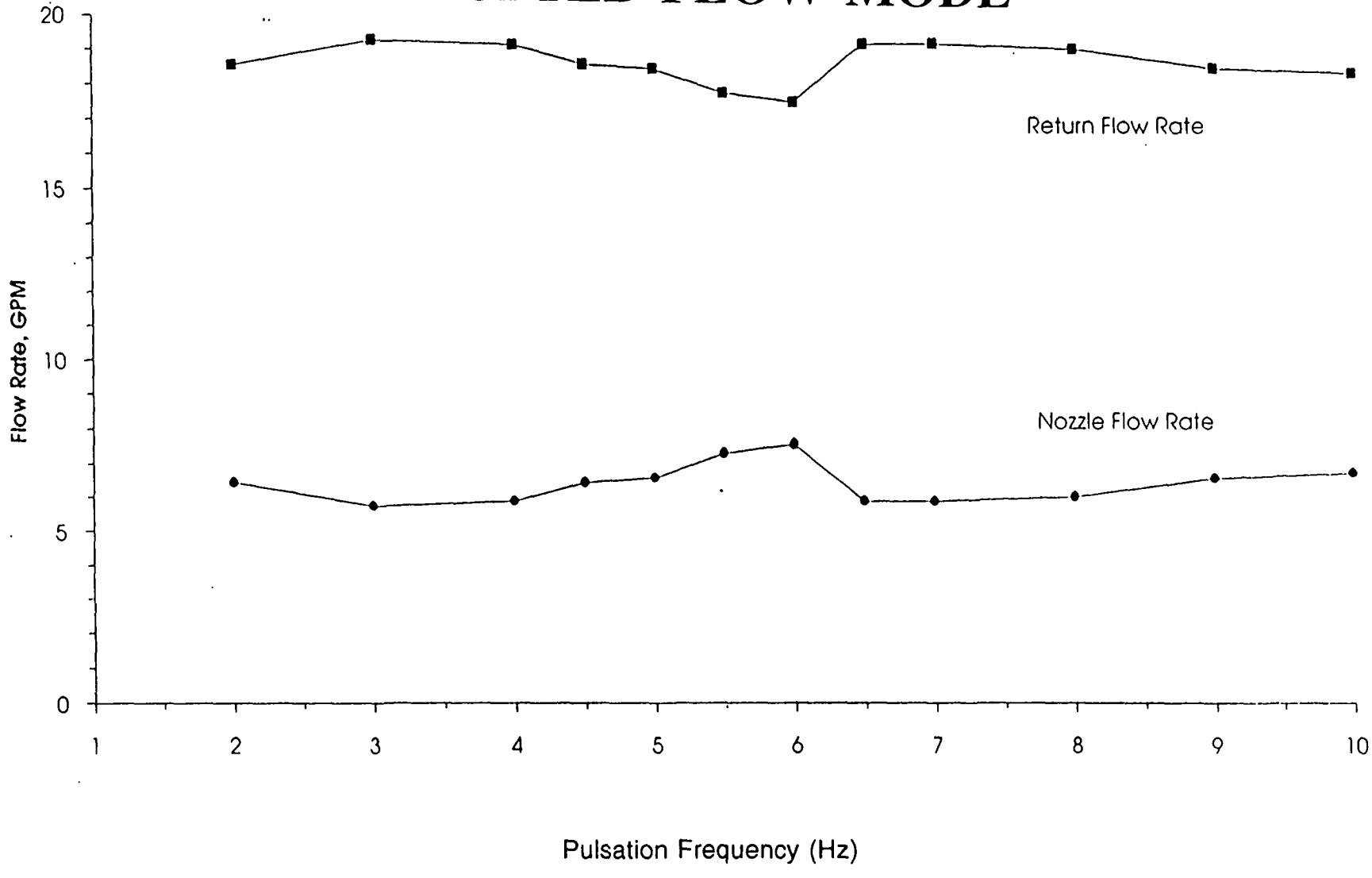

Figure 3.2

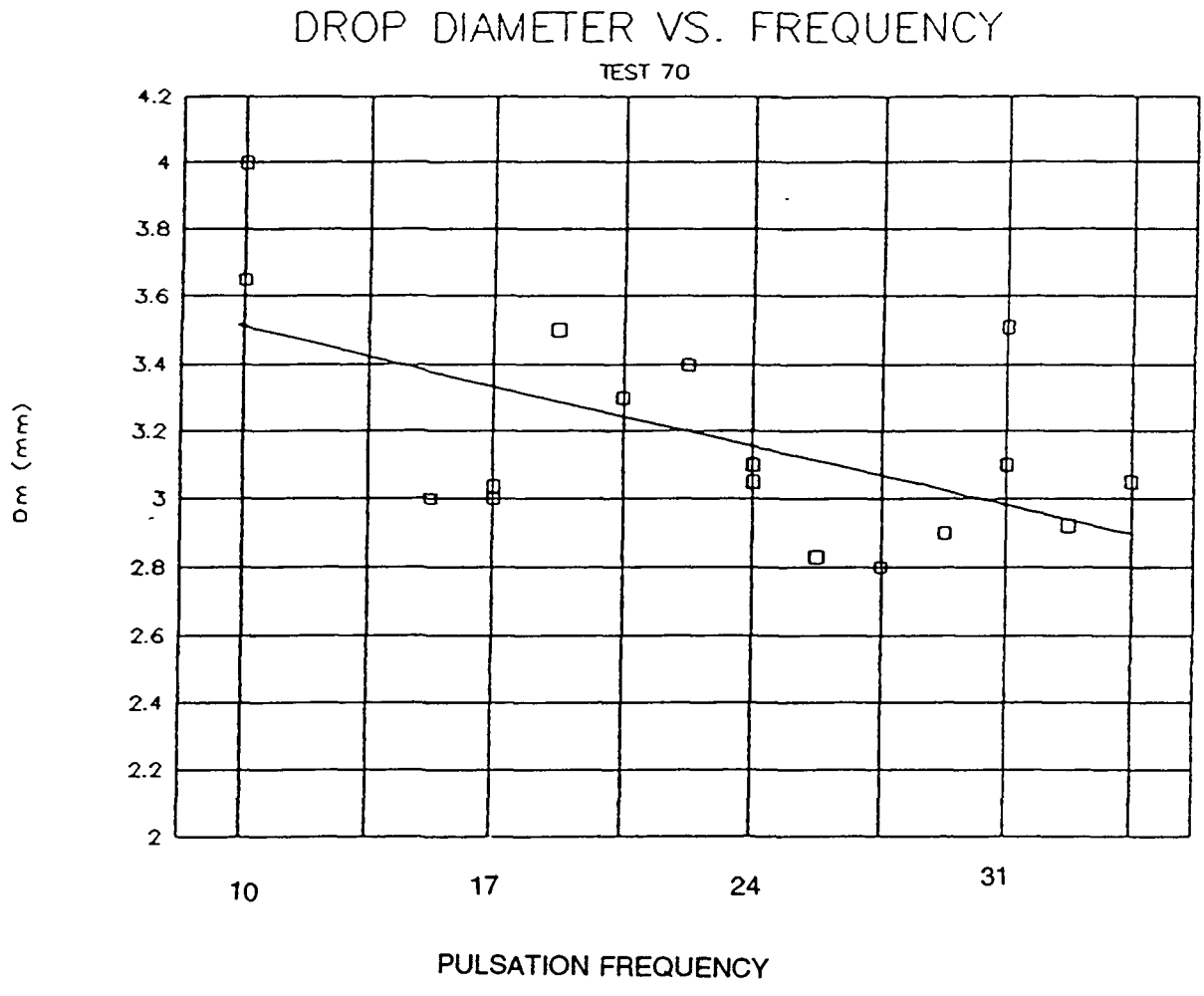

$$D_m = 3.77 - 0.0262\, f$$

Figure 3.3

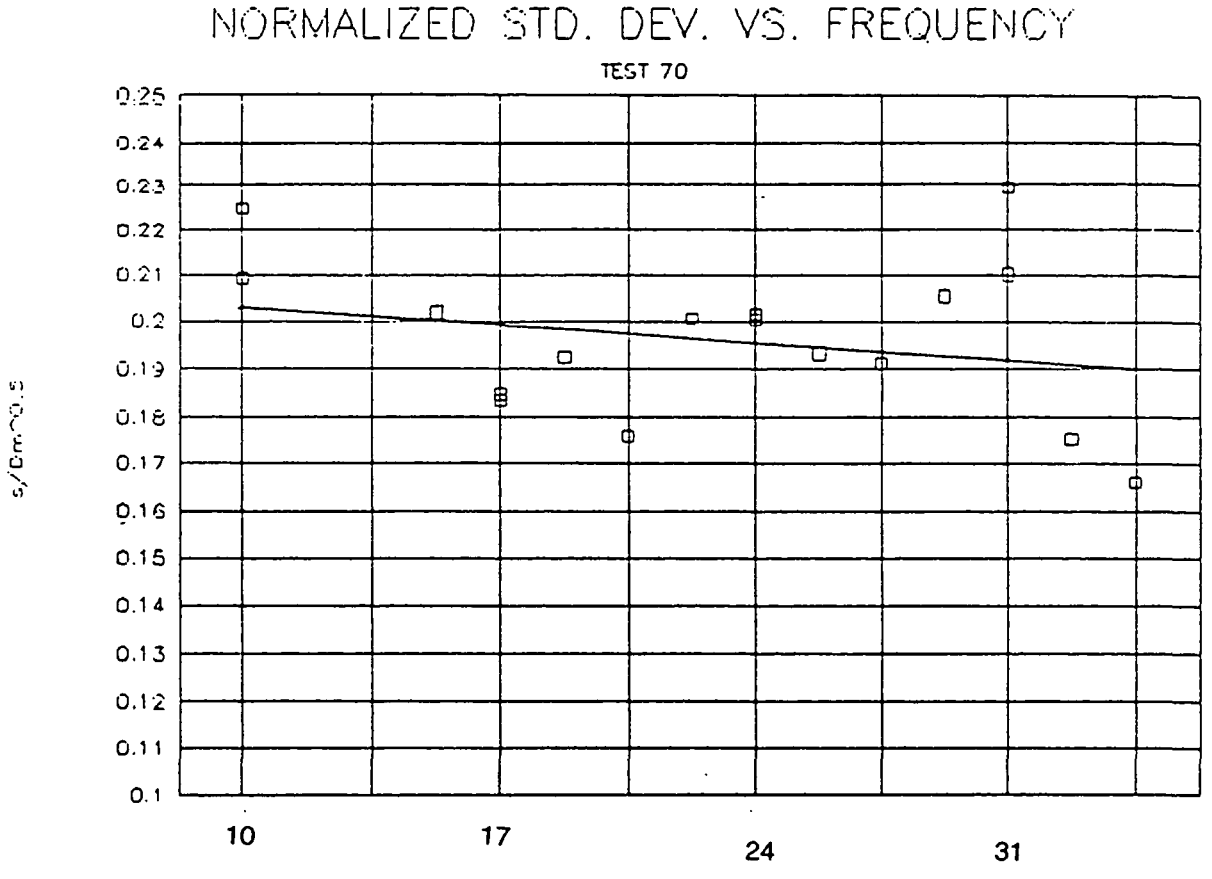

$$S/\sqrt{D_m} = 0.209 - 0.000557f$$

Figure 3.4

DROP DIAMETER VS. FREQUENCY - TEST 72 (LOW VISCOSITY)

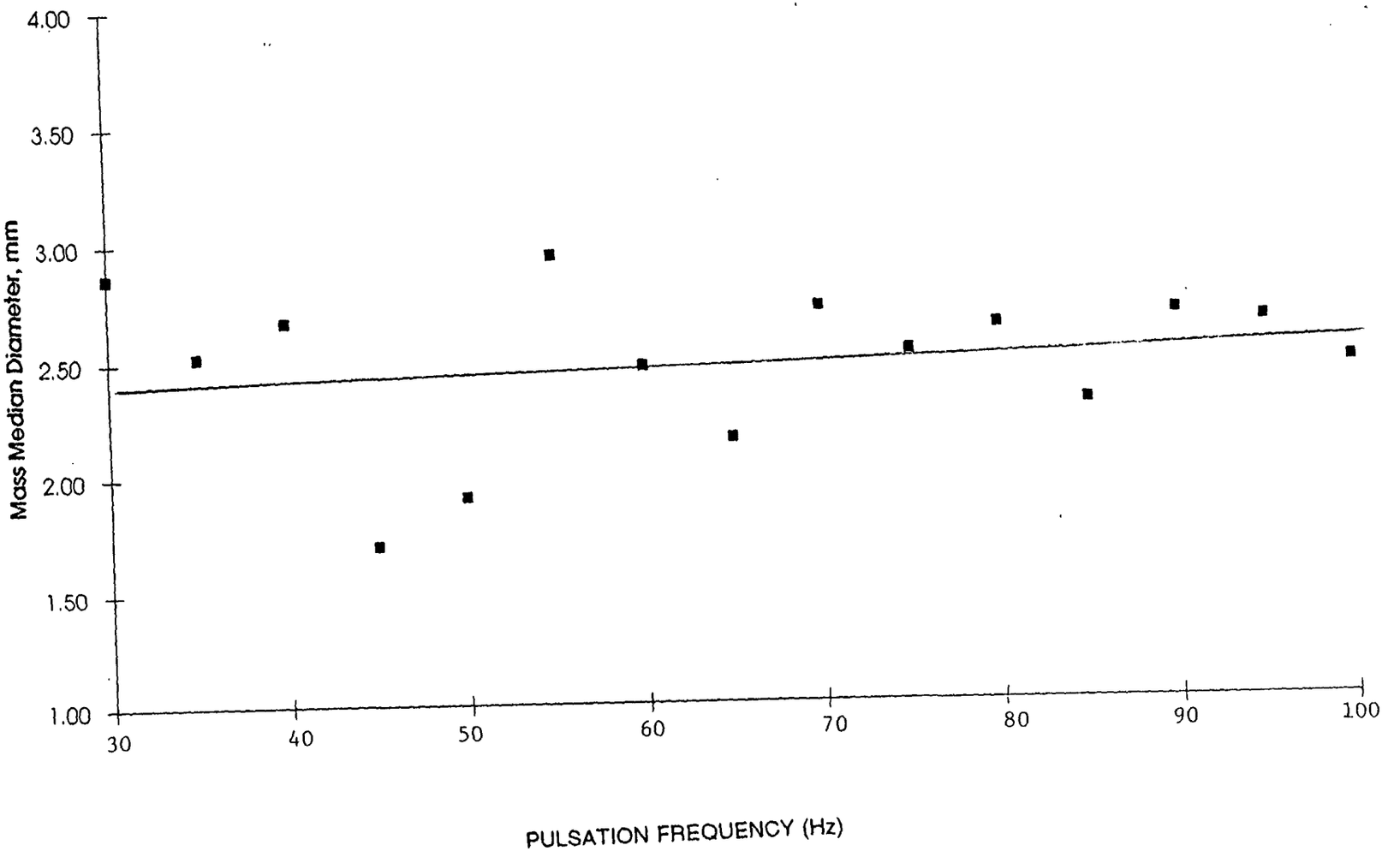

Figure 3.5

NORMALIZED STANDARD DEVIATION VS. FREQUENCY - TEST 72 (LOW VISCOSITY)

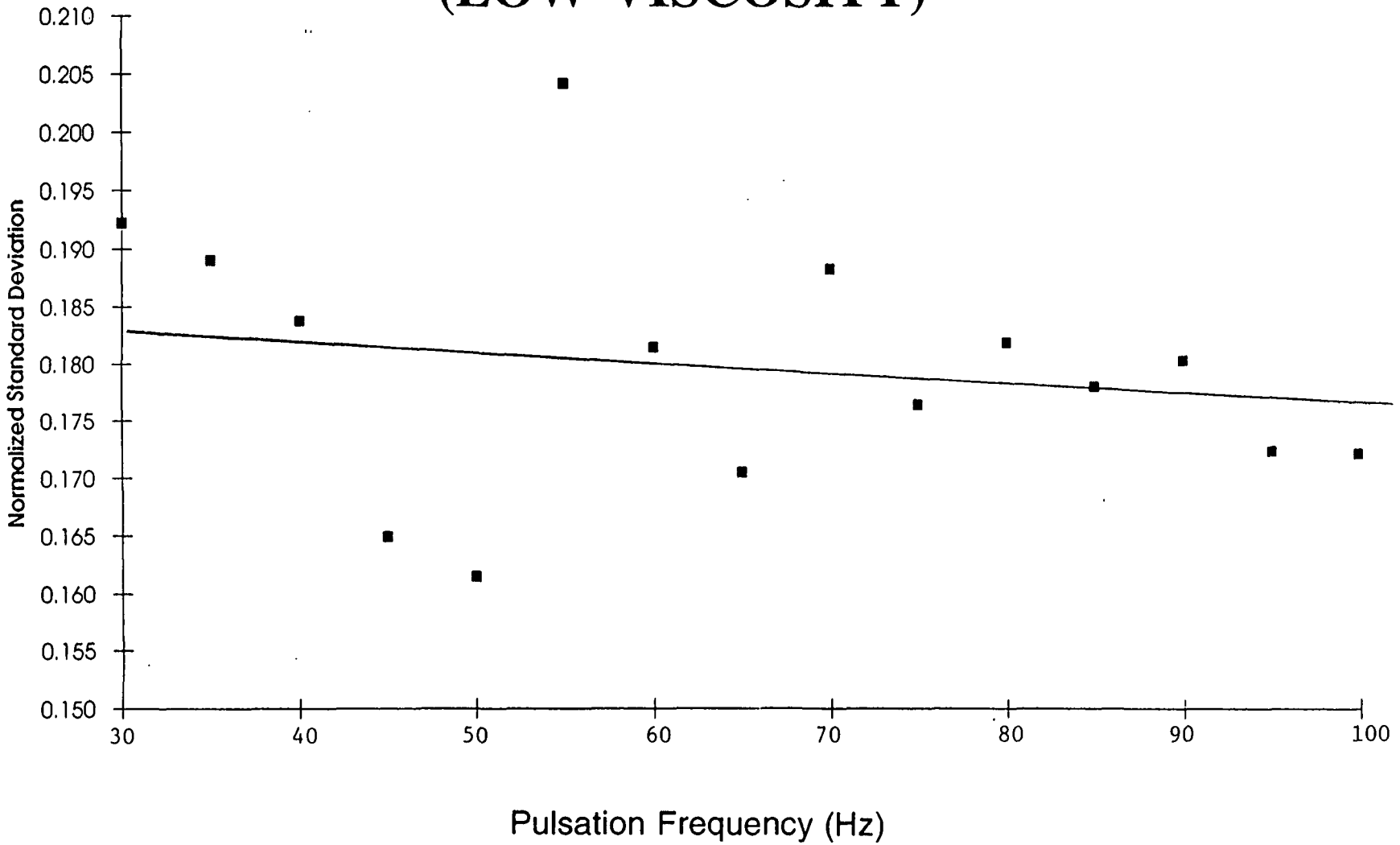

Figure 3.6

DROP DIAMETER VS. FREQUENCY - TEST 72 (HIGH VISCOSITY)

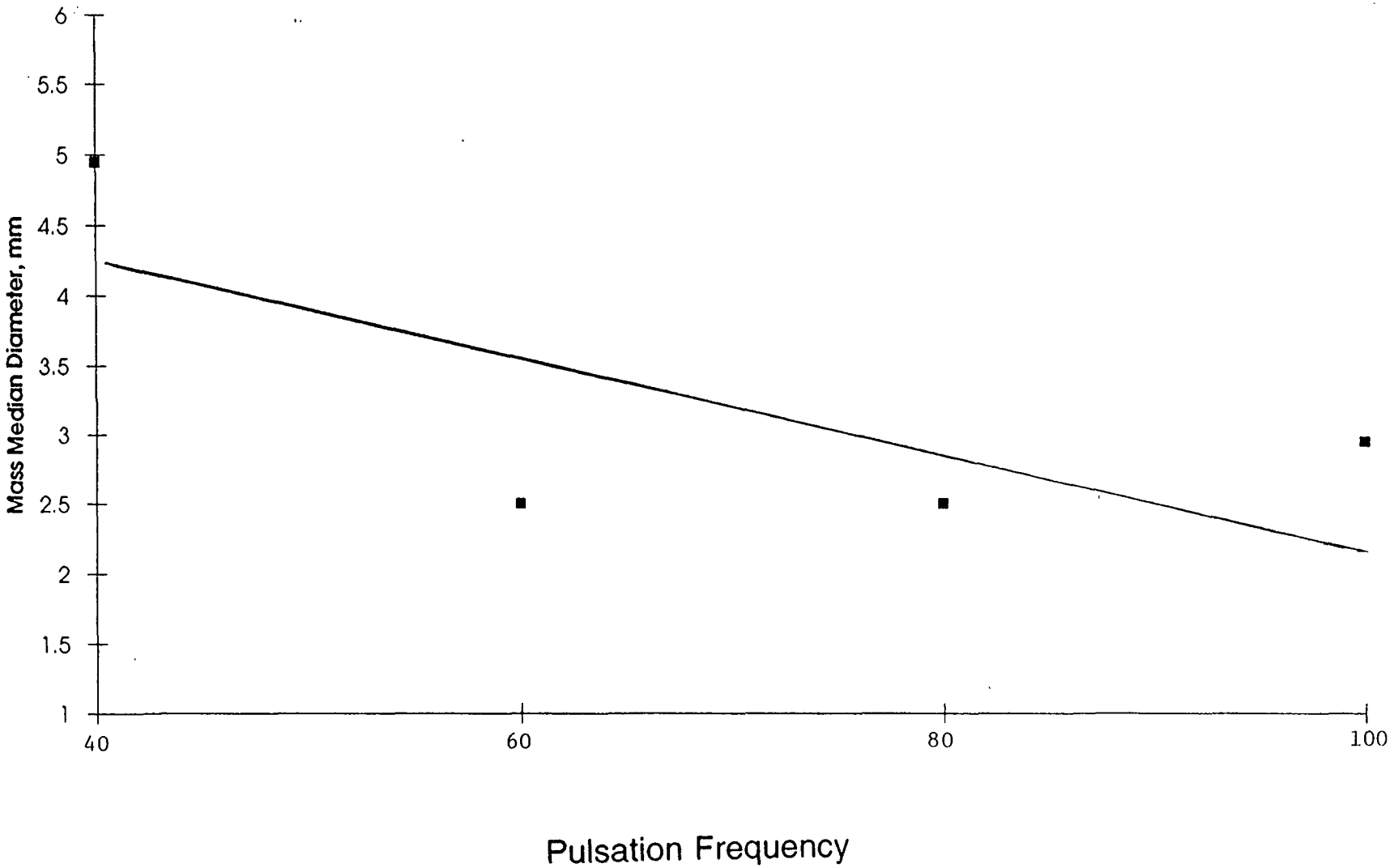

Figure 3.7

NORMALIZED STANDARD DEVIATION VS. FREQUENCY (HIGH VISCOSITY)

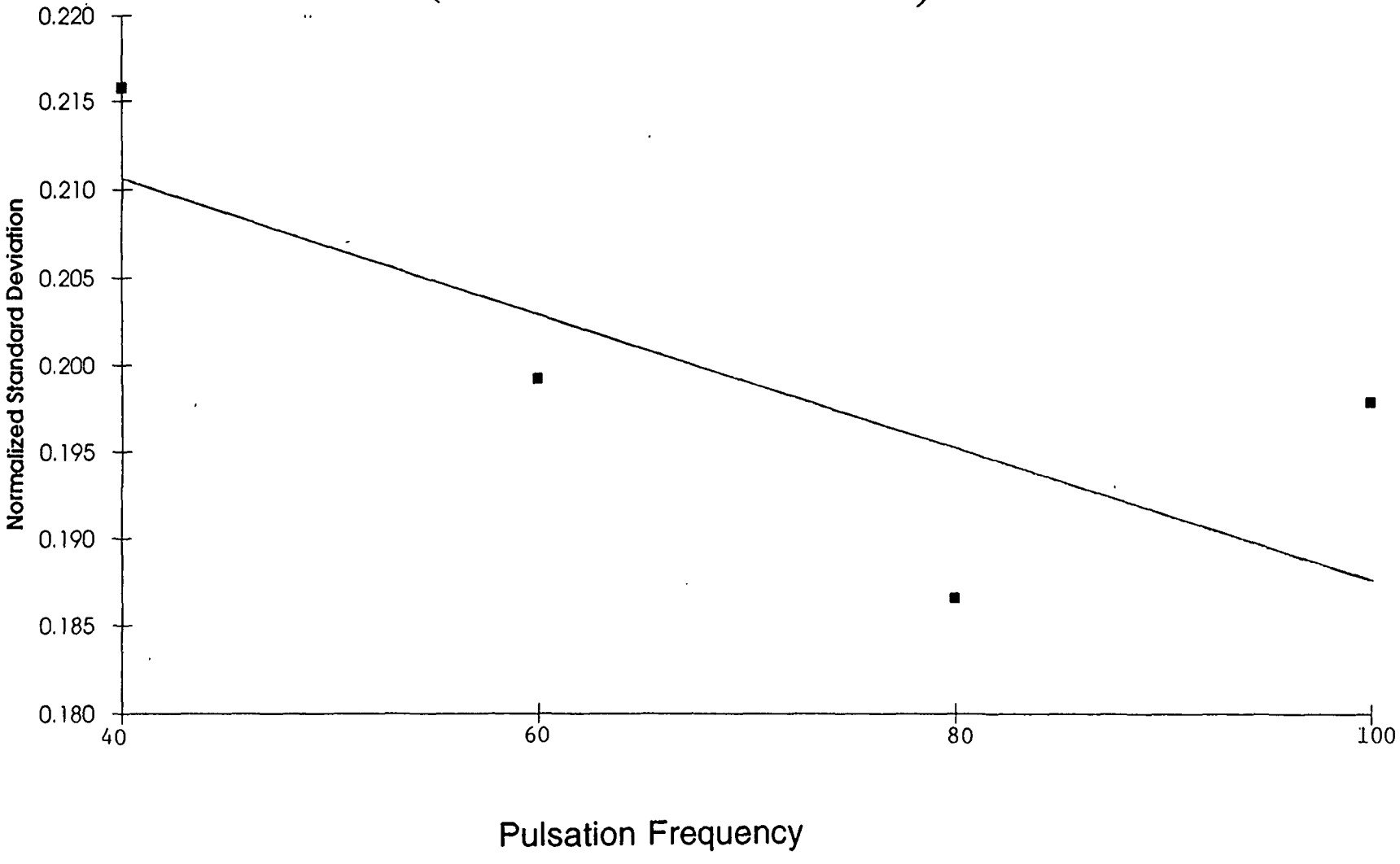

Figure 3.8

DROP DIAMETER VS. FREQUENCY (High RPM trial)

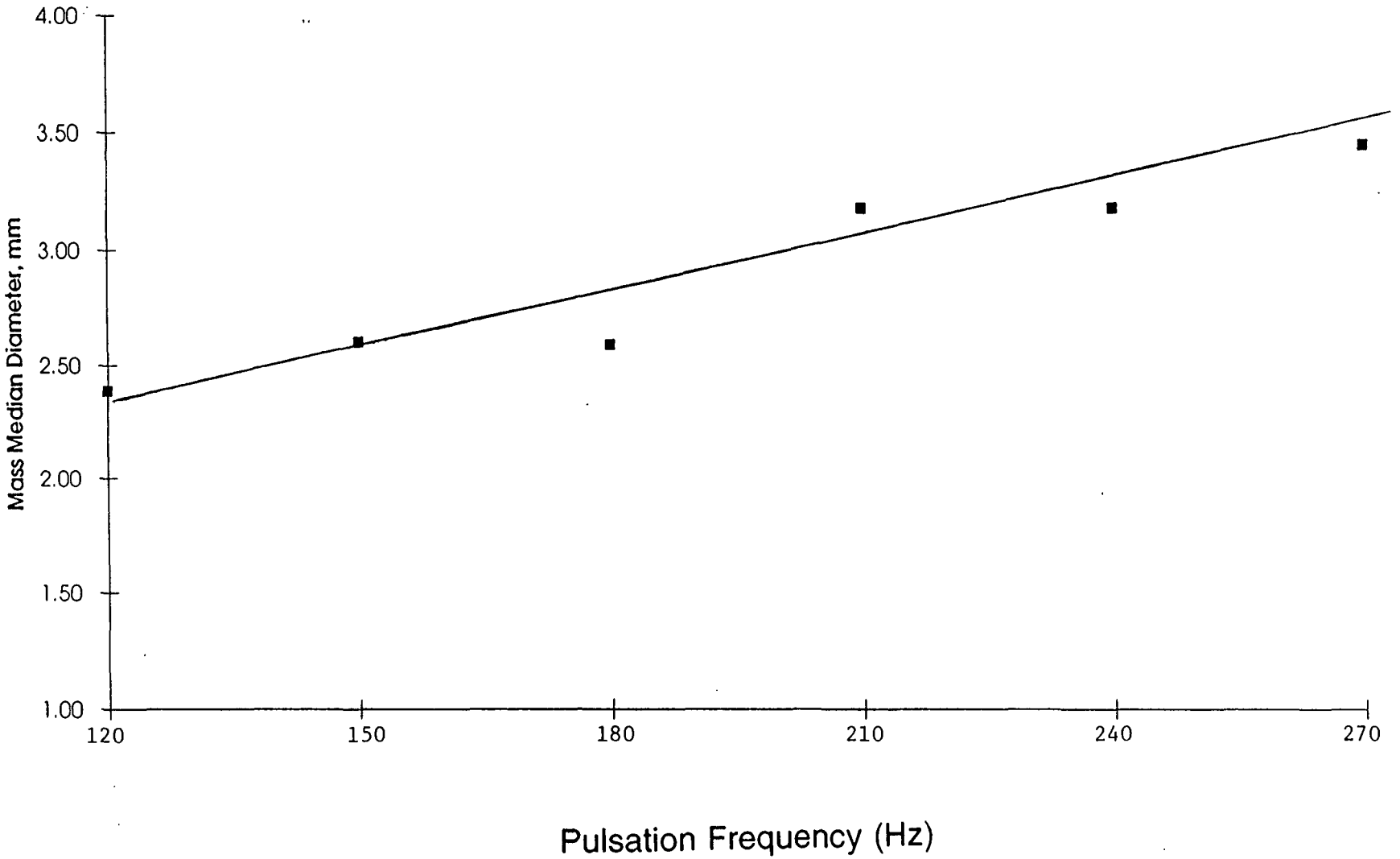

Figure 3.9

NORMALIZED STANDARD DEVIATION VS. FREQUENCY (High RPM trial)

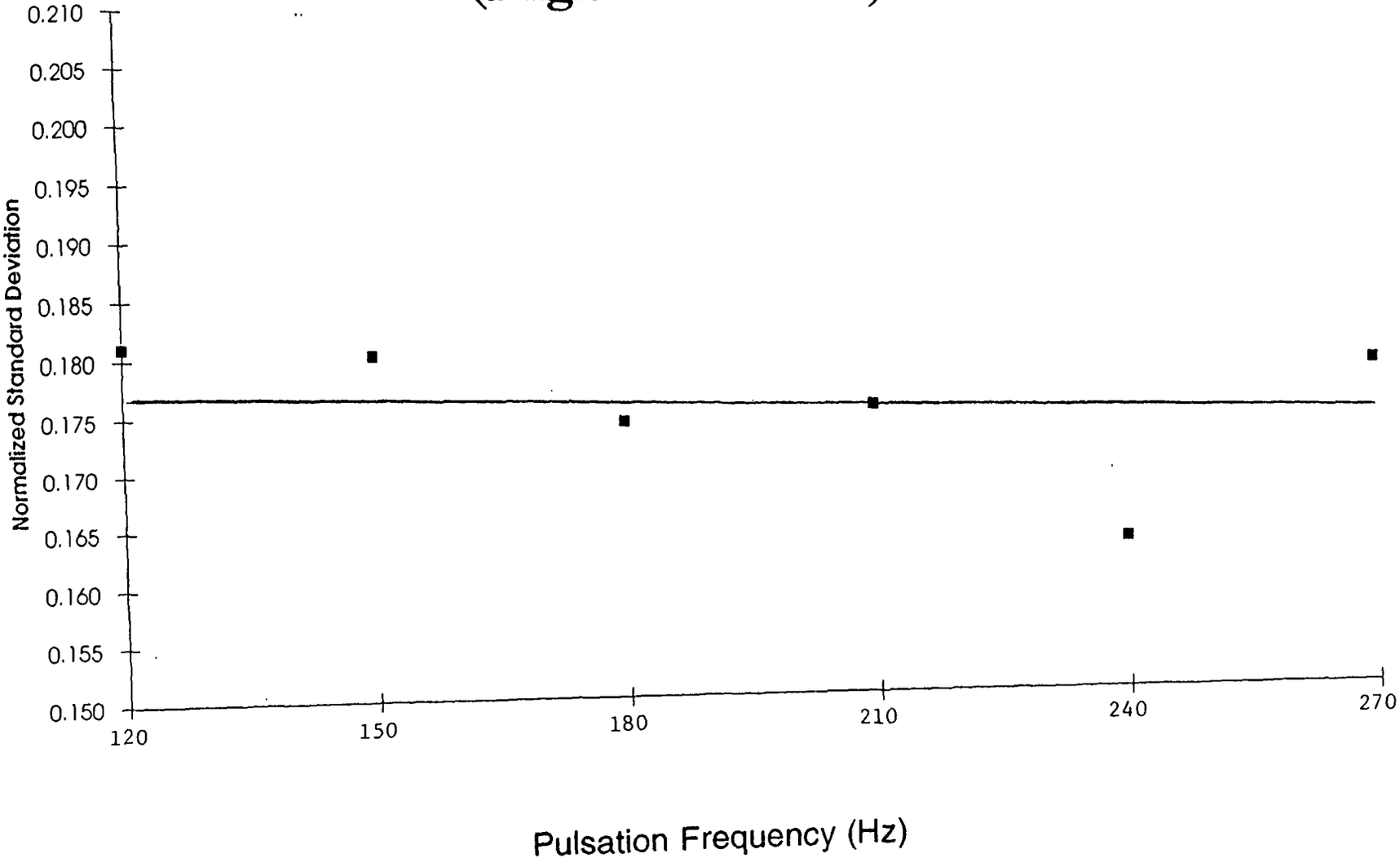

and H) are more than one standard deviation below the average 8 of 0.174. More data are needed to confirm or deny this possibility. Interestingly, this frequency agrees closely with the theoretical value of 230 Hz discussed earlier.

3.2 Dielectrophoresis

An exploratory test employing dielectrophoresis was conducted at 100°F using 48% solids black liquor flowing at 12.6 gal/min from a SS 15/65 V-jet nozzle. At these conditions, the liquor viscosity was 130 cP.

The electrodes were arranged as described previously. The tests were performed both with the spray sheet centered between the two electrode planes and with both sets to one side of the sheet. In both configurations, the closer electrode(s) is about 9 inches from the center of the spray sheet. Direct current voltages of 3.0 and 5.0 kV were applied between the electrode sets, yielding a maximum field strength of about 10 kV/m. Typically, dielectrophoretic effects are reported for field strengths on the order of 10-100 kV/m (11).

The voltage limitation in our system was determined by the cut-off current for the power supply. The electrodes were encased in insulating PVC tubing, but this did not prevent current flow for voltages above 5 kV. The key parameter here is the "spark-gap voltage" which, for a given dielectric medium between electrodes of known spacing, is the maximum voltage possible before breakdown occurs. For 5 kV with air as the dielectric, the minimum allowable distance separating the electrodes is 1-2 mm. With black liquor droplets effectively increasing the dielectric constant of the medium between the electrodes, the minimum separation distance is significantly increased. Hence higher field strengths with this electrode configuration do not appear to be possible.

Drop size determinations using dielectrophoresis conditions are summarized in Table 3.3. Tests 77B and 77C were performed with the spray sheet centered between the electrode sets, about 9 inches away; tests 77E and 77F had both electrode sets to one side of the spray sheet, the closer being about 9 inches away from the spray.

Table 3.3 - Effect of Dielectrophoretic Field Strength on Droplet Formation Characteristics

Test	Voltage (kV)	Median Diam. (mm)	Normalized Std. Dev.
77A	0	2.18	0.19
77B	5.0	2.15	0.18
77C	3.0	2.27	0.19
77D	0	2.25	0.20
77E	3.0	2.17	0.18
77E1	3.0	2.05	0.17
77F	5.0	2.10	0.17
77G	0	2.11	0.17

There does not appear to be any significant effect of field strength on drop size or size distribution for field strengths up to 10 kV/m.

4.0 CONCLUSIONS

1. Gaining independent control over drop size distribution in black liquor sprays from commercial nozzles will require an independently contolled external force, such as vibratory assist or a non-uniform electrostatic field.

2. Vibratory assist in the axial direction, as applied to black liquor spraying, was accomplished with two novel nozzle designs. The one achieving a pulsed flow by direct variation of the liquor flow by +/- 20% showed no significant effect on drop size distribution up to frequencies of 150 Hz. Higher frequencies and amplitudes of flow variation with this design were not possible.

3. Axial vibratory assist achieved by periodic flow interruptions has shown some promise, as evidenced by a weak narrowing of the drop size distribution with increasing frequency. There may exist a harmonic frequency where the distribution width exhibits a local minimum. More data extended to frequencies of 500 Hz are needed.

4. Application of dielectrophoresis to effect black liquor droplet coalescence and skew the drop size distribution away from the finer particles was unsuccessful in a limited trial. A maximum field strength of 5 kilovolts was achieved before dielectric breakdown occurred, as evidenced by the initiation of current flow

from the power source. It does not appear that drop size distribution can be significantly altered by this route.

5. To what extent the drop size distribution must be narrowed or skewed to have a positive impact on recovery boiler performance is not known at this time. An estimate can be obtained by specifying different drop size distributions as input to the recovery boiler model currently being developed by the Institute of Paper Science and Technology and calculating the model predictions.

5.0 REFERENCES

1. Empie, H.J., Lien, S.J., Rumsey, R.S., and Sachs, D.G., "Kraft Black Liquor Delivery Systems Report No.4," U.S. DOE Contract No. DE-FG02-88CE40839, IPST (Jan. 1993).

2. Empie, H.J., Lien, S.J., Yang, W., Samuels, D.B., and Adams, T.N., "Kraft Black Liquor Delivery Systems Report No.3," U.S. DOE Contract No. DE-FG02-88CE40839, IPST (Dec.1991).

3. Adams, T.N., Empie, H.J., Lien, S.J., and Spielbauer, T.M., "Kraft Black Liquor Delivery Systems Report No.2," U.S. DOE Contract No. DE-FG01-88CE40839, IPST (Dec. 1990).

4. Adams, T.N., Empie, H.J., Obuskovic, N., and Spielbauer, T.M., "Kraft Black Liquor Delivery Systems Report No. 1, "U.S. DOE Contract No. DE-FG02-88CE40839, IPST (Feb. 1990).

5. Crapper, G.D., Dombrowski, N., and Pyott, G.A.D., Proc. Roy. Soc. London A342, 209-224 (1975).

6. Crapper, G.D. and Dombrowski, N., Int. J. Multiphase Flow 10 (6), 731-736 (1984).

7. Mason, B.J. and Brownscombe, J.L., "Production of Uniform Size Drops at a Controllable Frequency & Spacing from a Vibrating Capillary," J. Sci. Instr. 41, (1964).

8. Lin, S.P. and Woods, D.R., "Induced Atomization," ICLASS-91 (Gaithersburg, MD), 383 (1991).

9. Schneider, J.M. and Hendricks, C.D., "Source of Uniform-Sized Liquor Droplets," Rev.Sci.Instr. 35 (10), 1349 (1964).

10. Dressler, J.L., "Atomization of Liquid Cylinders, Cones, and Sheets by Acoustically-Driven, Amplitude-Dependent Instabilities," ICLASS-91 (Gaithersburg, MD), 397 (1991)

11. Pohl, H.A., Dielectrophoresis, Cambridge Univ. Press (1978), Ch. 4.

12. Handbook of Chemistry & Physics (39th ed.), p. 2330.

PROPOSALS
SUBMITTED
TO THE
U.S. DEPARTMENT OF ENERGY

Proposal to U.S. Department of Energy

SMELT SOLIDIFICATION

by

Jeff Empie

Solidification of kraft smelt prior to dissolving to make green liquor represents a modification of the conventional recovery process that can improve energy efficiency, while eliminating the potential for smelt-water explosions in the dissolving tank and reducing TRS emissions levels in the dissolving tank vent stack. Use of a steam fluidized bed concept may provide an economic means for achieving these benefits. The objectives of this project are to: determine the technical feasibility of solidifying kraft smelt in a fluidized bed operating continuously at a temperature several hundred degrees below the melting point of the smelt; quantify the major impacts on the process of preparing green liquor; and implement the technology in a commercial pulp mill.

This proposal has resulted from some earlier work done under exploratory Project 3534-55 where a laboratory scale packed bed reactor containing ground solid smelt particles was steam purged at 800 F for two hours. Analysis of the processed smelt particles showed that all of the organic carbon originally in the smelt (dregs) had been gasified and 10-20% of the sulfide was unaccounted for. Sodium entrainment in the steam flow was only a few ppm. A check of the settling rate of the dregs before and after reaction showed an increase by a factor of 2 to 3. A check of the dissolving rate of the solid smelt particles showed it to be high enough that existing dissolving tanks should provide adequate residence time.

The proposed project will consist of three phases involving: additional laboratory fixed bed reactor experiments at elevated temperature and laboratory scale fluidized bed experiments using a cold flow system; a small pilot scale fluidized bed smelt solidifier to be operated under actual process conditions; and installation and operation of a demonstration scale unit at an operating pulp mill.

The operating characteristics of the fluidized bed solidifier, including fluidization properties and salt feeding/withdrawal procedures, can be established most easily by using a laboratory-scale cold flow system using model compounds that melt at near-ambient temperatures. In this way, the difficulties introduced by high

temperature operation (e.g. plugging, corrosion) can be minimized and left to larger scale operation.

The second phase will involve a pilot scale fluidized bed smelt solidifier. It will run with a molten smelt feed and establish operating characteristics at actual process conditions. Design and construction will take twelve months, and operation will require another twelve months.

After this work has been completed with positive results, we would anticipate a demonstration phase at a mill site with vendor participation. The goal would be to verify pilot plant results and establish operational reliability, leading to successful technology transfer to the industrial sector. Typically, this type of activity requires 2-4 years for design, construction, and start-up of the facility.

The critical milestones generally follow the technical issues identified previously. These would include:

*Definition of the process chemistry using steam as fluidizing gas. This will determine what purification technology, if any, will be needed to clean up the superheated steam product.

*Determination of the best way or ways to use, in the mill steam/power cycle, the atmospheric pressure superheated steam which would come off the fluidized bed.

*Quantification of other process impacts, including dregs reduction, increase in dregs settling rate, and ultimate deadload reduction in the liquor cycle.

*Definition of the operational methods for continuously and reliably feeding molten smelt to the fluidized bed and withdrawing solidified smelt particles. Molten smelt poses special challenges because of its corrosiveness and high melting point.

*Continuous, steady state operation of a fluidized bed smelt solidifier with a controllable particle size distribution in the bed.

*Quantification of the economic attractiveness of the smelt solidification process, including the improvement in operational safety and decrease in dissolving tank emissions.

Total budget for the forty month program involving the laboratory and pilot scale studies is $745,000, with the DOE share being $596,000.

Proposal to U.S. Department of Energy

DELIVERY OF HIGH SOLIDS BLACK LIQUORS TO KRAFT RECOVERY BOILERS

by

H. Jeff Empie
&
Cary Presser
(NIST)

For incremental recovery boiler capacity and energy efficiency improvement, it is desirable to be able to fire liquors of 80% solids and higher. Unfortunately, these high solids liquors are characterized by extremely high viscosities, making them difficult to fire into the furnace cavity where proper combustion processes can take place. Commercial systems are in-place which deliver 80% solids liquors by raising the liquor temperature to solve the viscosity problem. Unfortunately, there is a limit determined by the liquor boiling point above which flashing of the liquor occurs when it is sprayed. The result is droplets which are much smaller than normal, leading to increased carryover rates in the recovery boiler.

A second problem with firing high solids liquors is inadequate control of the heat release (brought about by the reduction in water vaporization in the sprating zone of the furnace cavity) such that the protective frozen salt layer on the furnace walls can be potentially melted away due to increased combustion zone temperature. Such an event can lead to a catastrophic smelt-water explosion if a tube leak should result from corrosion by molten smelt.

One candidate process concept to be considered would use black liquor oxidation (BLO) which can be used to convert residual sodium sulfide in the liquor to sodium thiosulfate. This has been the practice for odor control in older kraft recovery boilers where oxidation is generally conducted with the strong black liquor (approx. 50% solids) issuing from the multiple effect evaporator and prior to the final concentration step using a direct contact evaporator.

BLO can mitigate the heat release problem by oxidizing the liquor prior to final concentration and firing, effectively decreasing the liquor heating value by about 5%. The viscosity increase resulting from oxidation and additional water removal can be counteracted by increasing liquor temperature through adiabatic oxidation, and by establishing a two-phase flow of liquor and air ahead of the nozzle. This two-phase mixture will have an effective viscosity much lower than liquor alone, and may result in effervescent atomization of the black liquor. Effervescent atomization is a

technique used to generate fine droplets in other spraying applications (e.g. coatings). In the case of high solids black liquor, it should assist in the formation of properly sized drops which might otherwise be too large for good combustion. In between the oxidation and spraying steps would be a multi-stage flashing operation to concentrate the liquor to the final solids level.

Reaction kinetics for black liquor oxidation have been previously worked out for both weak and strong (i.e. 45%-55% solids) liquors at temperatures generally below 90°C. "High intensity" black liquor oxidation (HIBLOX) has been studied where higher temperatures (100-150°C) were employed to extend the oxidation reactions to include liquor organics (to decrease liquor heating value) in addition to the sodium sulfide. Both weak and strong liquors were studied: however, oxidation of concentrated liquor (>65% solids) has not been.

The project will consist of three phases involving:

1) A survey of potential low cost process technologies which will generate a high solids black liquor that can be fired into an existing recovery boiler and give state-of-the-art combustion and reduction efficiencies, while satisfying existing environmental constraints.

2) Laboratory studies to establish concept feasibility and provide necessary process performance data for design of a mill-scale demonstration of the technology. The information should stress impact on drop size and size distribution, along with combustion characteristics of those droplets.

3) Extended operation at a kraft mill to establish operability, reliability, and economic benefits of the modified liquor feed system.

Total budget for the twenty-four month program involving the technology survey and laboratory studies is $276,000, with the DOE share being $215,000.